REPORT DOCUMENTATION PAGE

Form Approved OMB NO. 0704-0188

1. REPORT DATE (DD-MM-YYYY)	2. REPORT TYPE	3. DATES COVERED (From - To)
23-11-2018	Final Report	23-Jun-2014 - 22-Jun-2018

4. TITLE AND SUBTITLE
Final Report: Self-Assembly of Multifunctional, Adaptive Nanomaterials.

5a. CONTRACT NUMBER
W911NF-14-1-0305

5b. GRANT NUMBER

5c. PROGRAM ELEMENT NUMBER
611102

6. AUTHORS

5d. PROJECT NUMBER

5e. TASK NUMBER

5f. WORK UNIT NUMBER

7. PERFORMING ORGANIZATION NAMES AND ADDRESSES
Ohio State University
1960 Kenny Road

Columbus, OH 43210 -1016

8. PERFORMING ORGANIZATION REPORT NUMBER

9. SPONSORING/MONITORING AGENCY NAME(S) AND ADDRESS (ES)
U.S. Army Research Office
P.O. Box 12211
Research Triangle Park, NC 27709-2211

10. SPONSOR/MONITOR'S ACRONYM(S)
ARO

11. SPONSOR/MONITOR'S REPORT NUMBER(S)
65672-MS.9

12. DISTRIBUTION AVAILIBILITY STATEMENT
Approved for public release; distribution is unlimited.

13. SUPPLEMENTARY NOTES
The views, opinions and/or findings contained in this report are those of the author(s) and should not contrued as an official Department of the Army position, policy or decision, unless so designated by other documentation.

14. ABSTRACT

15. SUBJECT TERMS

16. SECURITY CLASSIFICATION OF:			17. LIMITATION OF ABSTRACT	15. NUMBER OF PAGES	19a. NAME OF RESPONSIBLE PERSON
a. REPORT	b. ABSTRACT	c. THIS PAGE			Jonathan Parquette
UU	UU	UU	UU		19b. TELEPHONE NUMBER 614-292-5886

RPPR Final Report
as of 27-Nov-2018

Agency Code:

Proposal Number: 65672MS **Agreement Number: W911NF-14-1-0305**
INVESTIGATOR(S):

Name: Jonathan Robert Parquette
Email: parquett@chemistry.ohio-state.edu
Phone Number: 6142925886
Principal: Y

Organization: **Ohio State University**
Address: 1960 Kenny Road, Columbus, OH 432101016
Country: USA
DUNS Number: 832127323 EIN: 316025986
Report Date: 22-Sep-2018 Date Received: 23-Nov-2018
Final Report for Period Beginning 23-Jun-2014 and Ending 22-Jun-2018
Title: Self-Assembly of Multifunctional, Adaptive Nanomaterials.
Begin Performance Period: 23-Jun-2014 **End Performance Period:** 22-Jun-2018
Report Term: 0-Other
Submitted By: Jonathan Parquette Email: parquett@chemistry.ohio-state.edu
Phone: (614) 292-5886
Distribution Statement: 1-Approved for public release; distribution is unlimited.

STEM Degrees: 2 **STEM Participants:**

Major Goals: The long-term goal of this research is to understand how the collective structural features of noncovalently assembled systems can be used to create dynamic, stimuli-responsive systems that change color and structure upon light exposure. During the first two years as part of Aim 1, we have installed light-responsive molecular dyes, such as spiropyrans and dithienylethylenes, into the monomers of the nanostructures to allow light-triggered, local perturbations to disrupt the ability of the dye to efficiently participate in intermolecular ?-stacking interactions. We have also crosslinked the nanotube/nanofiber assemblies via photoinduced polymerization of diacetylene. This polymerization produced colored nanostructures that were stable to solvent conditions but reversibly change color with temperature. For Aim 3, we have templated gold nanoparticles onto the nanotubes, as part of a strategy to create light-modulated nanoparticle arrays. A very exciting development, that allows us to co-assemble a nanotube with two polymers into a single co-axial nanotubes with optoelectronic polymers on the surface. Thus, we will exploit this strategy to prepare photoresposive nanotube/polymer co-assemblies to more efficiently create light responsive nanomaterials. We expect that this work will ultimately contribute to the military's need for strong, camouflage materials with capabilities that respond colorimetrically and structurally to extrinsic input.

The long-term goal of this research is to understand how the collective structural features of noncovalently assembled systems can be used to create dynamic, stimuli-responsive systems that change color and structure upon light exposure. During the first two years as part of Aim 1, we have installed light-responsive molecular dyes, such as spiropyrans and dithienylethylenes, into the monomers of the nanostructures to allow light-triggered, local perturbations to disrupt the ability of the dye to efficiently participate in intermolecular ?-stacking interactions. We have also crosslinked the nanotube/nanofiber assemblies via photoinduced polymerization of diacetylene. This polymerization produced colored nanostructures that were stable to solvent conditions but reversibly change color with temperature. For Aim 3, we have templated gold nanoparticles onto the nanotubes, as part of a strategy to create light-modulated nanoparticle arrays. A very exciting development, that allows us to co-assemble a nanotube with two polymers into a single co-axial nanotubes with optoelectronic polymers on the surface. Thus, we will exploit this strategy to prepare photoresposive nanotube/polymer co-assemblies to more efficiently create light responsive nanomaterials. Recently, we have been able to create well-defined nanotubes by the assembly of the SP form of a bis-SP/MC pentapeptide. Furthermore, this process could be reversed by opening to the MC form. Based on our ability to uniformly coat positively charged nanotubes with negatively charged polyelectrolytes, we will explore the introduction of negatively charged, conjugated polyelectrolytes to coat the SP-pentapeptide nanotubes. The questions to be addressed are: (1) Will conversion back to the MC form result in loss of the nanotube structure when coated with polymer or will the polymer render the nanotube structure stable to the SP/MC interconversion? (2) Can we control the rate of energy transfer between the SP/MC chromophore and the polymer layer by

converting between the SP and MC states? Our recent results indicate that this system is uniquely capable of dissipating energy as a method of driving self-assembly. Nanomaterials that consume energy in order to self-assembly are potentially capable of mimicking natures methods of using chemical energy to control functional processes in the cell.
?
We expect that this work will ultimately contribute to the military's need for strong, camouflage materials with capabilities that respond colorimetrically and structurally to extrinsic input.

Accomplishments: see pdf document

Training Opportunities: Four graduate students (Dr. Nicholas Bewick, Mengmeng Liu; Cassidy Creemer; Thomas Reardon); several undergraduates have participated in the research supported by this project. Additionally, two Turkish graduate students from Ataturk University worked in my research group during 2014. Additionally, the PI has partnered with Prof. Ashton Hamme at Jackson State University through an NSF HBCU-RISE program, currently under review, to provide research experiences to minority students in the area of nanotechnology.

The PI served as a judge at the U.S. Army, Navy, and Air Force sponsored National Junior Science & Humanities Symposium in Dayton OH on April 28, 2016. This allowed the PI to mentor high school students in their quest to participate in science activities.

The PI obtained support from the ARO URAP program to support a hearing-impaired undergraduate student, Connor Paige, during Summer 2016. She participated in the research supported by the ARO program.

Results Dissemination: The results have primarily been disseminated by two publications. Several other manuscripts have been prepared and are either under revision or preparation.

The PI has presented one talk at an ACS meeting about the results of this work.

Undergraduates who have worked on this project presented at the OSU Denman Undergraduate Research Symposium. Students who have graduated have disseminated their work on this project as part of their theses (4 total).

Honors and Awards: Nothing to Report

Protocol Activity Status:

Technology Transfer: Nothing to Report

PARTICIPANTS:

Participant Type: Graduate Student (research assistant)
Participant: Cassidy Creemer
Person Months Worked: 5.00 **Funding Support:**
Project Contribution:
International Collaboration:
International Travel:
National Academy Member: N
Other Collaborators:

Participant Type: Graduate Student (research assistant)
Participant: Thomas Reardon
Person Months Worked: 5.00 **Funding Support:**
Project Contribution:
International Collaboration:
International Travel:
National Academy Member: N

Other Collaborators:

Participant Type: Graduate Student (research assistant)
Participant: Nicholas Bewick
Person Months Worked: 5.00 **Funding Support:**
Project Contribution:
International Collaboration:
International Travel:
National Academy Member: N
Other Collaborators:

Participant Type: Graduate Student (research assistant)
Participant: Mengmeng Liu
Person Months Worked: 5.00 **Funding Support:**
Project Contribution:
International Collaboration:
International Travel:
National Academy Member: N
Other Collaborators:

DISSERTATIONS:

Publication Type: Thesis or Dissertation
Institution:
Date Received: 31-Aug-2015 Completion Date:
Title: Intramolecular communication of peptide-dendrimer hybrids and the self-assembly of polymerizable NDI-diacetylene amphiphilic nanotubes
Authors:
Acknowledged Federal Support:

Publication Type: Thesis or Dissertation
Institution: The Ohio State University
Date Received: 30-Aug-2016 Completion Date: 12/22/15 5:00AM
Title: Decoration of Amphiphilic NDI-diacetylene Nanotubes with Gold Nanoparticles and the Anti-parallel ?-Sheet Assembly of Porphyrin Modified Tetrapeptides
Authors: Mary Nappi
Acknowledged Federal Support: **Y**

Publication Type: Thesis or Dissertation
Institution: The Ohio State University
Date Received: 30-Aug-2016 Completion Date: 1/5/16 5:00AM
Title: Stimuli responsive self-assembly of functional organic nanomaterials
Authors: Kwang Soo Lee
Acknowledged Federal Support: **Y**

RPPR Final Report
as of 27-Nov-2018

Publication Type: Thesis or Dissertation
Institution: Ohio State University
Date Received: 23-Nov-2018 Completion Date: 4/20/17 3:42AM
Title: Self-assembled Photo-responsive Nanostructures for Smart Materials Applications
Authors: Mengmeng, Liu
Acknowledged Federal Support: **Y**

Report: Self-Assembly of Multifunctional, Adaptive Nanomaterials.

Jon R. Parquette
The Ohio State University
Dept. of Chemistry and Biochemistry

Table of Contents

Project Overview. The expression of local molecular structure at size regimes ranging from nano- to mesoscopic has important functional significance in nature. Extraordinary properties emerge for molecules organized into structures with nanoscale dimensions, owing to the unique physical, chemical, and quantum phenomena that occur in this size regime. These properties critically depend on the size, shape, and internal/external surface structure of the nanostructures. Thus, many biomolecular systems such as hemoglobin, polymerases, membrane channels and photosynthetic systems achieve and modulate their functional characteristics via noncovalent self-assembly. Self-assembly provides a convenient, albeit often empirical strategy, to fabricate materials in the nanoscale regime where these properties are present. Although strategies to create nanostructured materials have been developed over the last decade, methods to dynamically modulate these structural features via external triggers are limited. Most self-assembled materials are static, thermodynamically stable structures that do not respond to variations in external conditions. The vast potential for these materials to display adaptivity, self-healing and other forms of "intelligent" behavior require a capability to transition between multiple states. In contrast, biological assemblies are dynamic systems capable of existing in non-equilibrium states capable of responding structurally and functionally to extrinsic input. To realize the functional diversity of these structures in Nature, we must learn how to design nanostructures capable of structurally reorganizing via non-equilibrium intermediates. A characteristic of non-equilibrium systems is that their function requires the dissipation of energy. This is an exceptionally challenging goal. **In this project, we will design self-assembled systems that undergo structural reorganizations that are driven photochemically. The long-term goal is to understand how the collective structural features of self-assembled nanomaterials can be used to create dynamic, stimuli-responsive systems.** Our recent results indicate that this system is uniquely capable of dissipating energy as a method of driving self-assembly. Nanomaterials that consume energy in order to self-assembly are potentially capable of mimicking natures methods of using chemical energy to control functional processes in the cell.

A Strategy for the Co-Assembly of Co-Axial Nanotube-Polymers.

Parquette, J.; Ji, Mingyang; Modarelli, D.M. *published*

Published: Ji, M.; Dawadi, M. B.; LaSalla, A. R.; Sun, Y.; Modarelli, D. A.; Parquette, J. R. Strategy for the Co-Assembly of Co-Axial Nanotube-Polymer Hybrids. *Langmuir* **2017**. *33 (36),* 9129..

ABSTRACT: Nanostructured materials having multiple, discrete domains of sorted components are particularly important to create efficient optoelectronics. The construction of multicomponent nanostructures from self-assembled components is exceptionally challenging due to the propensity of noncovalent materials to undergo structural reorganization in the presence of excipient polymers. This work demonstrates that polymer-nanotube composites comprised of a self-assembled nanotube wrapped with two conjugated polymers could be assembled using a layer-by-layer approach. The polymer-nanotube nanostructures arrange polymer layers co-axially on the nanotube surface. Femtosecond transient absorption (TA) studies indicated that the polymer-nanotube composites undergo photoinduced charge separation upon excitation of the NDI chromophore within the nanotube.

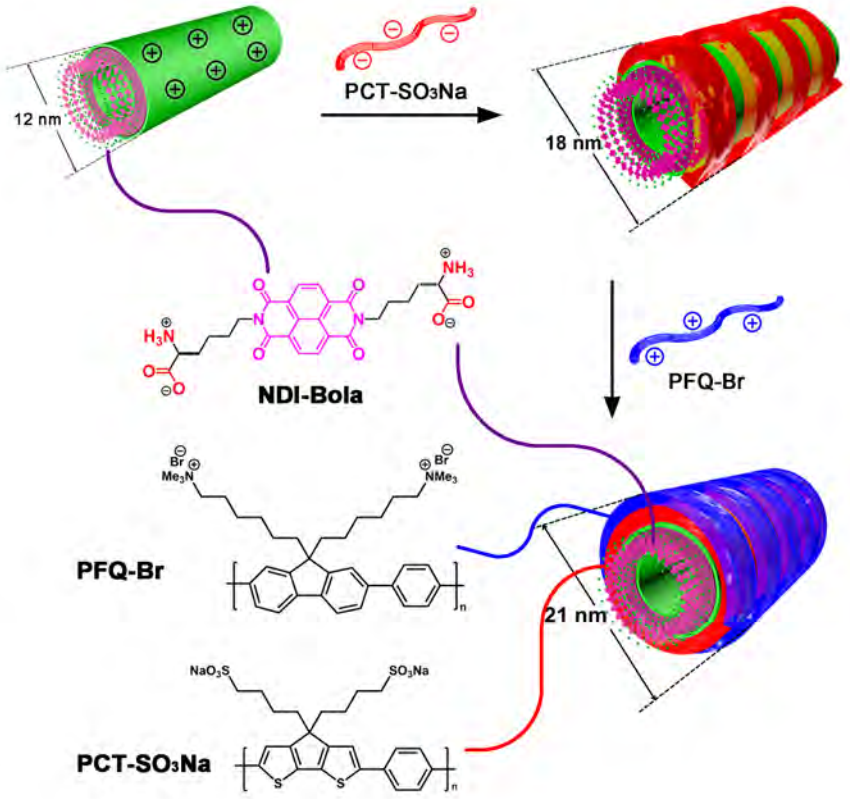

Figure 1. Structures of NDI-Bola nanotubes, conjugated polyelectrolytes PCT-SO_3Na and PFQ-Br. NDI-Bola nanotubes assembled via the progressive stacking of initially formed NDI-Bola monolayer rings. The NDI-Bola nanotubes were then sequentially wrapped with two oppositely charged polyelectrolytes, PCT-SO_3Na and PFQ-Br, to give NDI-Bola/PCT-SO_3Na and NDI-Bola/PCT-SO_3Na/PFQ-Br nanotubes.

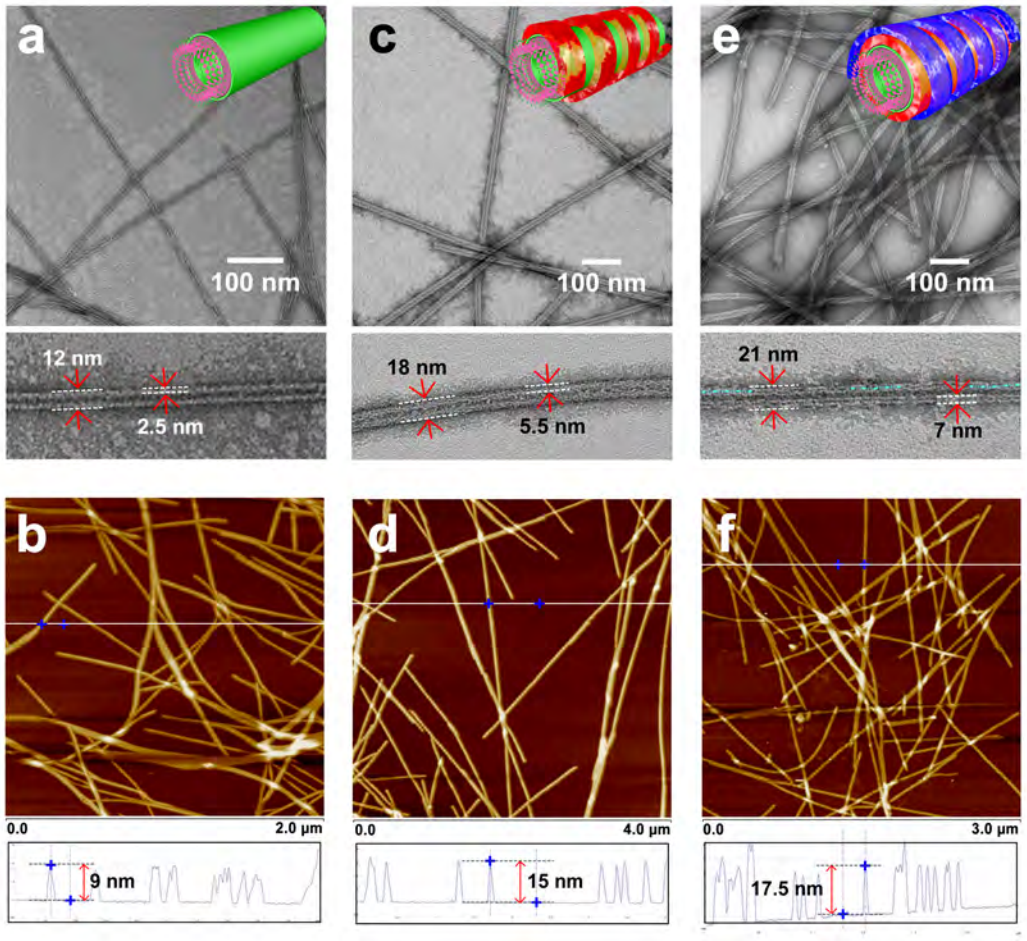

Figure 2. TEM and tapping-mode AFM images of (a, b) NDI-Bola, (c, d) NDI-Bola/PCT-SO_3Na (10:2, n/n), and (e, f) NDI-Bola/PCT-SO_3Na/PFQ-Br (10:2:2, n/n/n) in water (carbon-coated copper grid). The concentration of NDI-Bola in all samples was 2 mM. TEM insets: High-resolution images of individual nanotubes. Parts of the additional smaller channels in NDI-Bola/PCT-SO_3Na/PFQ-Br (10:2:2, n/n/n) are labeled in cyan. AFM insets: Section analysis showing uniform heights of corresponding nanotubes. NDI-Bola pre-assembled into nanotubes within 24 h. After treatment with polymers and incubating for 24 h, the resulting polymer-nanotube composites were centrifuged (5000 rpm) and redispersed in water for TEM and AFM tests.

Co-Assembly of MultiComponent Nanotube. Co-assembly of NDI-Bola and two conjugated polymers, PFQ-Br and PCT-SO_3Na.The darker internal line is a consequence of the negative stain wicking into the nanotube. Upon sequential addition of each polymer, another separate wall (light constrast line) along with a darker separation indicates the uniform coating of the polymer structures with a well-defined, nanoscale separation between the nanotube wall and the polymer coatings. **We have achieved a method to co-assemble an NDI nanotube with two conjugated polymers to create a polymer-nanotube with a co-axial arrangment of three functional chromophores. This advancement will greatly facilitate the assembly of multicomponent structures contain photoresposive surface polymers to explore how photoresponsivity of the surface would control nanostructure morphology and function.**

Controlling the Length of Self-Assembled Nanotubes by Sonication Followed by Polymer Wrapping

Mingyang Ji,[a] Brian Daniels,[a] Aileen Shieh,[a] David A Modarelli[b] and Jon R. Parquette[a]*

Published: Ji, M.; Dawadi, M.; LaSalla, A.; Sun, Y.; Modarelli, D.M.; Parquette, J.R. Controlling the Length of Self-Assembled Nanotubes by Sonication Followed by Polymer Wrapping, *Chem. Commun.* **2017**, *53*, 12806-12809

Abstract: This work demonstrates that sonication, followed by polymer-wrapping, is an effective strategy to modulate the length of self-assembled nanotubes. The length distributions of the nanotubes were controlled by varying the amplitude of sonication. Wrapping the nanotubes with ionic polymers suspended the propensity of the nanotube fragments to re-assemble over time into their elongated precursors.

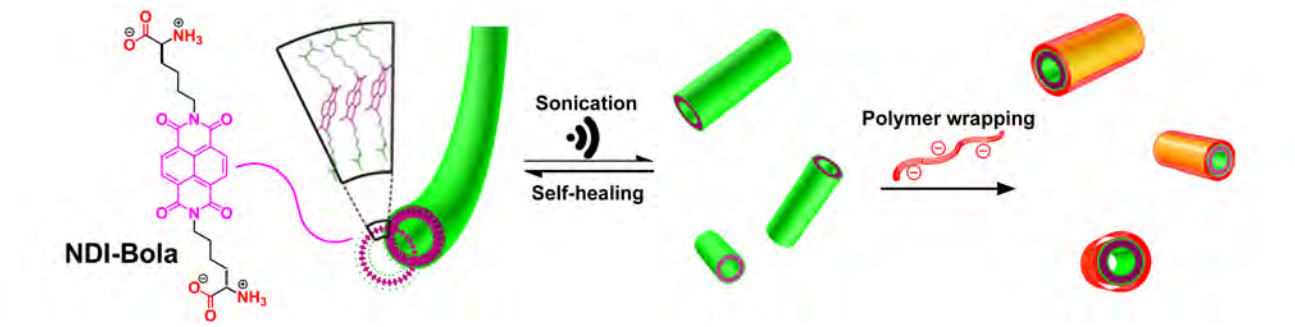

Fig. 1 Schematic illustration of sonication induced scission and polymer wrapping induced stabilization of self-assembled nanotubes.

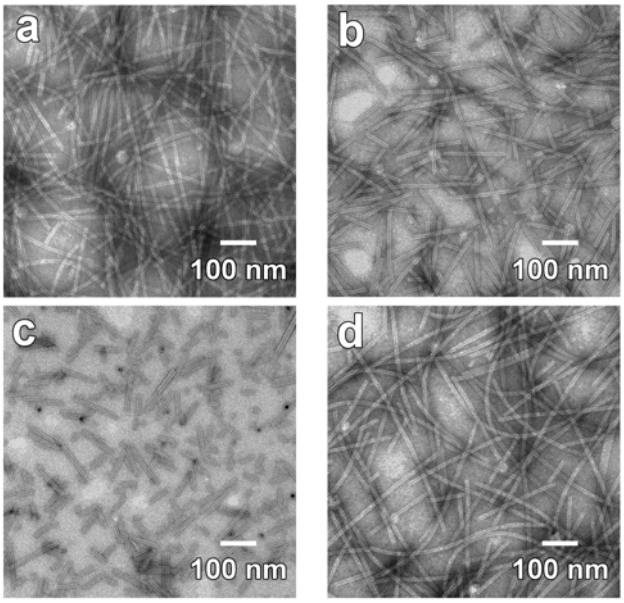

Fig. 2 Transmission electron microscopy (TEM) images of NDI-Bola (2 mM) in water (carbon-coated copper grid, 2% (w/w) uranyl acetate as a negative stain.). (a) Original nanotubes prepared by incubating in water (20 mM) for 12 h, then diluting to 2 mM for imaging. (b, c) After sonication at (b) 10% and (c) 20% amplitudes for 3 min, respectively. (d) Nanotubes sonicated for 3 min at 20% followed by 3 days of aging, indicating re-healing into elongated nanotubes.

The Light-Induced Active Assembly of Spiropyran Peptides

Biological systems use chemical fuels such as ATP to control the formation of active nanoarchitectures as a method to derive function and maintain life. These functional nanostructures exist in states that are "outside of equilibrium" in contrast to normal supramolecular assemblies that represent thermodynamically stable states. In an effort to create highly functional, controllable nanomaterials with functions that can potentially do work as in biological systems, there has been a recent, intense interest in creating synthetic, nanostructures that assemble when energy is consumed by the system. We have recently developed spiropyran peptides that assembles into either nanofibers or nanotubes when irradiated with light at 60°C but dissipate into dissociated states when the light is turned off.

Mono-Spiropyran Tetrapeptide Transiently Forms Nanofibers Under Irradiation.

This peptide remains in a dissociated state when in the open form after irradiation with UV light, but forms a self-assembled hydrogel, comprised of nanofibers, when irradiated with visible light in water (with 0.75% TFA). Heating at 60°C for 1 hour reverts the closed form to the open form, resulting in dissociation of the assembly and dissolution of the hydrogel. When the tetrapeptide is irradiated with visible light at 60°C, nanofibers progressively form from 30 minutes to 24 hours, as shown in the figure below. However, if the light is turned off, the fibers dissociate.

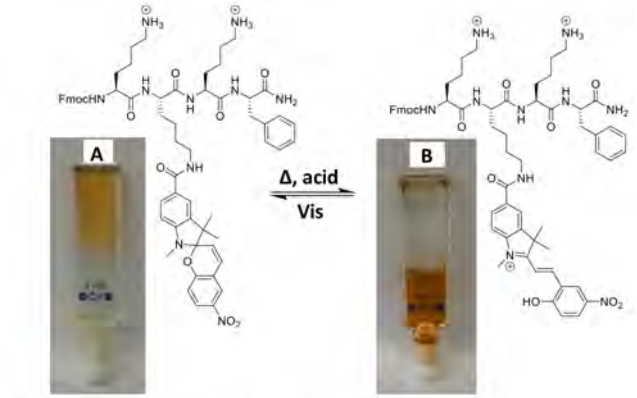

A 10 mM soln of tetrapeptide pre-heated for 1 h, then aged for 3 days in LED light/22°C (A), and re-heated for 1 h at 60°C/darkness (B).

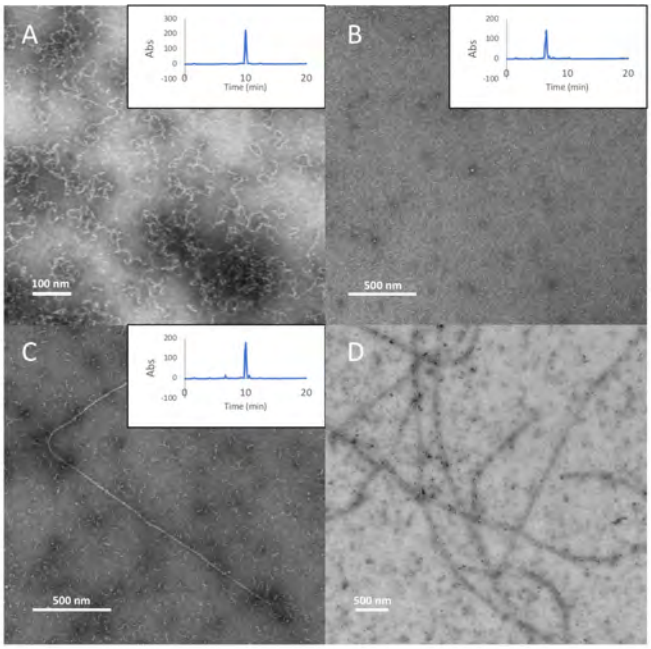

TEM images of SP0 (3 mM, 0.75% TFA in water, stained with uranyl acetate) assembly at A) T = 0 min, fully closed; B) T = 60 min, 60°C/darkness, fully open; C) T = 30 min, 60°C/LED visible light; and D) T = 24 h, 60°C/LED visible light. Graphic inserts show analytical reverse-phase HPLC traces corresponding to TEM samples.

Bis-Spiropyran Tetrapeptide Transiently Forms Nanotubes Under Irradiation.

The bis-spiropyran tetrapeptide, shown below, interconverts between four states: SP/SP; SP/MC; MC/SP and MC/MC. Whereas SP/SP state assembles into nanotubes, the other MC states do not form nanostructures. Similar to the mono-spiropyran system, irradiation with visible light induces the MC form to close into the SP form, whereas heating in 30% acetonitrile/water (0.75% TFA) converts the SP form to the open MC form. The HPLC traces below show the progressive transformation of the SP/SP form into the MC/MC form at 60°C over 45 minutes. TEM imaging shows that the SP/SP form assembles into well-defined nanotubes whereas the MC/MC form exhibits minimal self-assembly by TEM.

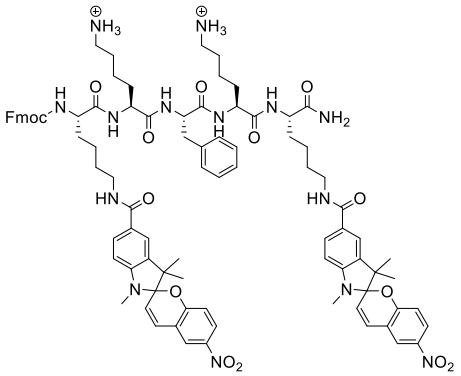

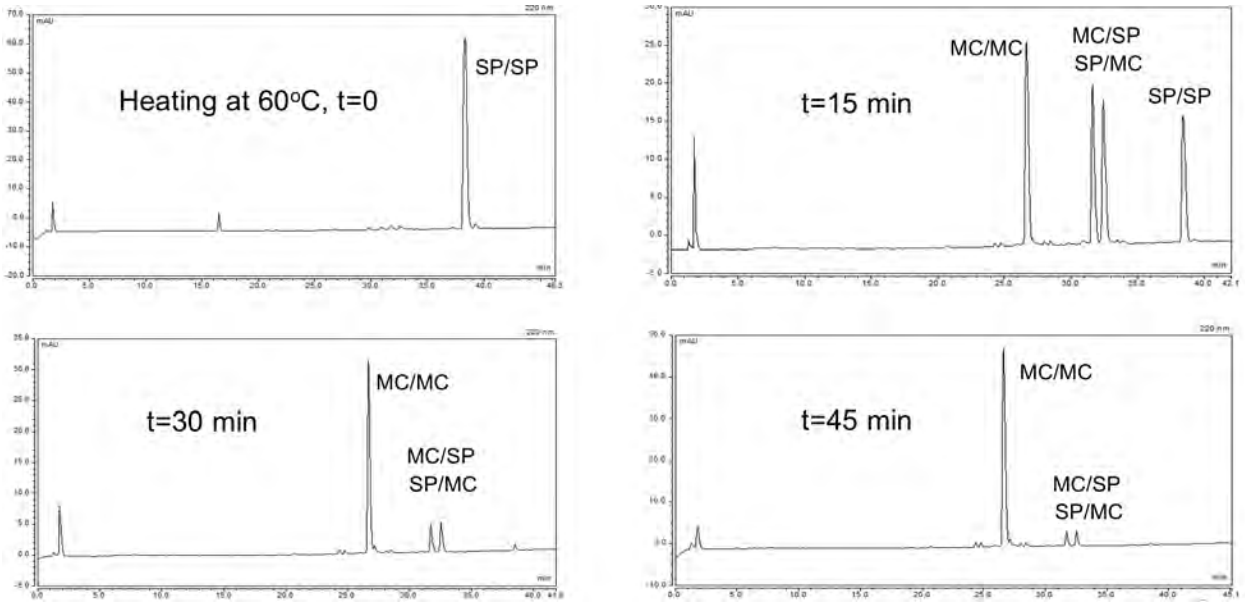

HPLC traces showing the thermal transformation of SP/SP form of peptide progressively into the MC/MC form upon heating at 60°Ç in 30% acetonitrile/water (0.75% TFA).

Remarkably, if the sample is heated to 60°Ç in 30% acetonitrile/water (0.75% TFA) in under visible light irradiation, nanotubes are formed. After the light is turned off, the nanotubes dissipate over several hours. These results indicate that this system is capable of displaying an active asssemly process driven by light as an energy source. More details about these systems are described in the following two sections of the report.

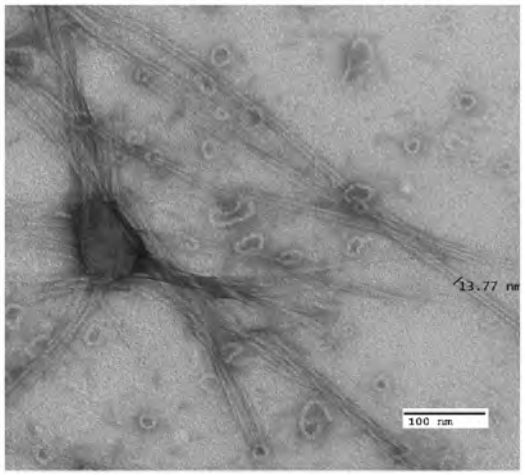

0.5 mM solution of **3** incubated in visible light overnight in 30% MeCN/water + 0.75% TFA
Visible light: 300 LEDs, 12V, 72W

Δ, 0.75% TFA
⇌
Vis

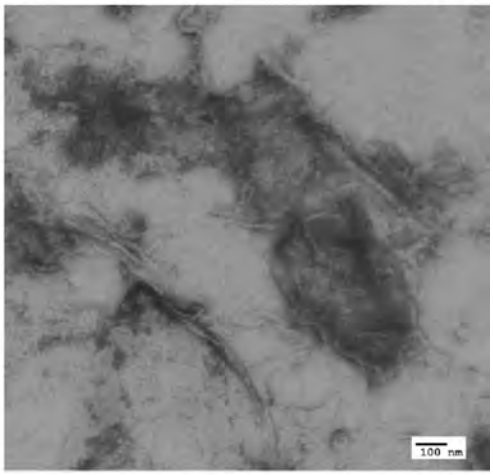

Same sample heated for 40 minutes

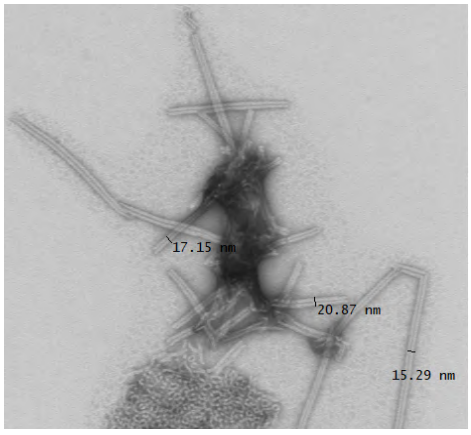

0.5 mM solution in 30% MeCN/water + 0.75% TFA heated at 60°C for 40 minutes, while constantly irradiated with visible light Visible light: 300 LEDs 12V, 72W

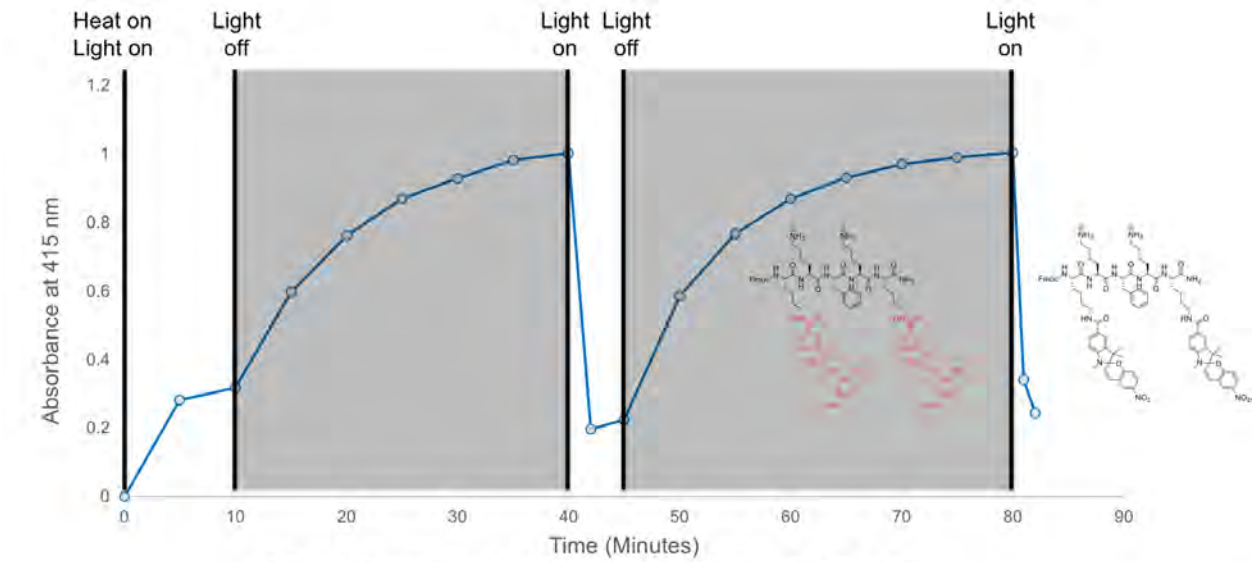

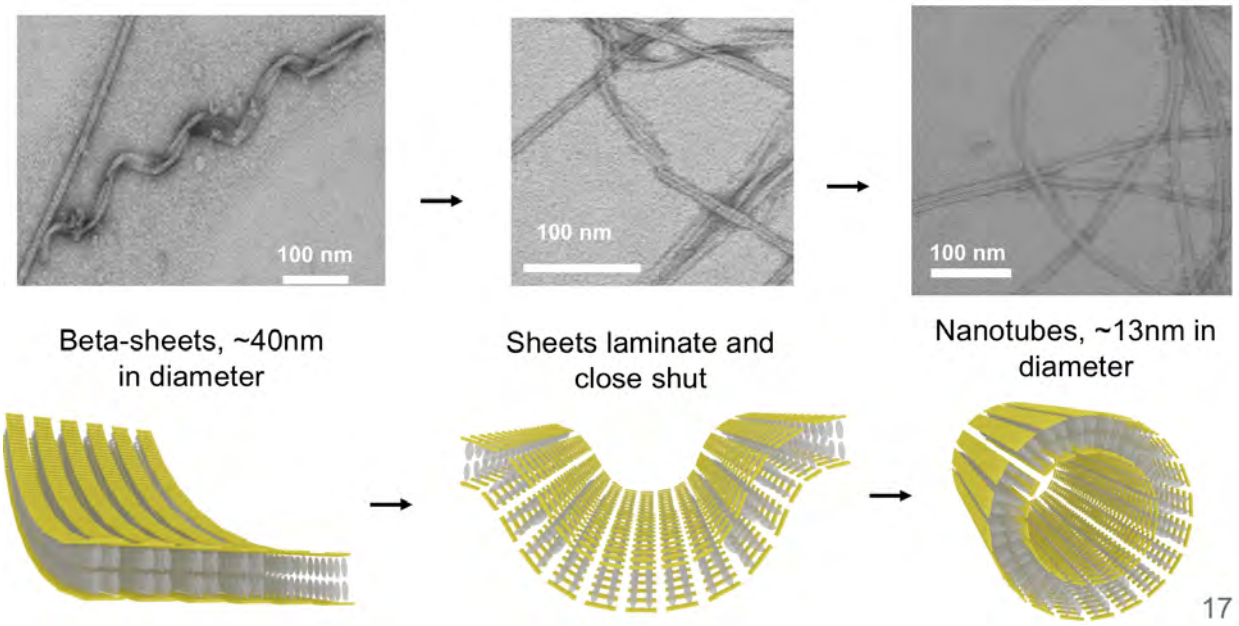

Proposed Mechanism of Nanotube Formation under Irradiation.

Photoresponsive Gelation of a Spiropyran Tetrapeptide

Mengmeng Liu, Allesandro Brunnetti and Jon R. Parquette

Spiropyrans constitute a well-studied group of light-switchable, photochromic dyes that exist as closed, nonpolar and nearly colorless molecules in the dark that absorb light in UV region. Light absorption induces a ring-opening process leading to a planar, merocyanine (MC) form that is highly colored and extensively pi-conjugated. Irradiation of this form of the dye with visible light returns the colorless spiropyran form. The position of the merocyanine-spiropyran equilibrium is also influenced by the polarity of the medium and can be induced thermally. In this work, spiropyran chromophores have been incorporated into a tetrapeptide to explore how local SP-MC isomerization would be expressed at the nanostructural level. The design of the SP-tetrapeptide, Fmoc-KK(SP)KF-NH_2, was based on a previous study of coumarin-tetrapeptides conjugates that we observed to self-assemble into nanofiber

structures. The Fmoc- group and the phenyl group of phenylalanine (purple part in Fig. 2-1) provides both hydrophobicity and also a potential to undergo π-π stacking as mechanism to drive assembly. The alternatating hydrophilic/hydrophobic peptide sequence creates amphiphilicity that is well-known to drive the β-sheet aggregation of de novo peptides in aqueous solution. The protonated lysine side chains provide water solubility and developing repulsive electrostatic interactions to attenuate uncontrolled aggregation that is commonly observed in pi-sheet assemblies. We hypothesized that the planar merocyanine form would be both be polar and potential capable of engaging in extensive -stacking interactions. In contrast, the closed, nonplanar spiropyran form would reduce these pi-piinteractions and would likely form amphiphilic structures rather than beta-sheet fibers. Accordingly, irradiation with UV-vis light would simultaneously modulate the color, spectroscopic properties, and nanostructure of the assemblies. These light-responsive chromophores were incorporated into the peptides to explore how local SP-MC isomerization would be expressed at the nanostructural level. We found in this study that the the spiropyran underwent most efficient thermal conversion (60 °C) into the open merocyanine (ME) whereas visible light efficiently converted the open ME back to the closed SP form. *Surprisingly, in this construct, we found that polar ME state of the peptide precluded self-assembly forming a dissolved solution; whereas conversion to the SP form resulted in beta-sheet hydrogelation.* This unexpected observation can be rationalized by the reduction in peptide amphiphilicity that occurs upon conversion from the nonpolar SP to the polar ME state.

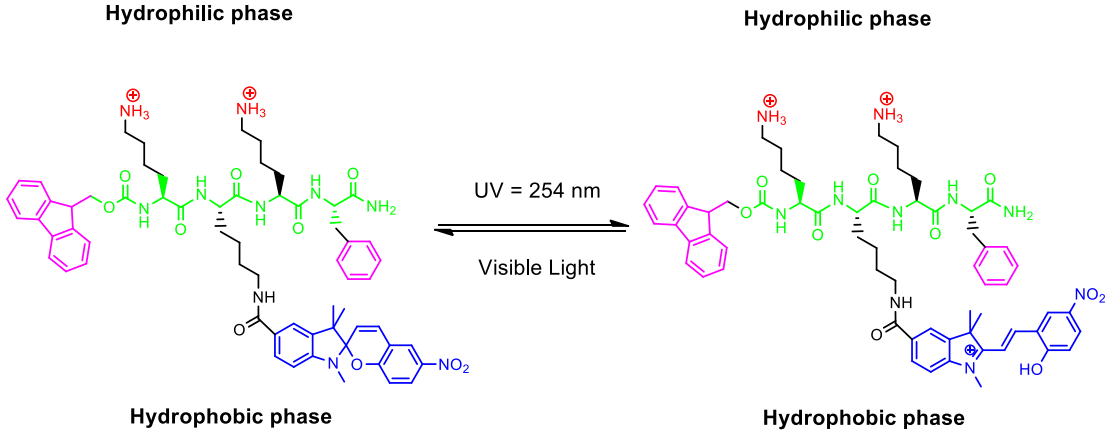

Figure 2-1. The structural design and of SP-tetrapeptides (Fmoc-KK(SP)KF-NH_2) conjugates which undergo structural change into the open form of protonated merocyanine form (Fmoc-KK(MC)KF-NH_2) with UV=254 nm irradiation in acidic condition.

Photo-Responsive Gel-Solution Conversion.

A 10 mM stock solution of Fmoc-KK(SP)KF-NH_2 in H_2O and 0.75% TFA were prepared. In H_2O, Fmoc-KK(SP)KF-NH_2 stays as a solution form under both visible light and UV=254 nm irradiation (Fig.2-2). In 0.75% TFA, under visible light, the tetrapeptide conjugates stay as the hydrophobic closed spiropyran form so that a rather fibril network can be established and even gel is formed (Figure 2-2; 2-3)

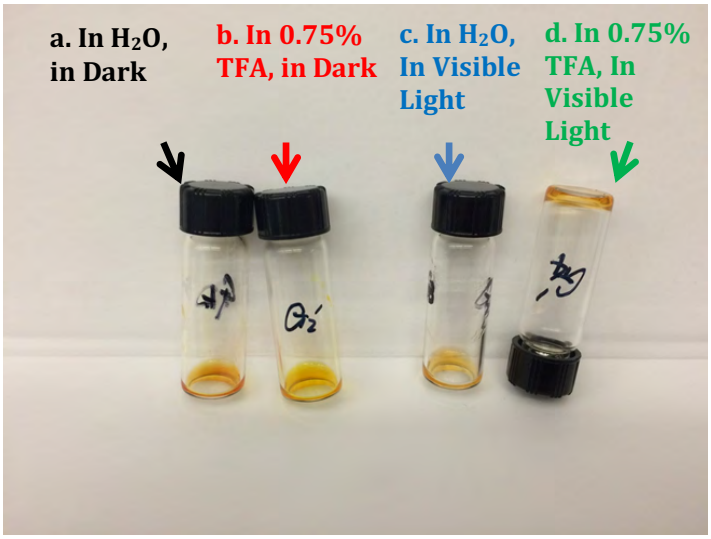

Figure 2-2. Solution images of Fmoc-KK(SP)KF-NH_2: Solution a. in H_2O kept in dark, b. in 0.75% TFA kept in dark, c. in H_2O and aged under visible light, d. in 0.75% TFA and aged under visible light

With UV=254 nm irradiation or heated up to over 60°C, the spiropyran part convert into the protonated merocyanine form. The hydrogel formed by Fmoc-KK(SP)KF-NH_2 form a hydrogel that transitioned into a liquid solution upon exposure to visible light, but was stable under dark conditions (Fig.4). With visible light irradiation, it can reversibly change back into the hydrogel state with the hydrophobic spiropyran reformation. The entire photo-responsive process is reversible for at least several cycles.

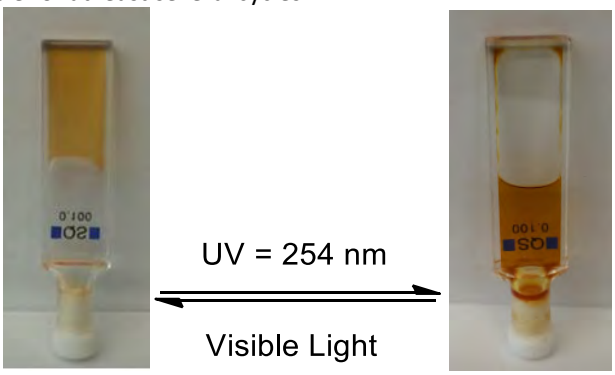

Figure 2-3. Conversion of Fmoc-KK(SP)KF-NH_2 in 0.75% TFA between gel and liquid states with irradiation of different wavelength.

Initial TEM analysis of the nanostructure of the SP and MC peptide states. Self-assembly behavior of the tetrapeptide solutions (a~d) was investigated by transmission electron microscopy (TEM). In pure H_2O, the SP-tetrapeptide solutions exhibited mostly amorphous aggregates in both the SP and MC forms (Fig. 2-4 a. and c.). However, In 0.75% TFA, the SP-tetrapeptides exhibited signficant gelation, which exhibited a well-defined nanofiber network by TEM imaging (Fig. 2-4d). Upon conversion to the open MC form upon heating to 60°C, the hydrogel disintegrated into a homogeneous solution with minimal nanofiber formation by TEM (Fig. 2-4 b.). These initial studies focused our attention on conditions using aqueous solutions containing 0.75% TFA, which likely protonate the zwitterionic MC form of the chromophore.

UV-vis Spectroscopy. The conversion between closed spiropyran form and the open merocyanine form can be observed by fluorescence microscopy. The spiropyran, merocyanine and protonated merocyanine have distinct absorption bands in UV-Vis spectra. In Fig. 2-5, a freshly prepared sample of Fmoc-KK(SP)KF-NH_2 in pure H_2O, after heating to 60°C for 1 h, then cooling and kept in dark, displays a small peak during 500~550 nm, indicating that only a very small fraction (80.8%) of the open MC form was produced under these conditions (Fig. 2-5. black line), which

is confirmed with analytical HPLC ratio (Fig. 2-6a). Upon visible light irradiation, this small peak disappeared, indicating the back conversion into closed spiropyran form (Fig. 2-5. blue line), which is 99.4% ratio from the HPLC study (Fig. 2-6c.). For the solution in 0.75% TFA, after UV irradiation and kept in dark, there was a distinct peak around 400 nm (Fig. 2-5, red line), which is the absorption band of the protonated merocyanine form. In this condition, a large portion of SP-tetrapeptides changes into the protonated open merocyanine form (85.6% in Fig. 2-6b.). With visible light irradiation, the decreased intensity of the peak around 400 nm reveals that the tetrapeptides convert back into the closed spiropyran form (Fig. 2-5, pink line) with a 99.5% ratio (Fig. 2-6d.). Both solutions in 0.75% TFA, compared to TFE solutions, exhibit red shift compared with the aqueous solutions, suggesting that J-type π-π interaction contribute to the self-assembly behavior.

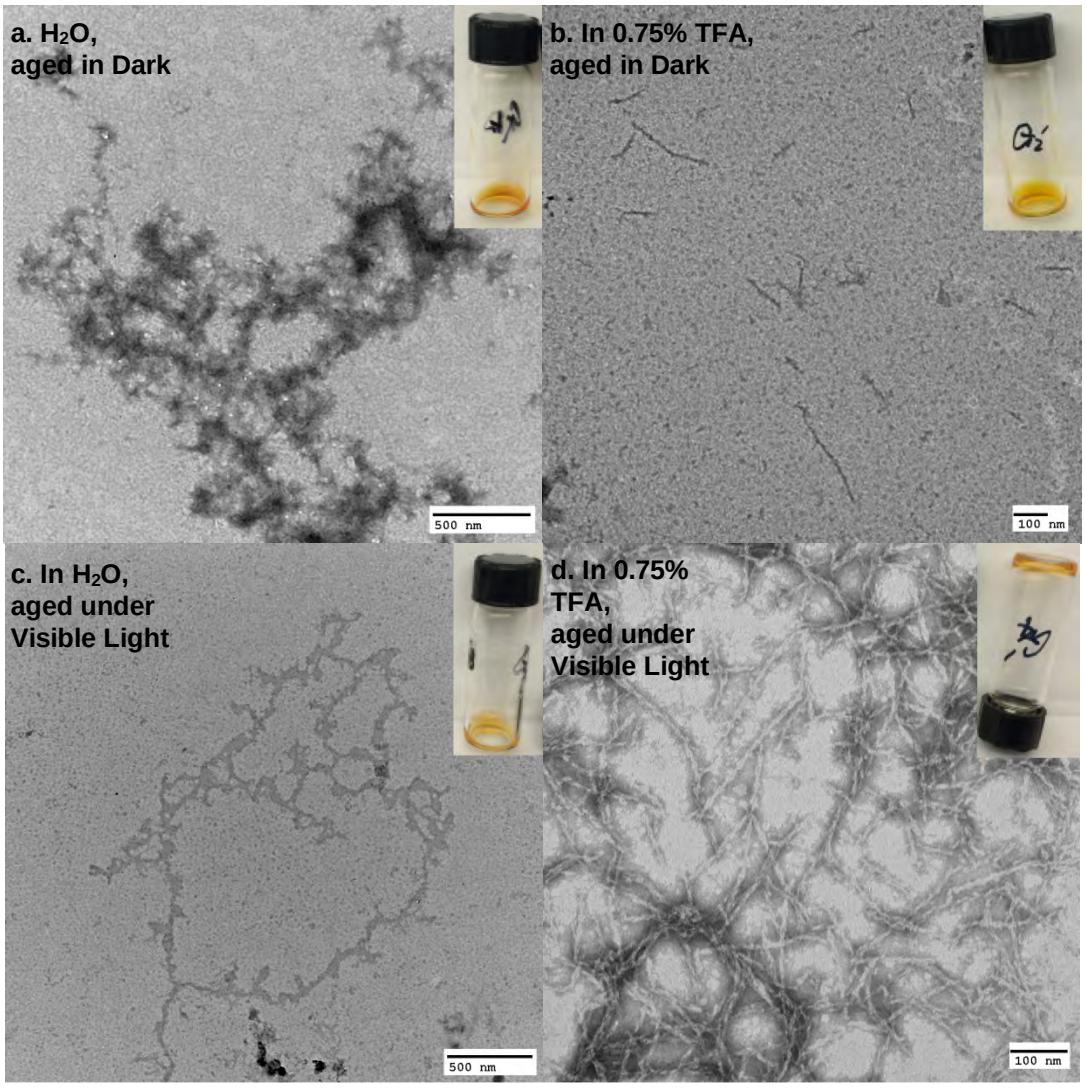

Figure 2-4. TEM images of solution a, b, c and d. All solutions were prepared at 10 mM concentration and aged under corresponding condition for 3 days and freshly diluted to 0.5 mM for microscopy

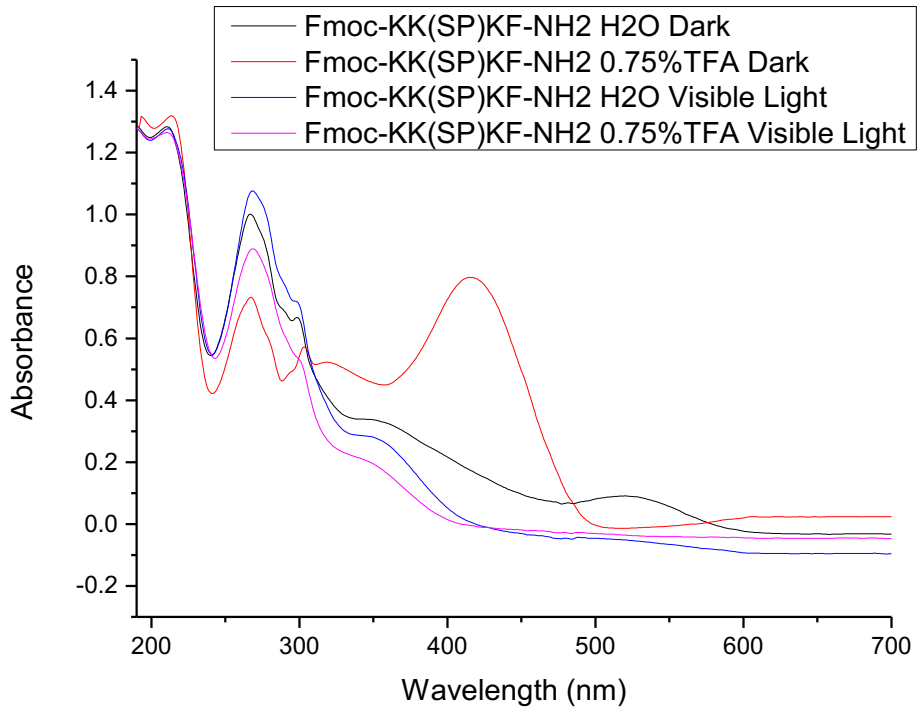

Figure 2-5 The UV-vis absorption of tetrapeptides Fmoc-KK(SP)KF-NH_2 solution a~d.

a. in H_2O in dark

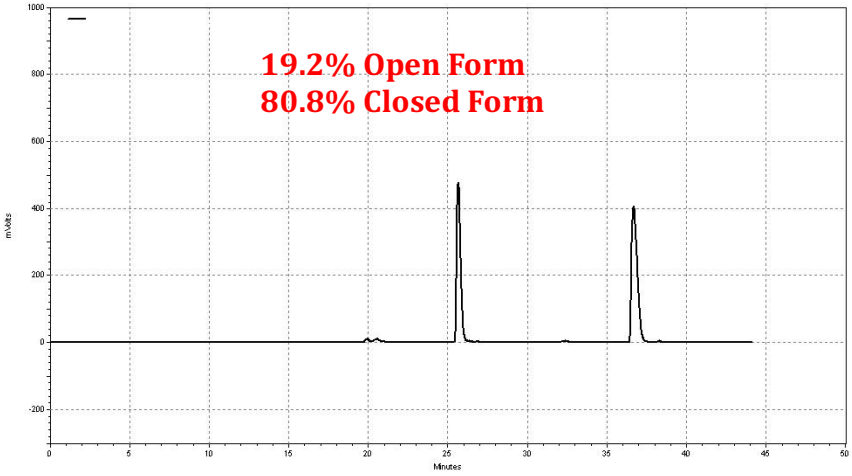

b. in 0.75% TFA in dark

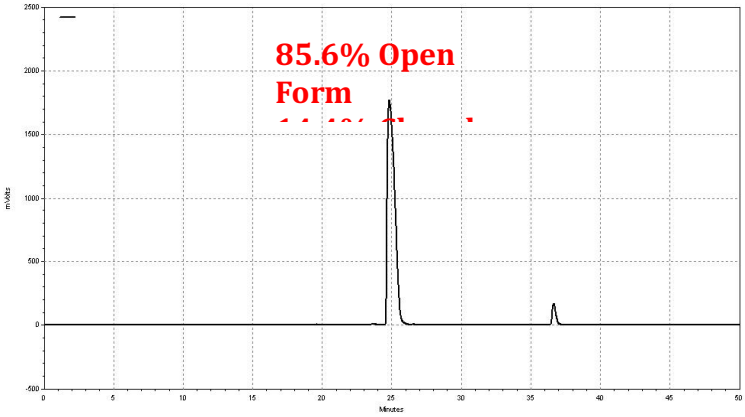

c. in H_2O under visible light

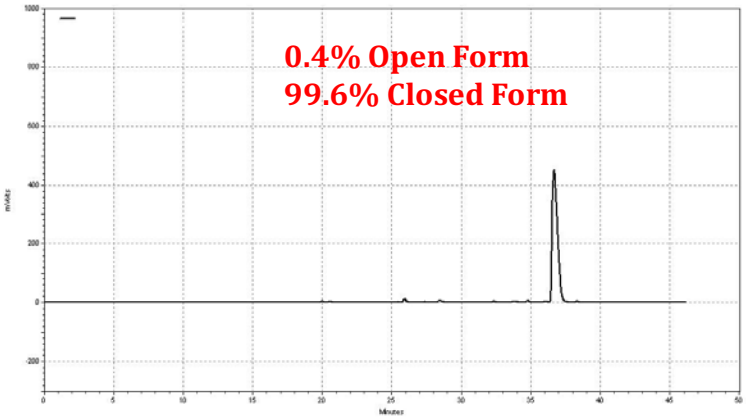

d. in 0.75% TFA under visible light

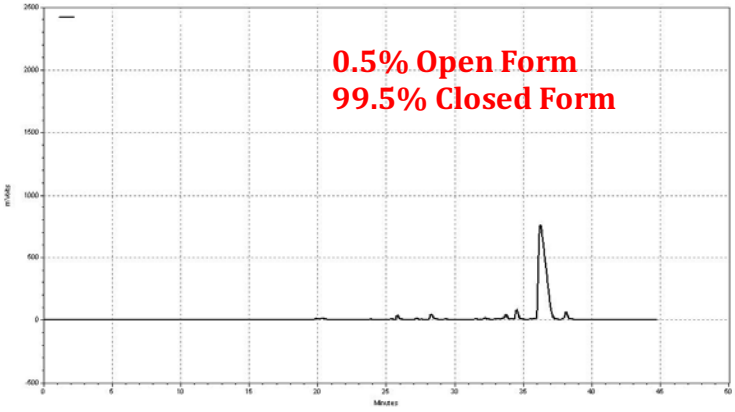

Figure 2-6. The corresponding analytical HPLC ratio of Fmoc-KK(SP)KF-NH2 for UV and CD study: a. in H_2O in dark (19.2% Open from, 80.8% Closed form), b. in 0.75% TFA in dark (85.6% Open form, 14.4% Closed form), c. in H_2O under visible light (0.4% Open form, 99.6% Closed form), d. in 0.75% TFA under visible light (0.5% Open form, 99.5% Closed form).

CD spectra. The corresponding CD spectra of a~d four solutions have also been tested. For both aqueous solutions (a,c black and blue lines), there was no distinct CD signal corresponding to the amorphous aggregates observed by TEM imaging. For the solution in 0.75% TFA in dark after thermal opening to the MC form (soln. b, red line), there was similarly no CD signals, corresponding to the non-gelled state showing no assembly by TEM (Fig. 2-4b.). For the sample in 0.75% of TFA under visible light (solution d), the CD spectra exhibied two distinct negative absorbance

bands, around 220 nm and around 280 nm, which correspond to the overlap of UV absorptions of both the Fmoc and SP chromophores.

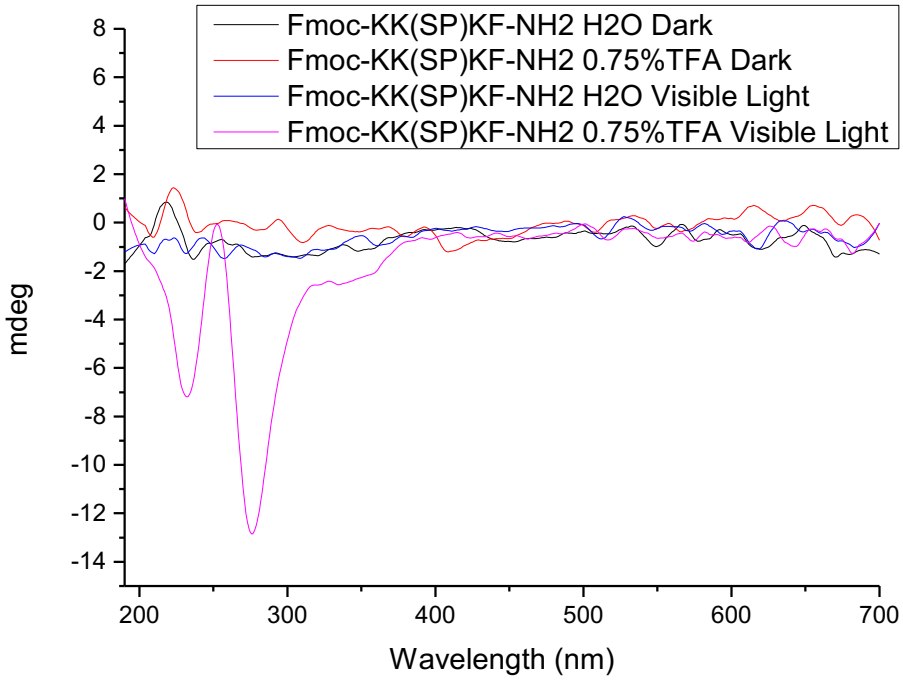

Figure 2-7. CD spectra of tetrapeptides Fmoc-KK(SP)KF-NH_2 solution a~d.

Quantification of the SP-MC interconversion thermally and via visible light by HPLC

The structural change of spiropyran can also be investigated by analytical HPLC since different closed and open forms of spiropyran are chromatographically distinct. The polar, merocyanine form exhibits a shorter retention time in reverse phase hplc compared with the closed spiropyran form.

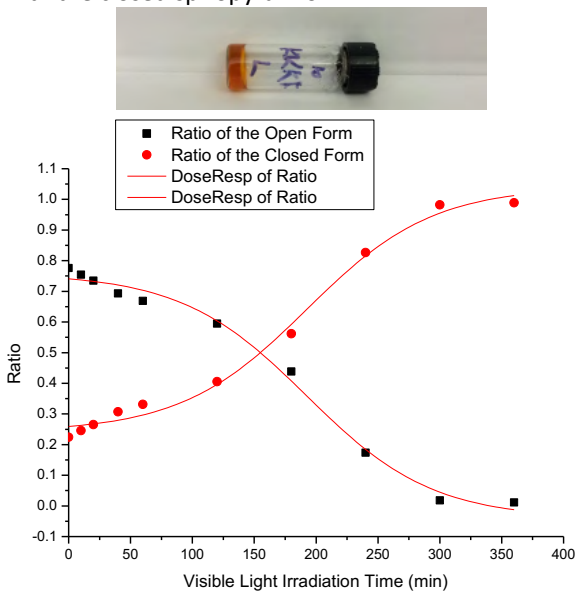

Figure 2-8. Ratio change of the open and the closed forms of 10 mM spiropyran tetrapeptides solution in 1% TFA under visible light irradiation. Solution b is the starting solution (time = 0)

The existence of closed form of spiropyran and the two different open form of spiropyran can be observed by analytical HPLC. From HPLC absorption, at time 0, solution b has 77.6% of open spiropyran form. After visible light irradiation, a new peak with a larger retention time appeared in the HPLC study increased drastically. With longer time irradiation, the open form peaks decreased as the closed form peak increased. After 6 h irradiation, the closed form ratio reaches 98.9% and the open form decreased to 1.10% (Fig. 2-8). The change in analytical HPLC study with visible light irradiation further confirmed the structural change from open protonated merocyanine form to the closed spiropyran form. Gelation also occurred after 3 days irradiation under visible light. The thermal process has also been investigated under UV=254 nm irradiation after the solution formed gel, but these conditions did not efficiently convert the SP form to the MC form, compared with the thermal conditions (Fig. 2-9).

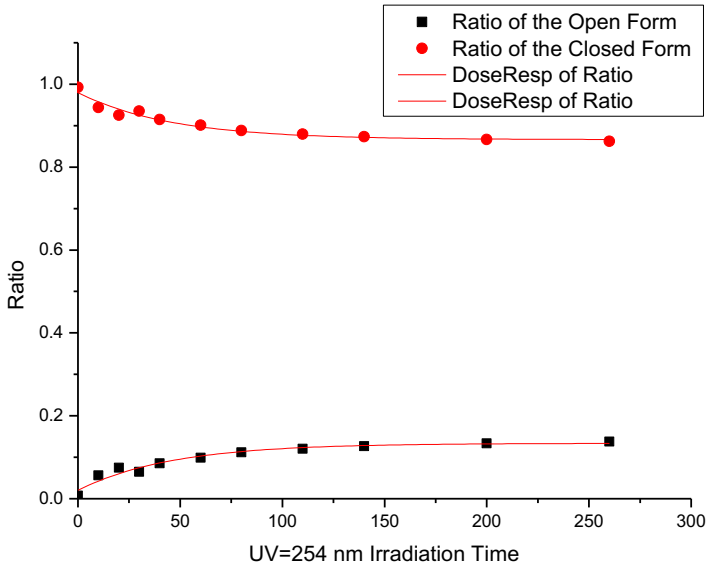

Figure 2-9. Ratio change of the open and the closed forms of 10 mM spiropyran tetrapeptides solution in 1% TFA under UV=254 nm irradiation.

After 3 days aging under visible light, gelation was observed havng the SP/MC ratio (96.0% closed) created upon visible light exposure. Although UV irradiation at 254 nm was not efficient, producing ~ 40% MC form, this was sufficient to dissipate the hydrogel gel into solution.

Thermal conversion of SP to MC form. Fresh 10 mM Fmoc-KK(SP)KF-NH_2 solution in 0.75% TFA was prepared and aged under visible light for 3 days at 20°C resulting in gelation. Then the solution was heated to different temperature by oil bath and for one hour in dark, and then the ratio was studied by analytical HPLC. As temperature increased to 60°C, the gel, formed by 97.6% of closed spyropyran form, changed into solution and the open form ratio increased drastically from 2.4% to 69.0 %. When heated to 85°C, the open form almost reaches 83.3%. The solution formed after heating was cooled down into 20°C and kept in dark for a week. It stayed as liquid form with no gelation occurred. When opposed under visible light for a week, the solution transitioned back into the hydrogel form as the open form converted back into the closed form. This solution-gelation conversion was repeated for 3 cycles.

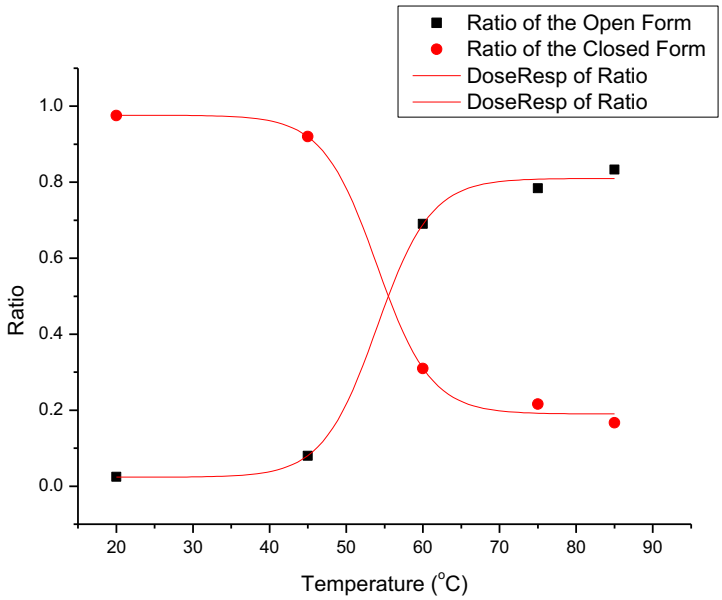

Figure 2-9. Ratio change of the open and the closed forms of 10 mM spiropyran tetrapeptides solution in 0.75% TFA at different temperature

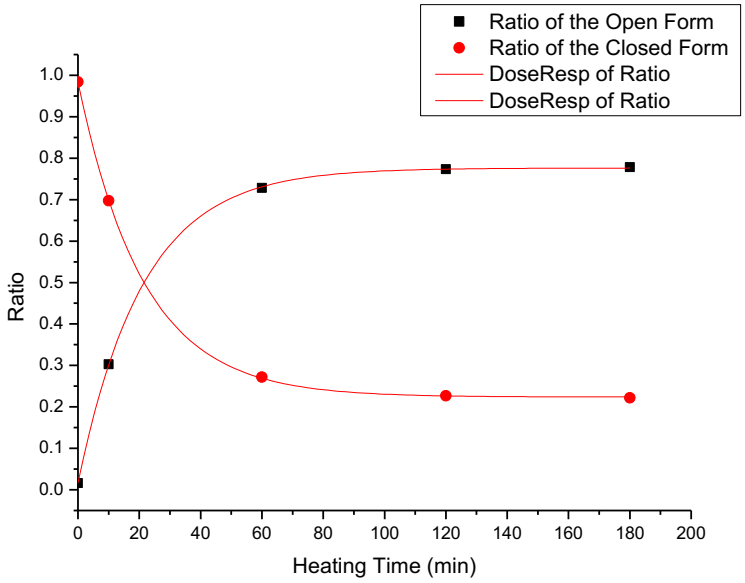

Figure 2-10. Ratio change of the open and the closed forms of 10 mM spiropyran tetrapeptides solution in 0.75% TFA heated and stays at 60°C for different time

The 10 mM Fmoc-KK(SP)KF-NH_2 solution in 0.75% TFA solution gelated in visible light was heated by 60°C oil bath in dark and the ratio was tested after different time. The ratio of the open form increased immediately from 1.60% to 72.8 % as the temperature increased during the one hour in the 60°C oil bath and stayed stably over 70% after 3 hours. The solution also formed during the process. This indicates that the ratio of the open and the closed form are rather stable after stay in oil bath for 1 hour. And the thermo-controlled closed to open form conversion is a rather quick process and is almost completed in one hour.

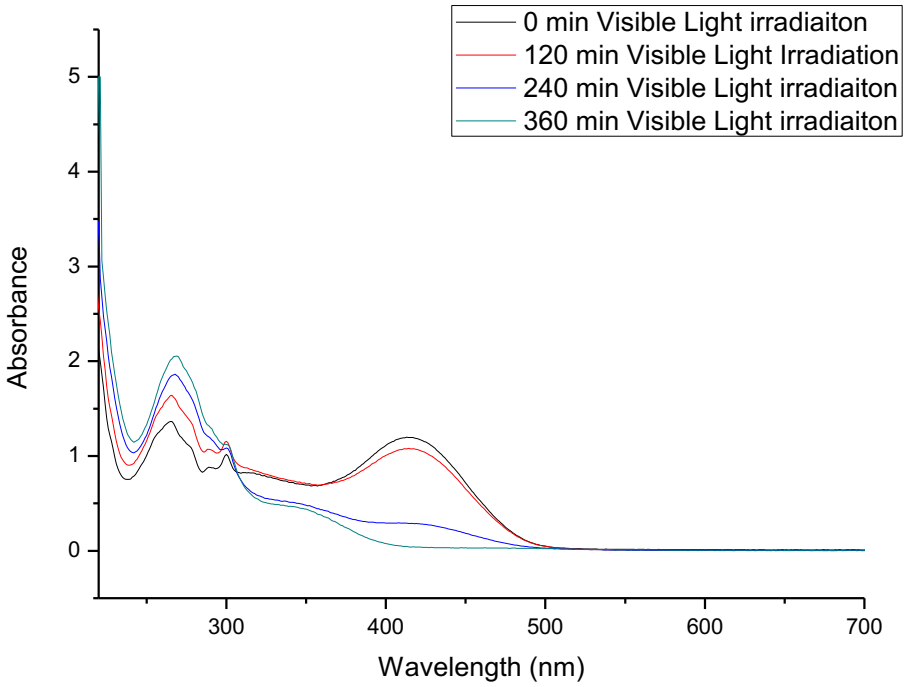

Fig. 2-10b UV of 1mM Fmoc-KK(SP)KF-NH_2 in 0.75% TFA Under Visible Light Irradiation

Driving Forces for self-assembly. Fourier-transform infrared (FT-IR) studies were conducted to investigate the secondary structure of spiropyran tetrapeptide conjugates in self-assembly. Two solutions were prepared in 0.75% TFA aqueous solution (10 mM) and aged for a week under visible light to form the gel and kept in dark, respectively, then lyophilized into solid states and dissolved in D_2O and lyophilized immediately to remove solvent. After repeating this process three times, TFA and solvent was removed. Then, the solids were dissolved in D_2O to prevent the overlap of strong around bending vibrational band of H_2O around 1600-1700 cm^{-1} region. Another solution was prepared by dissolve the spiropyran tetrapeptides in TFE.

(a) ~88% β-sheet
~12% Random Coil

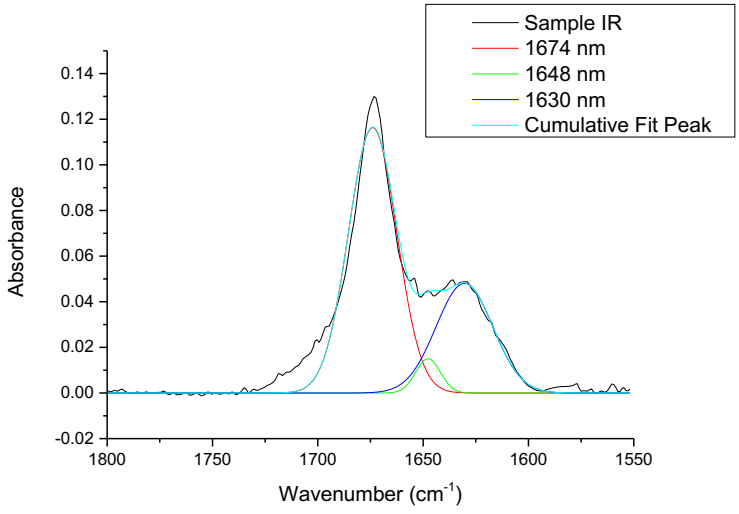

(b) Ca. 100% Random Coil

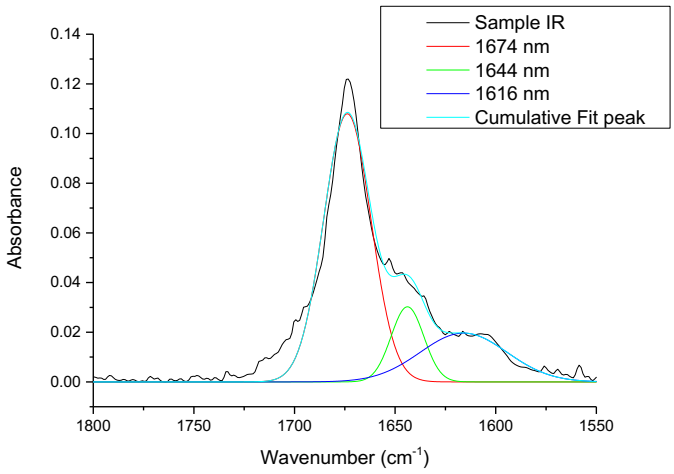

Figure 2-11. FT-IR spectra of tetrapeptides Fmoc-KK(SP)KF-NH_2 the closed and the open form in 0.75% TFA. (a) Gel solution under visible light (the closed form), (b) solution in dark (the open form)

From both Fig. 11.(a) and (b), both the major peaks appeared at 1674 cm^{-1} are referred to the C=O stretch absorption band of the amide group of spiropyran. The place of the amide I band vibrations arising from C=O stretch of amide group is a signature for different secondary structures in poly-peptides and proteins. For the gel solution under visible light formed by the closed spiropyran forms, a distinct peak at 1630 cm^{-1} indicates a β-sheet secondary structure, which is around 1620 -1640 cm^{-1} for amide I band. After deconvolution, a small peak around 1648 cm^{-1}, which is in the range of the nonordered region from 1640 -1650 $cm^{-1.}$ However, the major secondary structure for the closed spiropyran form assembly is β-sheet with a much stronger absorption band that takes up 88%. For solution in dark formed by the open merocyanine form, a non-ordered structure band around 1644 cm^{-1} is much stronger and no significant β-sheet band was observed, consistent with the CD spectra, indicating a dominate random coil secondary structure.

Rheology Study of gels. The Rheology Study has been conducted to investigate the physical property of gel formed by Fmoc-KK(SP)KF-NH_2. A 10 mM Fmoc-KK(SP)KF-NH_2 solution was prepared with 0.75% TFA added, the same solution was divided into tree part for gel formation. The rheology of gel three samples have been tested after 1 week, 2 weeks and 3 weeks respectively.

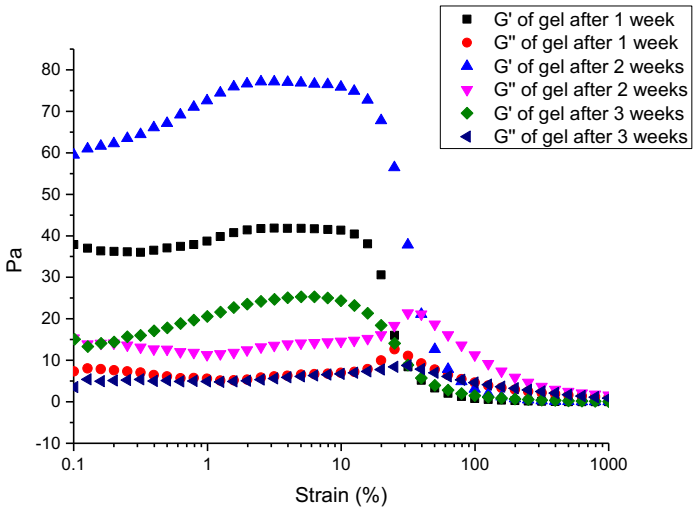

Fig. 2-12 Oscillatory stress sweep of hydrogel at 10 mM (0.75% TFA) over time.

The time dependence rheology of gel formed by Fmoc-KK(SP)KF-NH2 in 0.75% TFA has been studied. A strain dynamic sweep is shown in Fig. 2-12. The gel sample has the highest storage modulus and loss modulus after the second week. The storage modulus was around 75 Pa and rather steady before 10% of strain, showing a good tolerance to external forces. The loss modulus was around 15 Pa, much smaller than the storage modulus, indicates a rather viscoelastic property. Then, the storage modulus decreases drastically until smaller than loss modulus as the strain increases, which is the evidence of gel breaks down into liquid-like property. After 3 weeks, the storage modulus drops to around 20 Pa, which indicates a loss of viscoelastic property. During all three weeks, the gel samples broke down around a similar strain, which shows a strong property over strain tolerance. The closed SP form ratio remains similarly high, which is from 99.1~99.3%, but clearly small impurity peaks became higher after 3 weeks.

a. Corresponding HPLC ratio of gel after 1 week

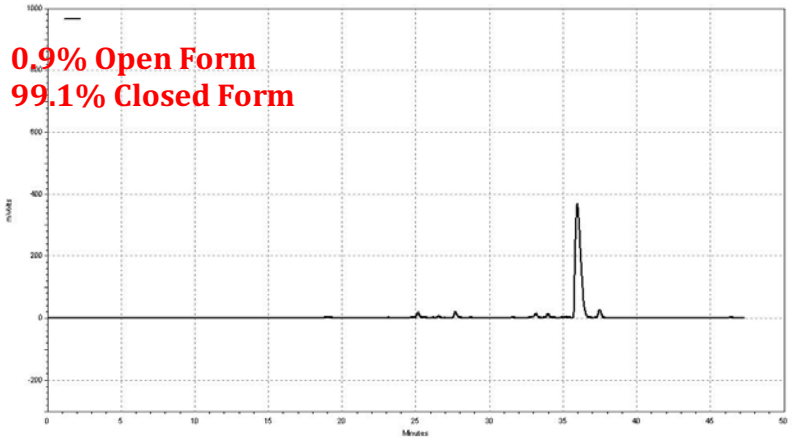

b. Corresponding HPLC ratio of gel after 2 weeks

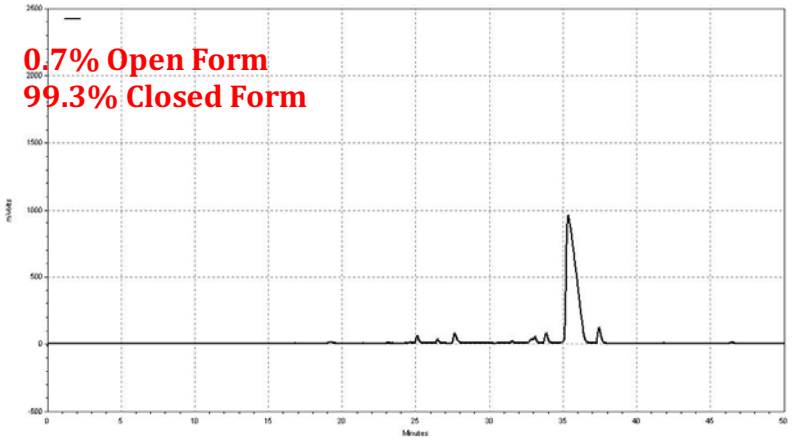

Fig 2-13. Corresponding HPLC ratio of gel: a. after 1 week, b. after 2 weeks.

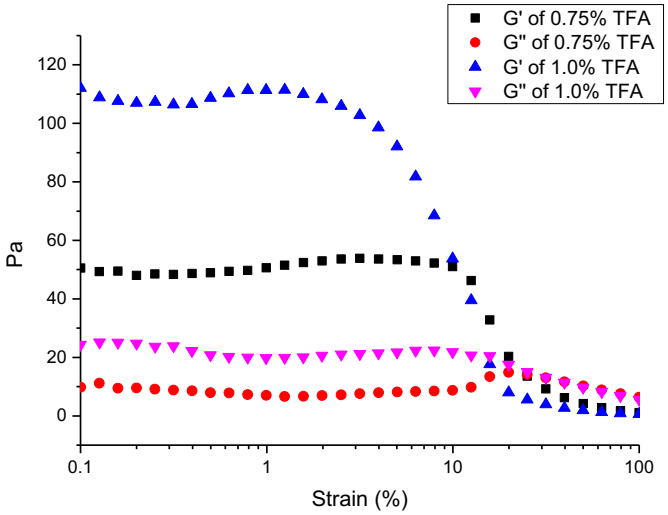

Fig. 2-14. Rheology of gel samples formed by 10 mM Fmoc-KK(SP)KF-NH_2 in 0.75% and 1.0% TFA

The influence of TFA concentration has also been studied, three 10 mM Fmoc-KK(SP)KF-NH_2 under 0.75%, 1.0% and 1.5% TFA concentration solutions were prepared. The sample under 1.5% TFA precipitated out and failed to form gel. Sample in 1.0% and 0.75% TFA formed gel successfully after two days' aging. The rheology of them have been tested after 1 week aging (Fig. 2-14). The sample in 1% TFA shows a better viscoelasticity than the sample in 0.75% TFA with a storage modulus of 110 Pa, but less tolerant to the external force as it started to break down under a much smaller strain of 2% strain.

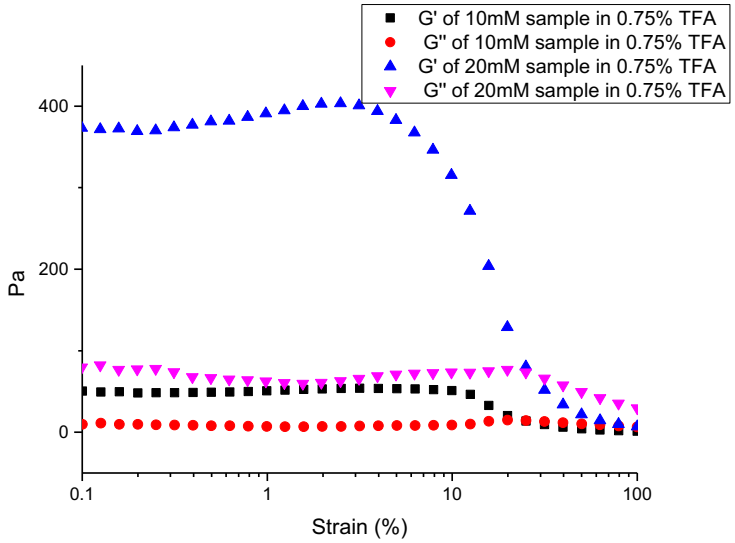

Fig. 2-15. Rheology of gel samples formed by 10 mM and 20 mM Fmoc-KK(SP)KF-NH_2 in 0.75% TFA

The influence of sample concentration has also been investigated. 10 mM and 20 mM samples under 0.75% TFA have been prepared and aged for a week. The rheology of samples have been tested. The 20 mM sample showed a much stronger viscoelasticity with a storage modulus of around 380 Pa and a similar tolerance of % strain (Fig. 2-15). It also takes much longer to form a gel since is more concentrated, which takes longer to be converted by visible light and forms a stronger gel with more fiber networks under higher concentration.

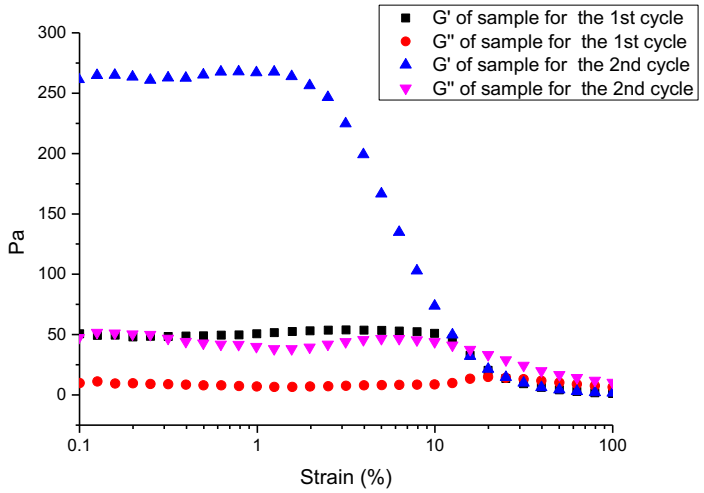

Fig. 2-16. Rheology of 10 mM Fmoc-KK(SP)KF-NH_2 sample gel in 0.75% TFA for 1st and 2nd heating cycle

The property of gel after annealing process has also been tested. The gel has been heated to 60°C for an hour and it turns into dark liquid solution as a large part of spiropyran opens. Then the solution was cooled down and aged for another week to form gel for the second cycle. The rheology of the second cycle gel was tested after one week of the heating up process. In Fig. 2-16, the second cycle gel was even more viscoelastic than the first cycle gel, with a significantly higher storage modulus of 260 Pa, the lost modulus has also increased to around 50 Pa. This increased viscoelasticity showed a rather good recovery of physical properties of gel and indicates that the changing process is reversible. The reason for this change remains unclear. One hypothesis is that the heating process did not break down the gel fibers completely, short fibers still remain in the solution. So after cooling down and aging, a further branched gel fiber network was formed with an even firmer gel.

Photoresponsive Nanotube Assembly and Gelation of a Bis-Spiropyran Pentapeptide

In order to promote an antiparallel packing interaction within the β-sheet peptide motif, we constructed peptides containing two SP/MC chromophores. Our previous work found that alanine-rich, 16-mer peptides, containing two appended dendrons and two lysine residues, underwent β-sheet assembly into well-defined nanotubes or nanofibers, depending on pH or salt concentration. In this design, the spacing of the dendritic substituents positioned the dendrons to pack cofacially along the long axis of the antiparallel β-sheet structure, thereby stabilizing the assemblies. Incorporating two spiropyran chromophores on one face of the peptide and charged lysine residues on the other face generally mimics the amphiphilicity and dendron positioning of the peptide-dendron sequences. In this design, two, SP-MC chromphores will be appended to lysine side-chains using standard solid-phase peptide synthesis. The SP-MC chromophores were separated by a three residue sequence (Lys-Phe-Lys) to reduce the potential for *intra*molecular association. *Inter*molecular packing within the antiparallel β-sheet nanostructure would induce pairwise packing of the SP-MC chromophores.

Preliminary Results. A pentapeptide sequence, shown below, was prepared using a solid-phase, Fmoc peptide synthesis strategy. The conversion between closed spiropyran form and the open merocyanine form of the peptide could be observed by ultraviolet spectroscopy (Fig. 1). The spiropyran, merocyanine and protonated merocyanine have distinct absorption bands in UV-Vis spectra. In the figure shown below, a freshly prepared sample of the pentapeptide in 30 %CH_3CN/H_2O (0.75% TFA), after heating to 55°C for 1 h, then cooling and kept in dark, displayed a progressively increasing peak at 425 nm, indicating a predominantly open, protonated MC form was produced under these conditions (Fig. 1). Upon visible light irradiation, this peak disappeared, indicating the back conversion into the closed spiropyran form. TEM imaging (10 mM 30 %CH_3CN/H_2O) indicated that the closed SP form, which forms a rigid gel, was comprised of homogenous nanotubes that formed by the progressive rolling of initially formed nanoribbons

(Fig. 1). In contrast, the open MC form, existed primarily in the monomer state, as indicated by the lack of any structures observable by TEM.

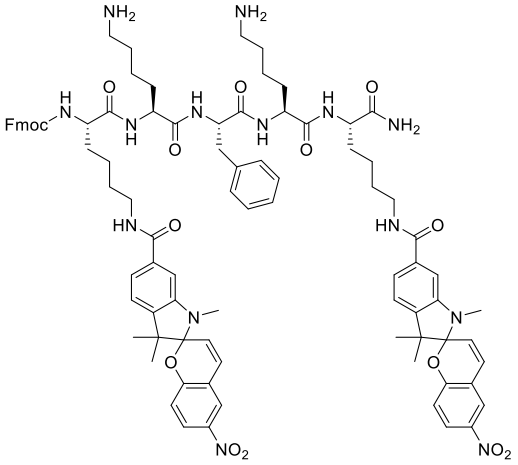

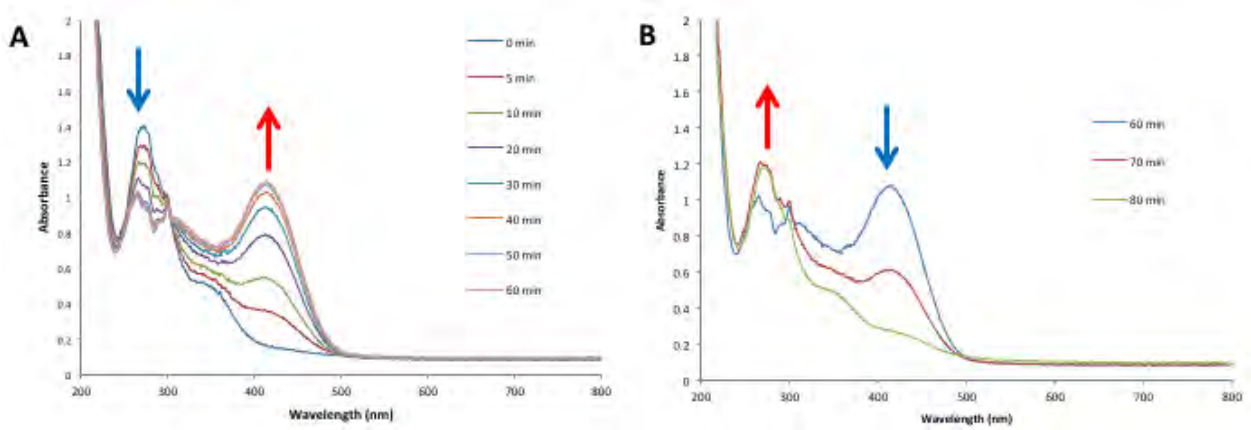

Figure A) UV-Vis of 0.35 mM sample of the bis-SP/MC pentapeptide in 30% MeCN/H_2O w/ 0.75% TFA after heating at 55°C and B) removed from the heat source and irradiated with an LED visible light source.

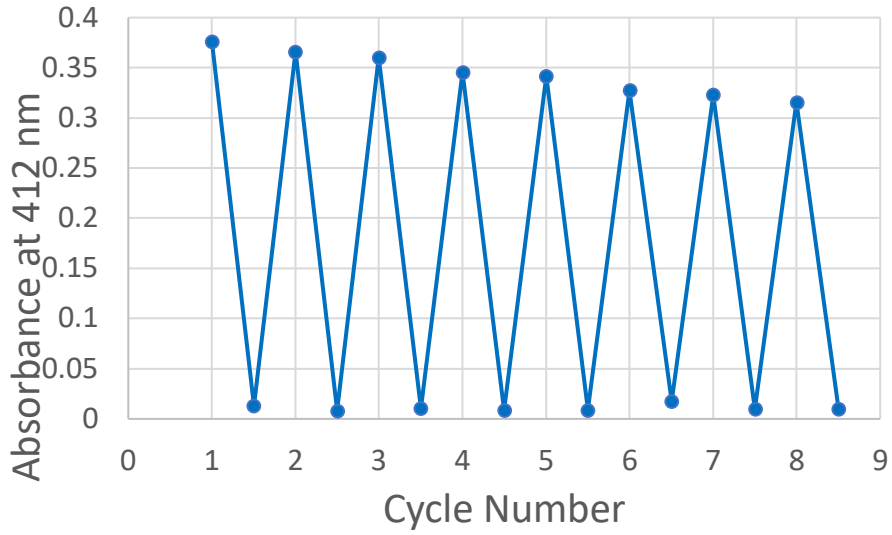

Repeated Cycling of the SP→MC interconversion is stable over 10 cycles. 1 cycle = heating at 60 °C for 30 minutes, followed by visible light for 5 minutes; Visible light: 300 LEDs 12V, 72W

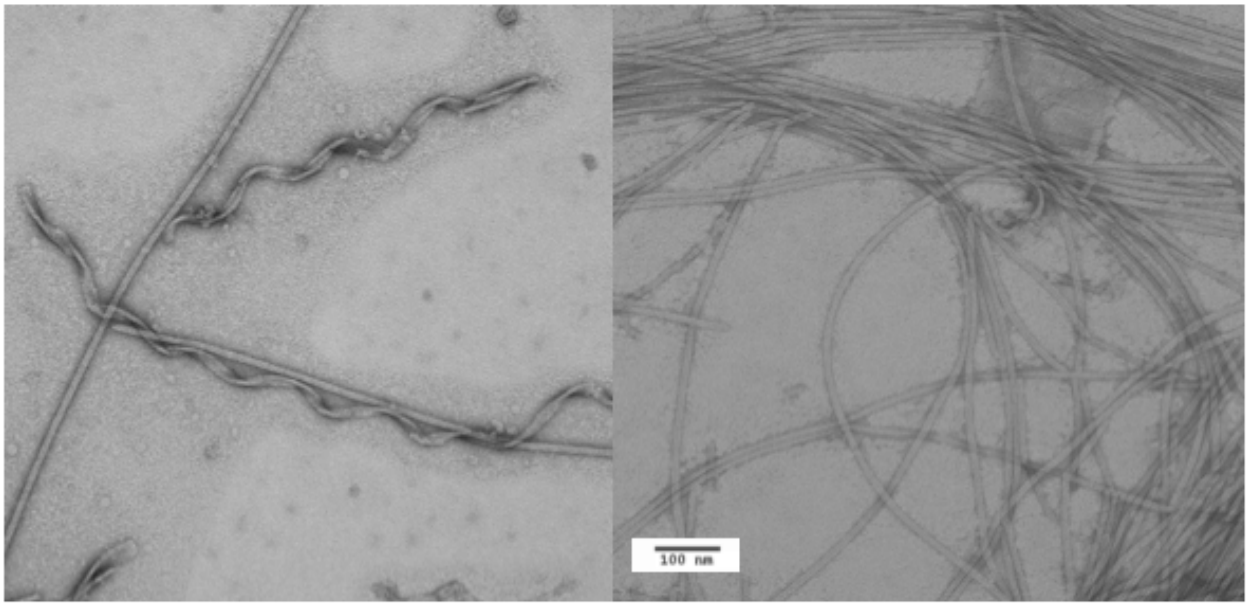

TEM image of **bis-SP/MC pentapeptide** in 30% CH_3CN/H_2O at 10 mM after irradiation with visible light, which converted MC→SP form and resulted in the formation of a gel state. The images show that in the closed SP form, the pentapeptide assembles into well-defined ribbons (left image) that progressively fold into nanotubes (right image).

The Self-Assembly of Naphthalene diimide-based amphiphiles containing bisindolylmethane.

Sinan Bayindir, Kwang So-Lee, Nurullah Saracoglu, and Jon R. Parquette

ABSTRACT: The self-assembly of naphthalene diimide-based amphiphiles containing bisindolylmethanes for metal complexation are reported. In the present work, three naphthalene diimide (NDI) amphiphiles containing bis(indolyl)methane and *L*-lysine head groups were successfully synthesized as monomers to assemble into well-defined nanotubes. In this context, their self-assembly in different solvents and at pH values led to nanostructures such as nanotubes, liposomes, and nanofibers. In addition, the Fmoc protected amphiphile underwent a transition from nanotubes to liposomes, depending on a copper-driven structural transition at pH 7.

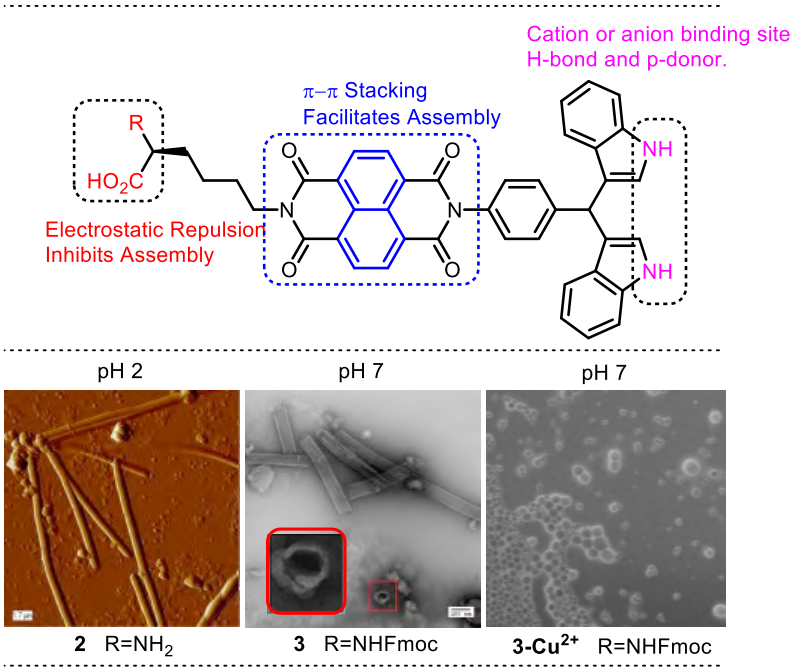

Details of Study.

Introduction. The use of peptide-based amphiphilic molecules in recent years has also attracted much interest.[4] Peptide self-assembly processes are highly sensitive towards changes in stimuli such as pH or temperature.[5] Increasing interest in ion recognition through supramolecular chemistry have seen a tremendous growth in the development of highly selective colorimetric and fluorescent chemosensors for various analytes in the last decade[6] Among these chemosensor candidates, design of specific sensors for biologically active cations such as Na^+, K^+, Ca^{2+}, Cu^{2+}, and Zn^{2+} are extremely useful and important[7] towards the study of physiology, medical diagnostics,[8] and even selective light harvesting[9] due to the modulation of optical properties in these moieties in respond to the change in the local environment. Moreover, copper (II) ion is a cofactor of various metalloenzymes and used by various metabolic processes such as gene expression and neuro-signal transductions. Therefore, detecting copper(II) has gained enormous attention. Consequently, organisms tightly regulate internal concentrations of copper. After Czarnik and co-worker reported rhodamine-B based chemosensors,[10] rhodamines,[11a] iminoquinolines,[11b] 1,8-naphtalimides,[11c] and bis(indolyl)methanes[11d] as colorimetric and ratiometric probes for detection have been studied. In this work, we have designed and synthesized new NDI amphiphiles **1**-**3** containing bis(indolyl)methane and *L*-lysine head groups. In these structures, NDI serves as a hydrophobic component to control stacking, while *L*-lysine serves as the polar head group and drives chiral amplification of the 1D self-assembly process in a polar solvent. The bis(indolyl)methane site can act as both an acidic H-bond donor and a basic π-donor. Self-assembly of the amphiphiles **1**-**3** was largely induced by balancing the repulsive electrostatic

interaction created by polar ammonium functional groups with the attractive interactions; hydrogen bonding interaction from the *L*-lysine backbone and hydrophobic π-π interactions induced by the adjacent NDI chromophore.

RESULTS AND DISCUSSIONS

Synthesis of NDI-Based Amphiphiles. The synthetic strategy of the NDI-based amphiphiles is shown in Scheme 1 and 2. Bis(indolyl)methane **6** was synthesized through $Bi(NO_3)_3{\cdot}5H_2O$-catalyzed electrophilic substitution reaction of indole (**4**) and 4-nitrobenzaldehyde (**5**). Compound **6** was reduced to produce 4-(di(1*H*-indol-3-yl)methyl)aniline (**7**) using sodium borohydride/nickel acetate in methanol or by catalytic hydrogenation over the Pd/C catalyst in 98% and 93% yields, respectively (Scheme 1). The target compound **1** was obtained through two different pathways (Scheme 2). The first includes the reaction of NDI **9** with both N^{α}-Boc-*L*-lysine to yield monoimidation product **8**, which was converted to the desired compound **1** using bis(indolyl)methane **6** in DMF at 100 °C. An alternative strategy begins with primarily imidation between NDI and the key compound **6** in DMF to produce **10**. Compound **1** was obtained through a reaction between **10** and N^{α}-Boc-*L*-lysine (**11**) in DMF. The Boc deprotection of **1** was carried out with triethylsilane and trifluoroacetic acid (Et_3SiH-TFA) in dichloromethane to give another amphiphile **2** in 85% yield (Scheme 2). With imides **1**-**2** in hand, we turned our attention to the synthesis of amphiphilic N^{α}-Fmoc-*L*-lysine-NDI-3,3'-bis(indolyl)methane **3**. Upon exposure to TFA in CH_2Cl_2 at room temperature, the Boc group in (N^{2}-Fmoc)-(N^{6}-Boc)-*L*-lysine (**12**) was deprotected to give N^{α}-Fmoc-*L*-lysine (**13**), which was then coupled by **10** in DMF at 100°C to produce the amphiphile **3** (Scheme 2).

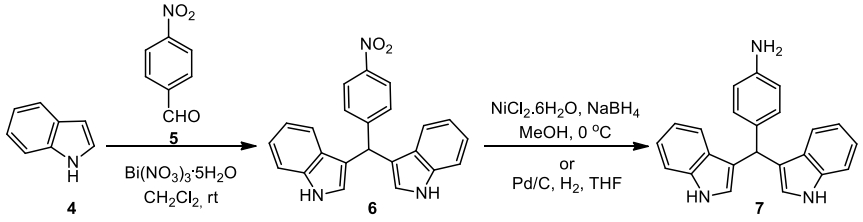

Scheme 1

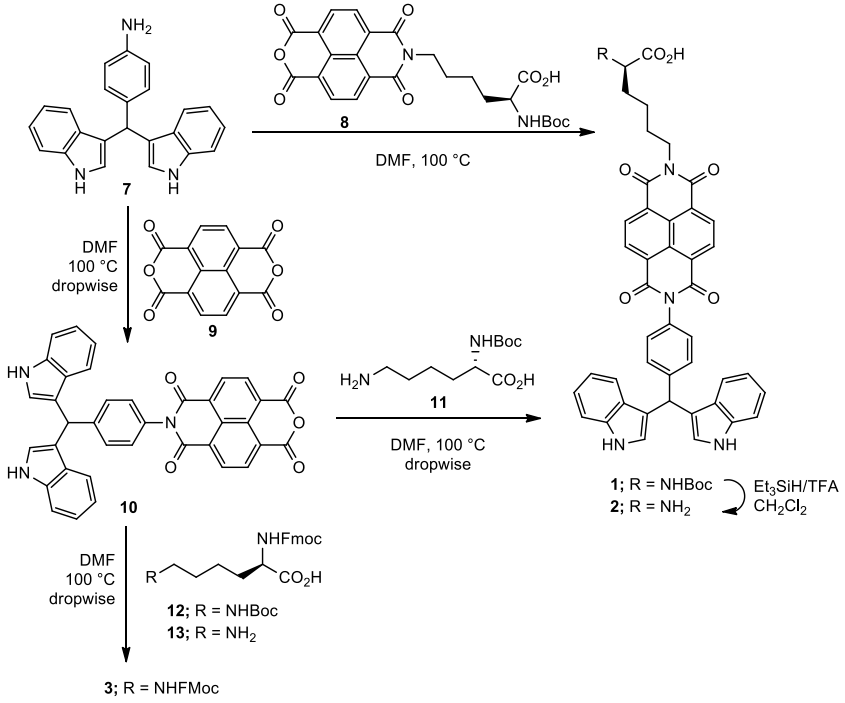

Scheme 2

Spectral Studies and Sensing Ability of Amphiphiles. We initially performed ultraviolet-visible (UV-Vis) and circular dichroism (CD) experiments at different pH conditions and solvents systems such as TFE, TFE-H_2O, MeOH, MeOH-H_2O, MeCN-H_2O etc. UV-vis studies of amphiphile **2** in different pH conditions (pH 2, 7 and 11) caused a max red-shift in MeCN-H_2O at pH 2. The changes in electronic properties of **2** can also be probed by UV-vis spectroscopy whereby the UV-vis spectra of **2** (1×10^{-4} M) showed absorbance band of NDI chromophore at 232 nm (Band II) and 358/379 nm (Band I) at natural conditions (Figure 2A, black line). Upon addition of TFA (%10) to **2** in MeCN-H_2O, the corresponding absorbance band of NDI undergoes a bathochromic shift to 283 nm (Band II) and the absorption band at 360/381 nm (Band I), which correspond to *J*-aggregate of the NDI chromophore (Figure 2A, red line). Likewise, the CD studies of amphiphile **2** were conducted at different pHs (pH 2, 7 and 11). The formation of the amorphous aggregates at pH 2 and 7 in MeCN-H_2O, was accompanied by broad, red-shifted peaks. However, circular dichroism (CD) spectra at pH 2 and 7 are characteristically different when compared to those obtained at pH 11 in MeCN-H_2O. Particularly, the CD spectrum of **2** in MeCN-H_2O showed cotton affects between 300 and 400 nm due to a band I of the NDI chromophore and corresponding to NDI (Band II) transitions, respectively (Figure 2B).

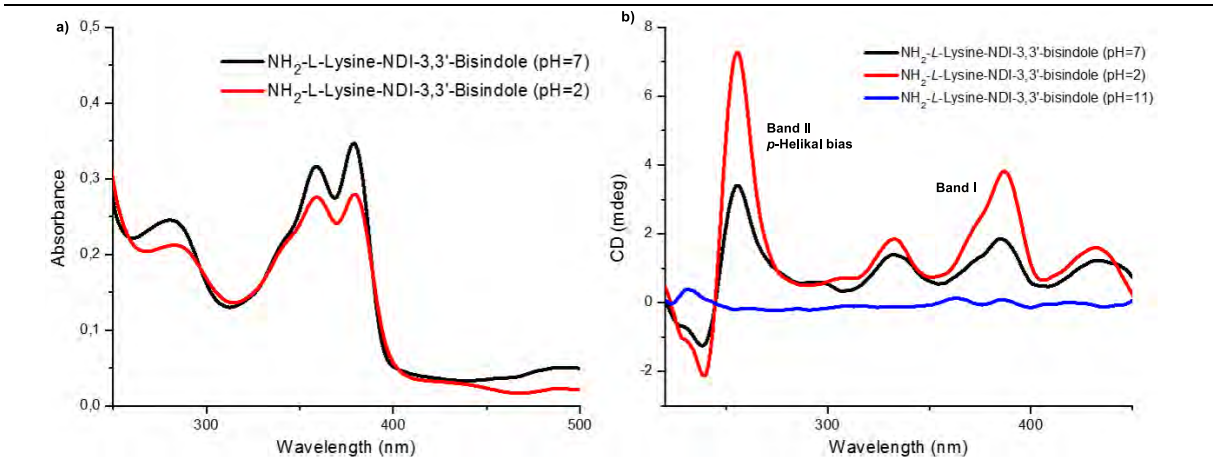

Figure 2. A) UV-vis and B) CD spectra of (NH_2-*L*-lysine)-NDI-3,3'-bis(indolyl)methane **2** in MeCN/H_2O (v/v, 1:1) at pH 7 and 2.

The UV-Vis and CD spectra of Fmoc-protected amphiphile **3** in MeCN-H_2O (v/v; 1/1) at pH 2, 7 and 11 are shown in Figure 3A and B, respectively. The UV-Vis spectra of **3** in MeCN-H_2O (v/v; 1/1) at pH 2 similarly exhibit to the red-shifts (Figure 3A). To probe the change in electronic properties of **3**, TFA (%10) was added to a solution of **3** in MeCN-H_2O. The UV-Vis absorption spectrum of the amphiphile **3** exhibits two peaks with a maximum at 284 nm (Band II) corresponds to NDI chromophore and second absorption bands appearing at 359/380 nm (Band I) which are attributed to *J*-aggregate of the NDI chromophore (Figure 3A, red line), along with a new peak at 506 nm, which is resulted from the addition of TFA (%10). However, CD spectra of **3** at pH 2 is characteristically different from pH 7 in MeCN-H_2O (Figure 3B). While the CD spectrum of **3** at pH 7 revealed maximum at 211 nm (Band II)/345 nm (Band I) and minimum at 237 nm (Band II)/384 nm (Band I) with a crossover at 220 nm (Band II)/358 nm (Band I) indicating a turn-like conformation, CD spectrum at pH 2 conditions revealed maximum at 232 nm (Band II)/351 nm (Band I) and minimum at 211 nm (Band II)/386 nm (Band I) with a crossover at 211 nm (Band II)/366 nm (Band I) indicating a turn-like conformation. As a result of these studies, we commented that while the Y-polarized (Band II) region exhibit M-helical tendency at acidic (pH 2) conditions, Z-polarized (Band II) region exhibit a *p*-helical tendency in both acidic (pH 2) and basic (pH 11) conditions (Figure 3B).

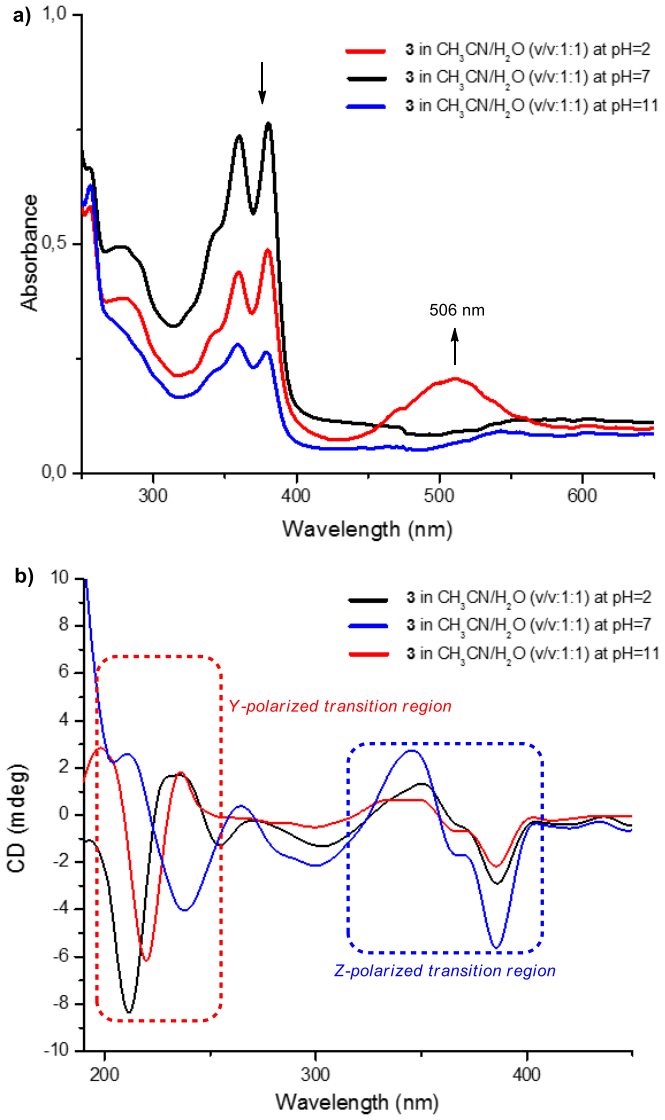

Figure 3. A) UV-vis and B) CD spectra of *N*$^{\alpha}$-Fmoc-*L*-lysine-NDI-3,3'- bis(indolyl)methane **3** in MeCN-H_2O (v/v, 1:1) at pH 2, 7, and 11.

The metal ion binding ability of **3** in MeCN-H_2O was studied by UV-Vis spectroscopy. The binding studies of **3** with various metal ions such as Cr^{2+}, Co^{2+}, Cd^{2+}, Mg^{2+}, Sn^{2+}, Fe^{2+}, Cu^{2+}, Hg^{2+}, Mn^{2+}, Zn^{2+} (in the form of chloride salts) showed that it exhibits a high binding affinity for Cu^{2+} with a distinct color change from pale yellow to red suggesting a red-shift. The interaction of **3** with the addition of Cu^{2+} resulted in a color change visible to the naked eye (Figure S1), and this phenomenon is also monitored by the UV-vis spectroscopy studies (Figure S2). Figure 4A shows that UV-Vis absorption spectra of **3** (1×10^{-4} M) exhibit absorption bands for NDI chromophore at 359 and 380 nm and absorption bands for indole chromophore at 225 and 284 nm, which are typical for a $\pi-\pi$ transition. The addition of 1 equivalent of $CuCl_2$ to **3** caused bathochromic shifts in the absorption maxima of chromophores.[14] Interestingly, stepwise addition of the equivalent of $CuCl_2$ to a solution of **3** in MeCN/H_2O (v/v, 1:1) resulted in the formation of a new absorption band at 509 nm, which can be probed by Job's plot analysis (Figure 4B and C). The Job's plot shows a 1:1 stoichiometry between **3** and Cu^{2+} in MeCN-H_2O solution (v/v, 1:1) (Figure 3B). Unfortunately, ^{1}H NMR spectroscopy of the **3**-Cu^{2+} complex in DMSO-d_6 was not informative because of resonance broadening caused by the paramagnetic nature of the Cu^{2+}.

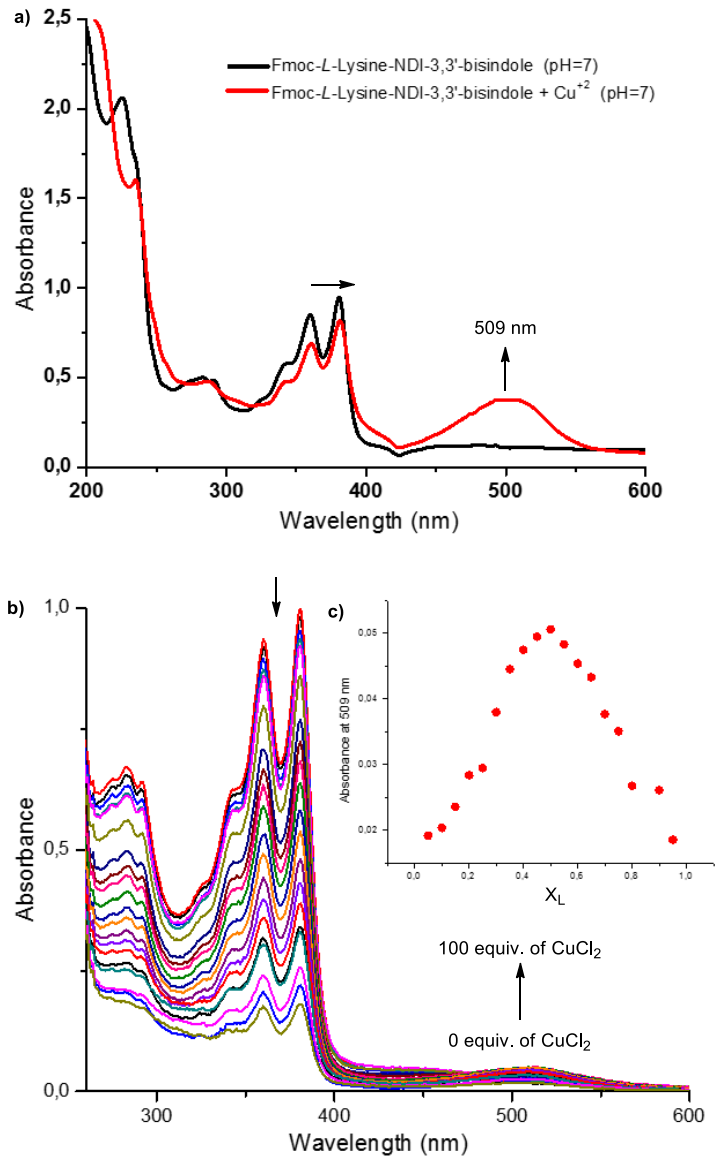

Figure 4. A) UV-vis spectrum of **3** and **3**-Cu^{2+} (1×10^{-4} M) in MeCN/H_2O (v/v, 1:1), b) UV-vis titration of **3** with Cu^{2+} in MeCN/H_2O (v/v, 1:1) and B) Job plot showing the 1:1 stoichiometry of complex **3**-Cu^{2+} in MeCN-H_2O (v/v, 1:1).

The last UV-vis and CD studies were also carried out on N^{α}-Boc-*L*-lysine-NDI-3,3′-bisindole **1**. The characteristic peaks, Band I (356-378 nm, z-polarized π-π* transitions) and Band II (232 nm, z-polarized π-π* transitions) of NDI unit, were determined with the UV-vis studies of **1** in MeCN/H_2O (v/v, 7/3) at pH 7. When the UV-vis spectrum of **1** in MeCN /H_2O solution at pH 11 is examined, the Band I (356 nm to 378 nm) peaks of the NDI unit appears to decrease in intensity and resonate at 359 and 381 nm by shifting to the red area. The red-shift that was observed is an evidence of π-π interactions in the molecule (Figure 5A). In addition to UV-vis studies of amphiphile **1**, we also performed CD studies of **1**. While the NDI unit peaks (Band II) that were being the resonance at 232 nm of amphiphile **1** was exhibiting a weak *p*-helical tendency at pH 7, it was exhibiting a strong M-helical tendency at pH 11 (Figure 5B).

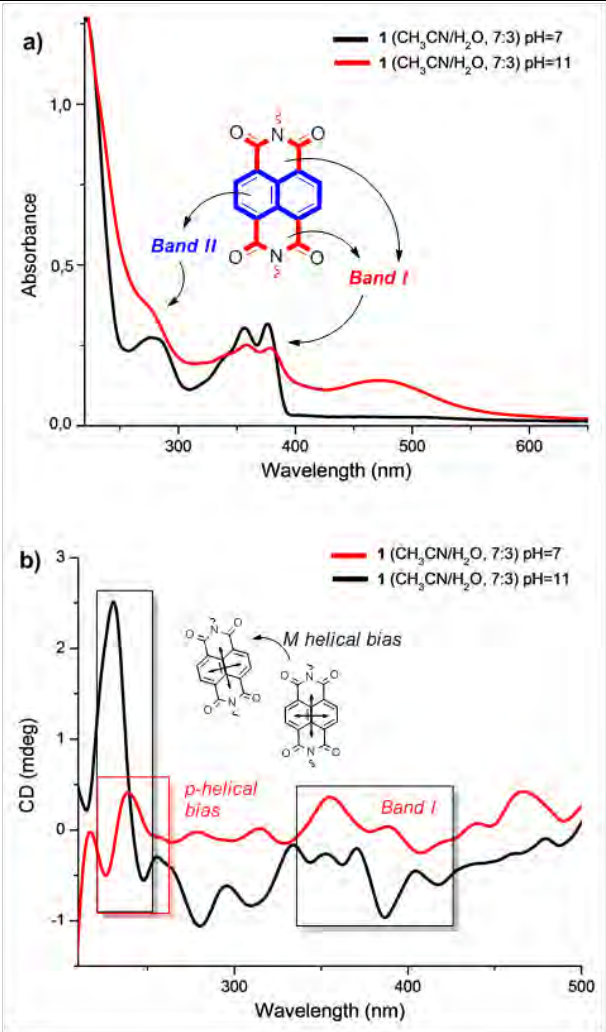

Figure 5. A) UV-vis and B) CD spectra of *N*$^{\alpha}$-Boc-*L*-lysine-NDI-3,3'-bis(indolyl)methane **1** in MeCN-H_2O (v/v, 7:3) at pH 7, and 11.

Similar to **3**, the interactions of Nᵅ-Boc-L- lysine -NDI-3,3′-bisindole **1** with various metals in different solvents at pHs were investigated. The ligand-Cu^{2+} interaction was determined by the color change visible to the naked eye in the solution. This interaction phenomenon was also monitored by UV-vis spectroscopy (Figure 6A and B). The UV-vis and CD spectra of the interaction of **1** with Cu^{2+} ions at pH 7 and 11 have indicated that π-π interactions between the NDI units of active power in the spectral behaviours and formation of nanostructures. When the UV-vis spectrum taken at pH 7 of the 1-Cu^{2+} complex was examined, it was seen that there is a red-shift of characteristic peaks from 282 nm (Band II) and 358-381 nm (Band I) to 289 nm (Band II) and 360-382 nm (Band I). Similarly, a red-shift of characteristic peaks of NDI units from 282 nm and 358-381 nm to 292 nm and 365-386 nm was observed from the UV-vis studies of 1-Cu^{2+} at pH 11 conditions. Further, a new red-shift interaction peak was also observed at 501 nm (Figure 6A). The CD spectrum of the **1**-Cu^{2+} complex has provided important knowledge on how meaningful aggregation would be. According to the information obtained from the CD spectrum, while the NDI unit peaks that were being the resonance at 289 nm of amphiphile **1** was exhibiting a weak M-helical tendency at pH 7, it was exhibiting a strong M-helical tendency at pH 11 (Figure 6B). Although significant results have been obtained from UV-vis and CD studies, the low water solubility of amphiphile **1** has made it difficult to work with 1. Therefore, the formation of nanostructures was seen to occur approximately two weeks later due to the low water solubility of amphiphilic **1**.

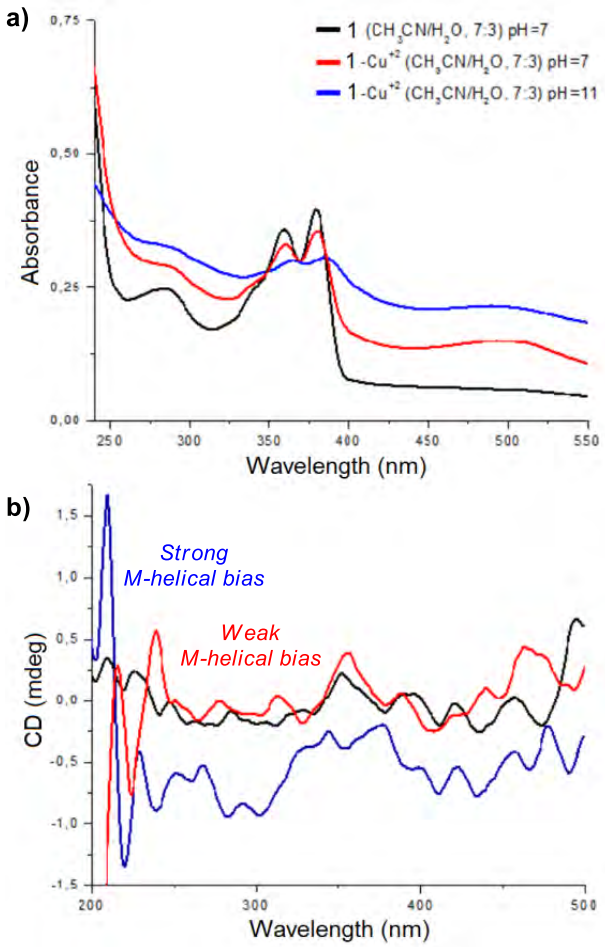

Figure 6. A) UV-vis spectrum and, B) CD spectra of *N*$^{\alpha}$-Boc-*L*-lysine-NDI-3,3'-bis(indolyl)methane **1**-Cu^{2+} (1×10^{-4} M) in MeCN-H_2O (v/v, 7:3) at pH 7, and 11.

Self-Assembly of Amphiphiles. Following UV-vis and CD experiments, the self-assembly studies of amphiphile **2** were studied in a different solvent and pH systems and nanostructures were morphologically characterized by transmission electron microscopy (TEM), scanning electron microscopy (SEM) and atomic force microscopy (AFM). The self-assembly of **2** in MeCN-H_2O at neutral pH revealed that the formation of irregular nanofiber structures, which were confirmed by TEM, SEM and AFM studies, whereas the self-assembly at pH 11 did not provide any formation of a nanostructure. Figures 7 A-D show the self-assembly studies at pH 2 afforded very uniform nanotubes with an outer diameter of 21.2 nm, an inner diameter of 4.8 nm and a thickness of 16.4 nm. On the other hand, the AFM measurement gives the thickness of 15.8 nm for this tube (Figure 7F). The AFM image is consistent with the TEM images, which show a 1-D proliferation of the nanotube assemblies (Figure 7D). The shifts in the UV-vis and CD spectra and the increases in peak intensities appeared to affect only the quality of the formed nanostructure, and have no effect on the type of the nanostructure.

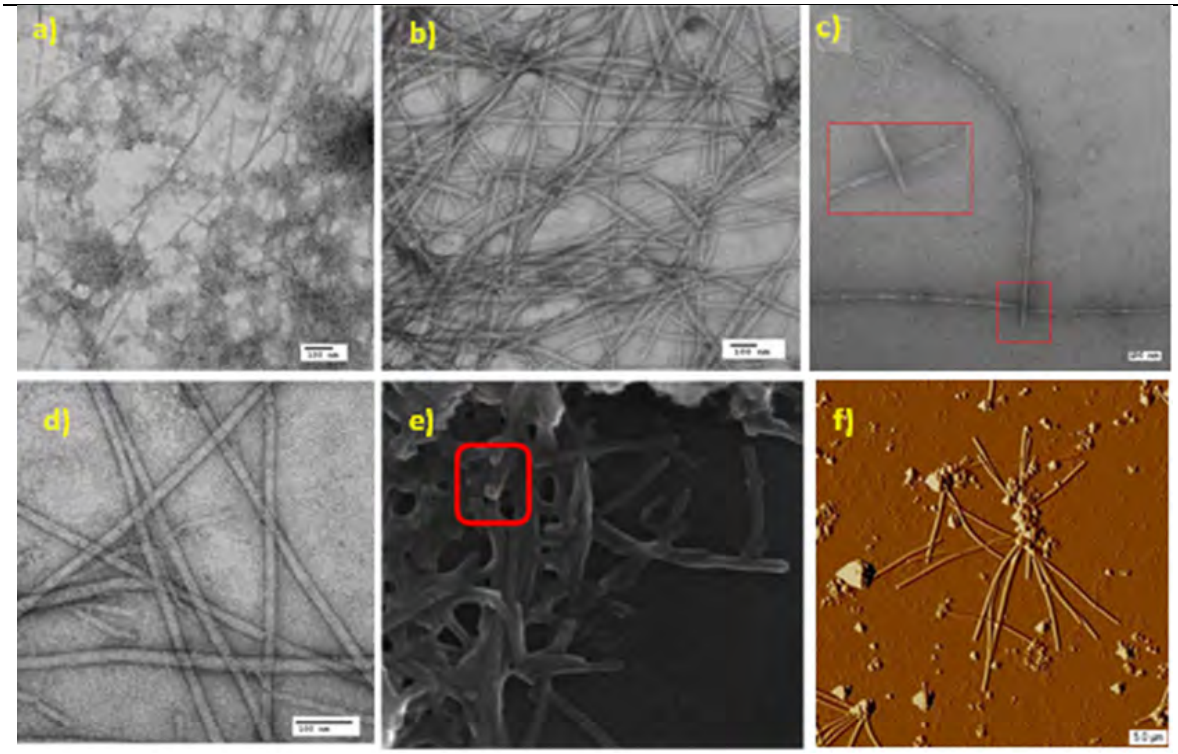

Figure 7. A) TEM (pH 7), B-D) TEM (pH 2), E) SEM (pH 2) and F) AFM (pH 2) images of **2** in MeCN-H_2O (v/v, 1.1).

While the basic conditions (pH 11) for **3** also lacked the variety of different nanostructures, the **3** under acidic conditions (pH 2) self-assembled into the irregular nanospheres (Figure 8A-C). TEM image of amphiphile **3** at neutral pH have revealed a formation of uniform nanotubes with a wide exterior diameter of 58.1 nm (Figure 8D-E). The walls of the tube were approximately 8.6 nm thick, resulting in an inner tube diameter of about 40.9 nm. Considering the wall thickness on the nanotube for **2** and **3**, the length brings to mind of the tetra-layer assembly of the amphiphilic building blocks which constructed the nanotube. SEM image of **3** indicates a very uniform and well-defined nanotube which has a dark, hollow cross-sectional view that symbolized the tubular structure whereby at the surface of the nanotubes were coated with uranyl acetate (Figure 8F). Hereby, a protruding tip of a single nanotube wedged between two intersecting nanotubes was visible in one image on the SEM further confirms the tubular morphology of the assemblies.

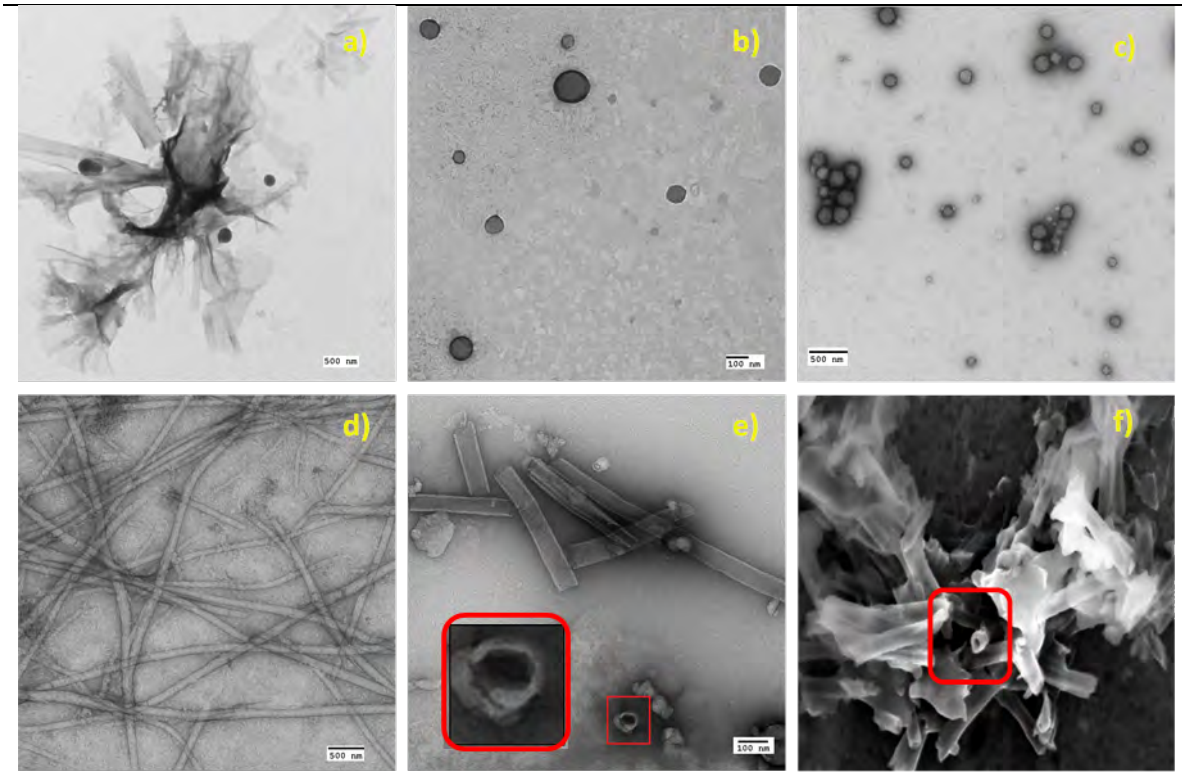

Figure 8. A) TEM (pH 11), B-C) TEM (pH 2), D-E) TEM (pH 7) and F) SEM (pH 7) images of **3** in MeCN/H_2O (v/v, 1:1)

Following the addition of 1 equiv. of $CuCl_2$ to **3** (1 x 10^{-2} M) in MeCN / H_2O (v / v, 1: 1), we observed a drastic structural transformation from nanotube to a liposome, which was confirmed by TEM, AFM and SEM images (Figure 9). The liposome appears as a black circular line that separates the dark interior from the light exterior as the interior space of the liposome was filled with negative stain, uranyl acetate. The exterior diameter was 88-250 nm, and the wall thickness of 8.6 nm is similar to that of the nanotube. The interior diameter was 71-235 nm.

As a result of the spectroscopic studies carried out in this work, it seems that significant accumulation nanostructures occur. All these data demonstrate that π-π and the other non-covalent interactions exist of **1** in CH_3CN/H_2O (v/v, 7/3) at pH 11, and as a consequence of the accumulation of meaningful forms of nanostructures are seen such as the nanotube, nanomisel, and nanoshell from TEM and SEM images (Figure 10 A-D, S3, and S4). When the TEM images of **1** in CH_3CN/H_2O (v/v, 7/3) at pH 11 are examined, it is seen that the inner diameter of the nanotube is 19.0 nm, the outer diameter is 23.8 nm and the wall thickness is 4.8 nm (Figure 10B). While no nanostructure formation was observed at pH 7, irregular nanomisel structures were observed from **1**-Cu^{+2} complexes under the same conditions at about two weeks (Figure 10A and C). Within about the same time, regular nanomisel structures were obtained from the self-assembly studies of the **1**-Cu^{+2} complex in CH_3CN/H_2O (v/v, 7/3) at pH 11.

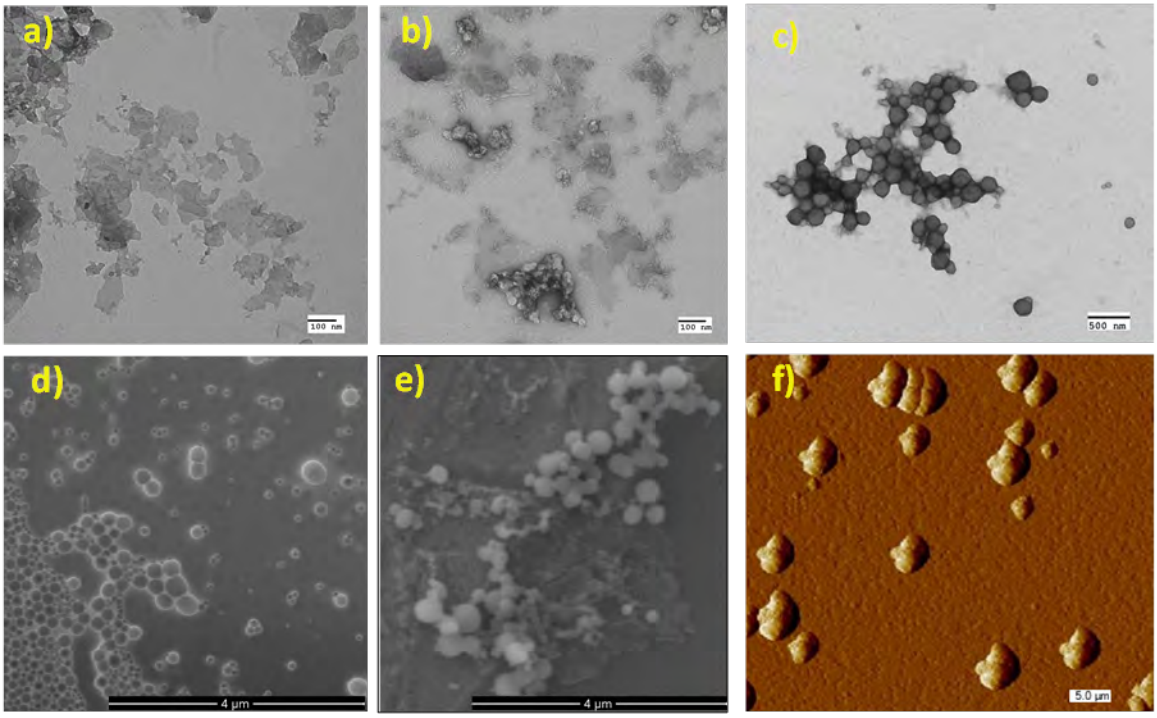

Figure 9. A) TEM (pH 11), B) TEM (pH 2), C) TEM (pH 7), D-E) SEM (pH 7) and F) AFM (pH 7) images of **3** and 1 equiv. of Cu^{2+} in $MeCN/H_2O$ (v/v, 1:1)

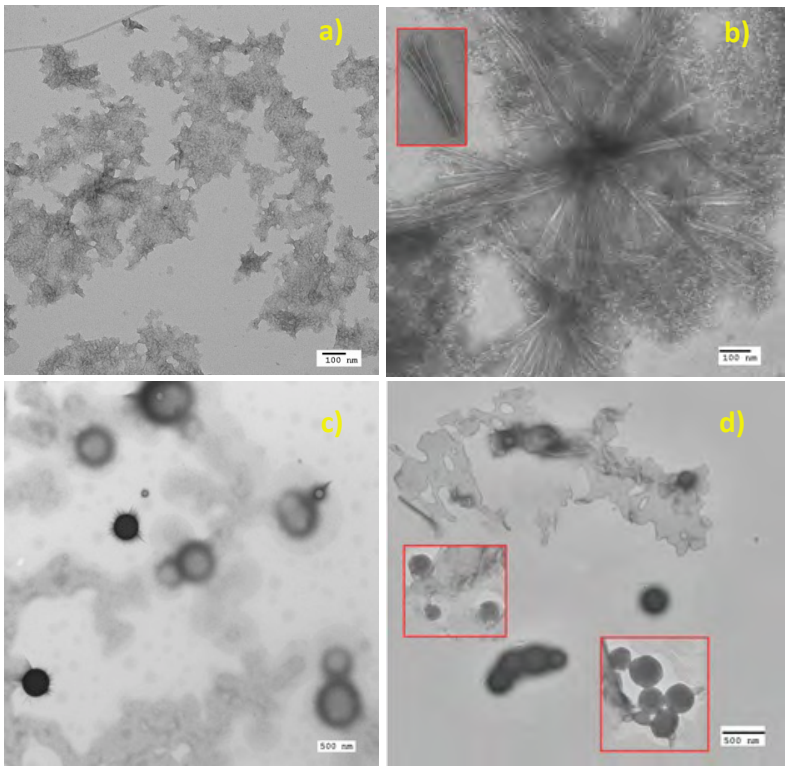

Figure 10. A) TEM (pH 7), B) TEM (pH 11) images of 1 in $MeCN/H_2O$ (v/v, 7/3), C) TEM (pH 7), and D) TEM (pH 11) images of **1** and 1 equiv. of Cu^{2+} in $MeCN/H_2O$ (v/v, 7:3)

Characterization. Dynamic light scattering (DLS), X-ray Diffraction (XRD) and X-ray photon spectroscopy (XPS) were used to understand the formation morphology of nanomaterials. DLS studies showed large aggregates of **3** (1×10^{-2} M) in MeCN/H_2O (v/v, 1:1) with dispersive size over large variable measurement size. However, the addition of 1 equivalent $CuCl_2$ to **3** resulted in the formation of uniform liposomes over the range of 500 – 1400 nm (maximum at 844 nm) (Figure 11). XRD also exhibited evidence of change in stacking distance between the amphiphilic building blocks from 3.20 Å to 4.02 Å. In XRD spectrum, initial d-spacing (3.2022) of **3** is an evidence of efficient π-π stacking of the NDI and bis(indolyl) chromophores (Figure 12). On addition of Cu^{2+} coordinate with bisindole chromophore, the d-spacing between the building blocks increased significantly due to change in bisindole structural conformation that deviates away from planarity during coordination with Cu^{2+} cation. This resulted in increased steric repulsive interaction between indole chromophores that pushes the building blocks further apart and affected the directionality of the assembly process. The structure of **3**-Cu^{2+} complexes was also studied with XPS analysis, and the C (1s), N (1s) and O (1s) spectra of the nano-assemblies of **3** were obtained in the absence and presence of Cu^{2+} ions. The XPS spectrum showed a double carbon peak at 283.05 and 286.50 eV, corresponding to the carbon of bisindole, NDI and lysine chromophores of amphiphile **3** in the absence of Cu^{2+} ions. The presence of only a two peak indicates that the surface is made up of stacking aromatic carbons from amphiphiles while lysine is embedded within the nano-assemblies (Figure 13).

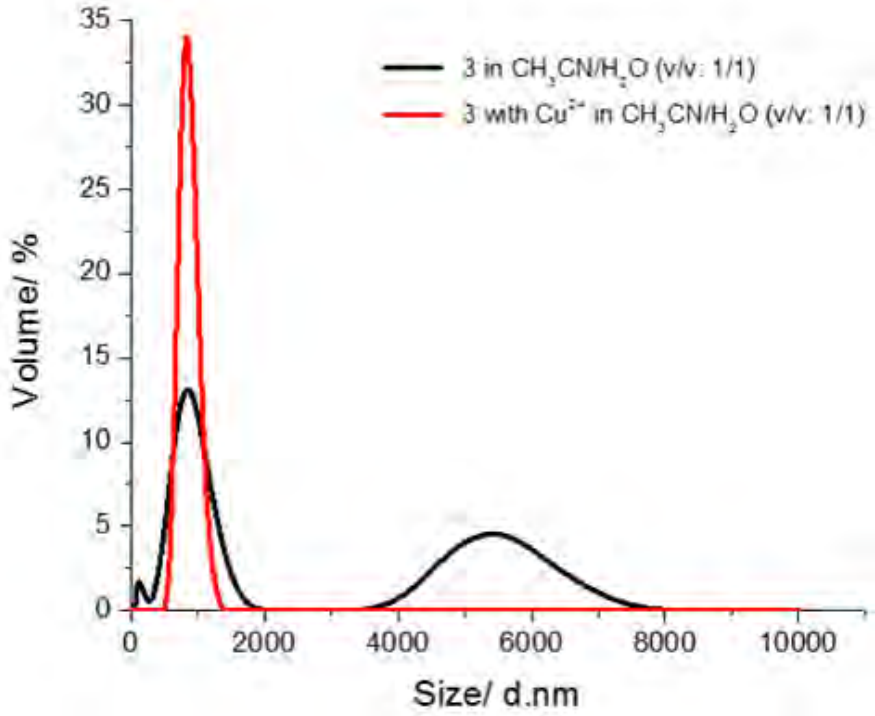

Figure 11. DLS spectra of **3** (black) and **3** + Cu^{2+} solution (red) in MeCN/H_2O (v/v, 1:1)

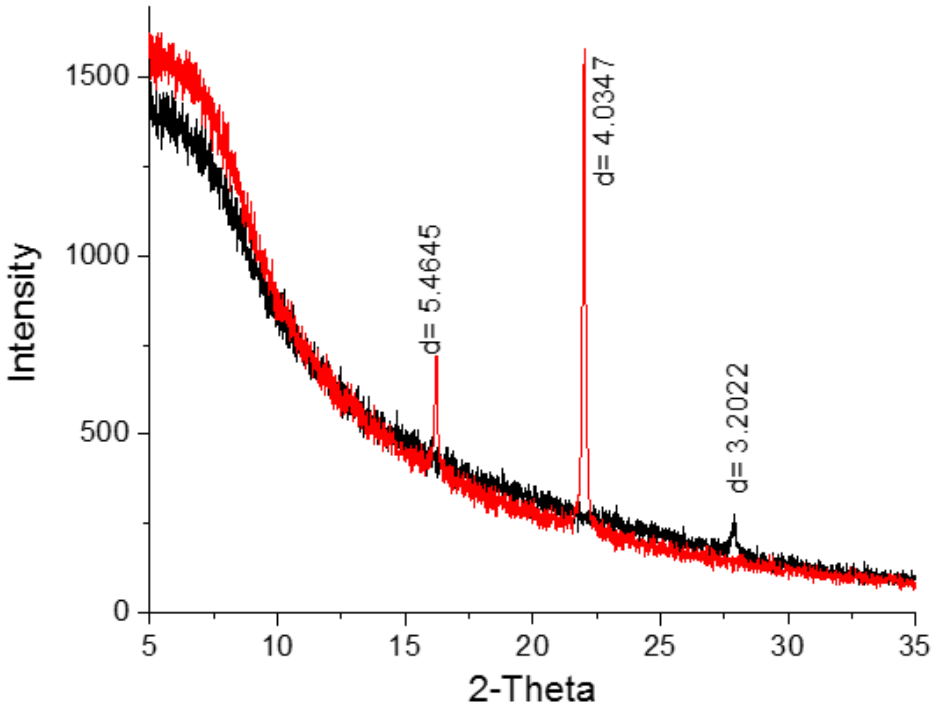

Figure 12. XRD spectra of **3** (black) and **3** + Cu^{2+} solution MeCN/H_2O (v/v, 1:1)

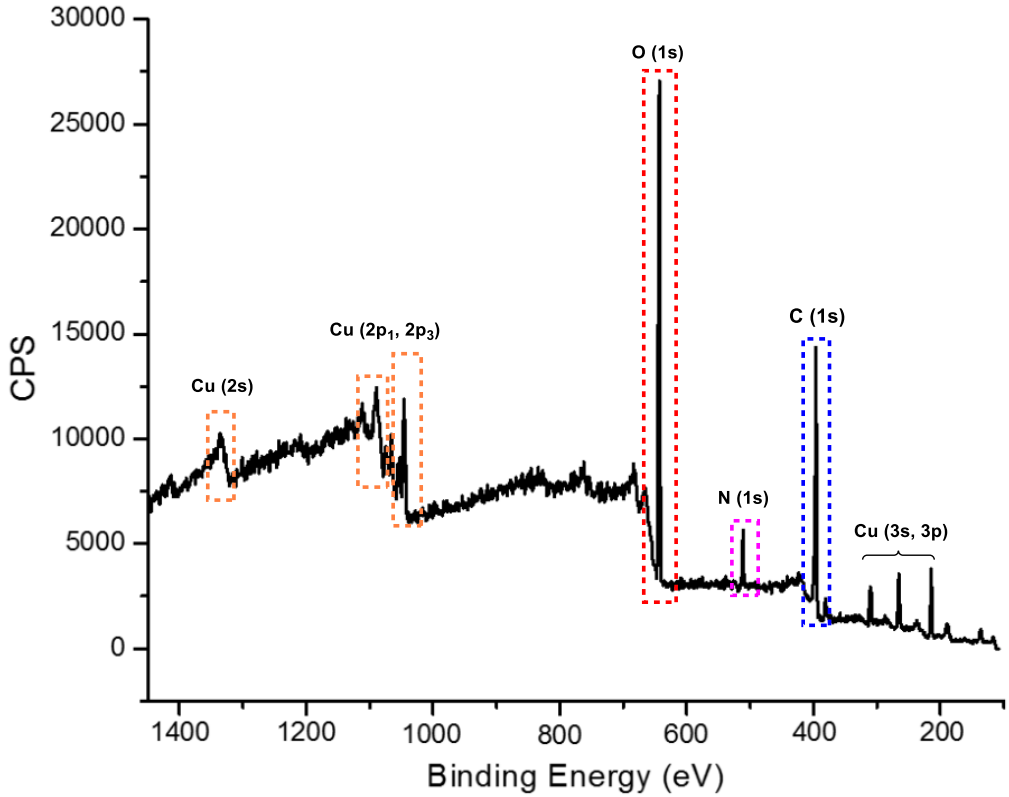

Figure 13. XPS spectrum of amphiphile **3** with $CuCl_2$.

When Cu^{2+} ions were present, a shift in both peaks towards higher energy appeared in the C (1s) spectrum at 283.15 and 286.59 eV. The peak with the lower binding energy at 283.15 eV corresponds to C-H element as the addition of Cu^{2+} lead in an increase of +0.1 eV. The absence of peak around 290 eV suggested that lysine moieties are encapsulated within the nano-assemblies rather than located on the surface of the structure (Figure 14C).[15] N (1s) spectra showed an association of Cu^{2+} with the nitrogen of the indole moieties. The amine group of indole appeared as a peak with a binding energy of 398.5 eV in the absence of Cu^{2+} ions. We assigned the other broad peak at 398.4 eV to nitrogen in the imide moiety of the NDI chromophore.[16] A change in the N (1s) spectrum was observed after addition of Cu^{2+} ions. The high energy peak at 398.4 eV disappeared, and a resulting broad peak appeared at 398.5 eV, which indicated that out-of-plane deprotonated amine from bisindole formed distorted tetrahedral coordinate around copper ions (Figure 14B).[11d] Changes were also observed in O (1s) spectrum where a doublet peak at 529.94 eV and 529.65 eV were formed in the absence of Cu^{2+} ions. The addition of Cu^{2+} ions resulted in a negative shift of a higher energy peak by -0.02 eV to 529.92 eV while the lower energy peak increases by +0.07 eV to 529.72 eV (Figure 14A). The changes in energy are relatively small as the element found in NDI chromophore is further away from the binding site between indoles and Cu^{2+} cation. This new peak clearly indicated that the amine groups of bisindole complexed with the Cu^{2+} ion, consistent with our UV-Vis spectroscopy results.

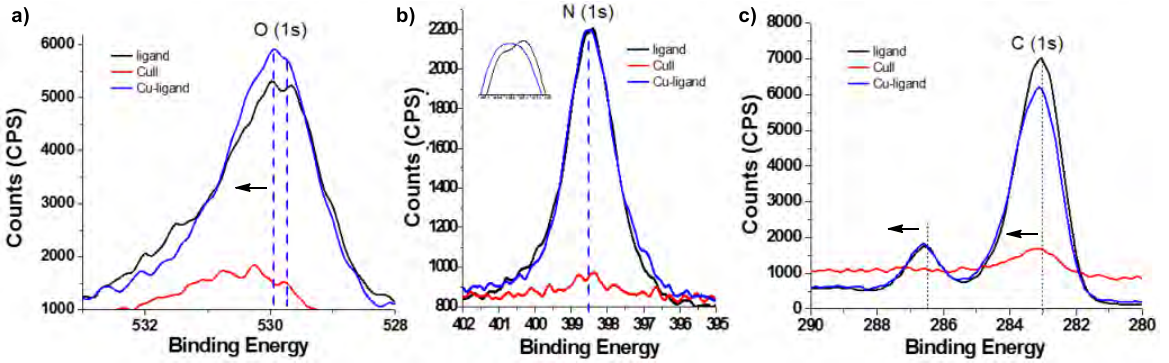

Figure 14. A) XPS O (1s) spectrum of amphiphile **3** (black), amphiphile **3** +$CuCl_2$ (blue) B) XPS N (1s) spectrum of amphiphile **3** (black), amphiphile **3** +$CuCl_2$ (blue) and $CuCl_2$ (red) and C) XPS C (1s) spectrum of amphiphile **3** (black), amphiphile **3** + $CuCl_2$ (blue) and $CuCl_2$ (red).

XPS spectrum of copper proved that most of the copper was present in a divalent oxidation state (Cu^{2+}), this is obvious from the strong satellite peaks from $Cu2p_{3/2}$ and $Cu2p_{1/2}$ spectra at 939- 945 eV and 960-964 eV respectively.[17] Based on the $Cu2p_{1/2}$ peak, a change in peak after adding **3** to Cu^{2+} was observed from 950.78 eV to 951.00 eV, with an increase of +0.22 eV. Also, it is interesting to observe that in $CuCl_2$, a strong peak at 953.06 eV was observed at a greater intensity than 950.78 eV, whereas in the mixture, a strong peak at 951.00 eV has a greater intensity due to suppression of peak at 952.80 eV (Figure 16A and B). Chemical shift was also observed in $Cu2p_{3/2}$ peak, from 930.96 eV to 931.36 eV measures an increase of +0.4 eV. A similar change in intensity was also observed, whereby a strong peak at 933.31 eV at a greater intensity than 930.96 eV in $CuCl_2$, whereas addition of **3** to $CuCl_2$ caused a suppression of the strong peak at 933.31 eV resulted in a greater intensity peak at 931.36 eV than 933.03 eV (Figure 15B). The more conspicuous chemical shift was observed in Cu LMM Auger spectrum where energy increased by 9.19 eV from 569.71 eV to 570.90 eV while a quenching of 575.19 eV was observed (Figure 15A). The XPS results imply that Cu^{2+} ions form bisindole–Cu complexes due to copper binding to the nitrogen of indole chromophores rather than formation of an oxygen-bound complex with the lysine group. Both C1s and N1s spectra are indicative of a bisindole–Cu complex structure where the Cu^{2+} ion is surrounded by an adjacent amine from indole moieties to form a distorted tetrahedral dimer complex. Figure 17 propose a structure for tetrahedral dimer complex.

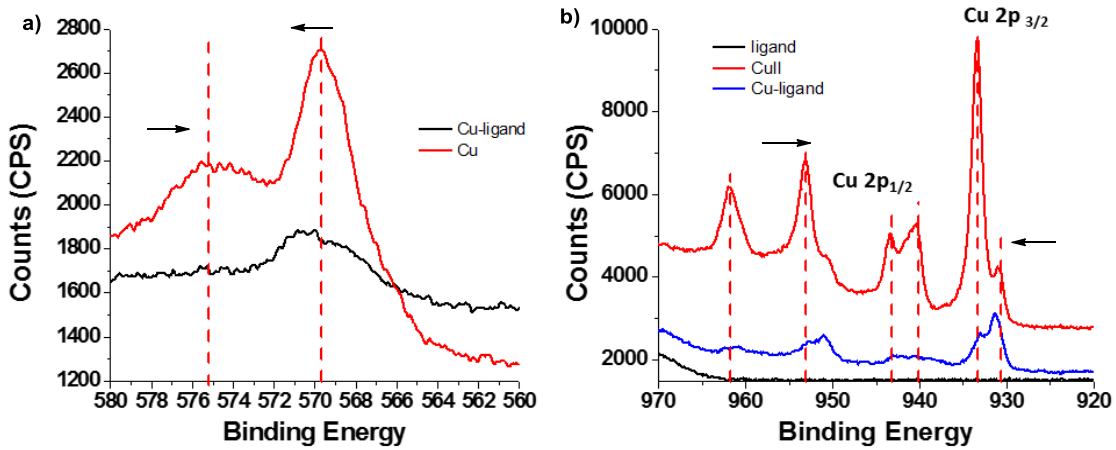

Figure 15. A) Auger Cu LMM spectrum of amphiphile **3** +$CuCl_2$ (black) and $CuCl_2$ (red), and B) XPS Cu $2p_{1/2}$ and $Cu2p_{3/2}$ spectrum of amphiphile **3** (black), amphiphile **3** +$CuCl_2$ (blue) and $CuCl_2$ (red)

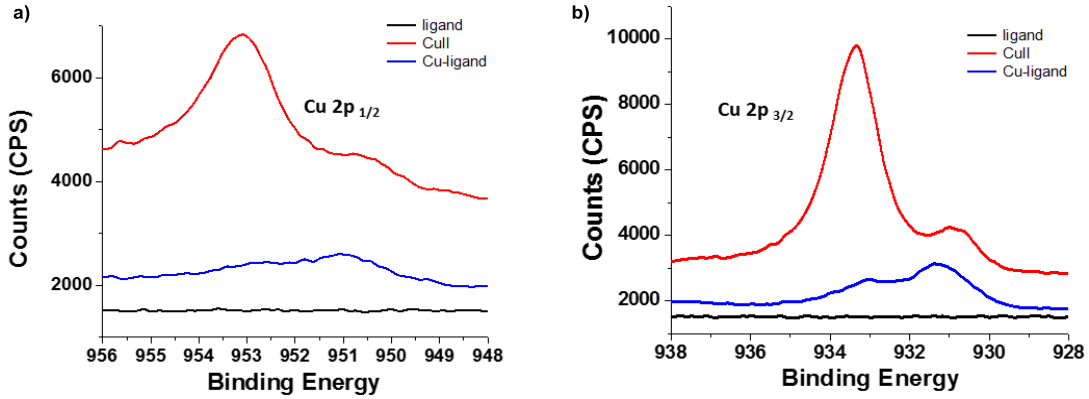

Figure 16. A) $Cu2p_{1/2}$ spectrum of amphiphile **3** (black), amphiphile **3**+$CuCl_2$ (blue) and $CuCl_2$ (red), and B) $Cu2p_{3/2}$ spectrum of amphiphile **3** (black), amphiphile **3** +$CuCl_2$ (blue) and $CuCl_2$ (red)

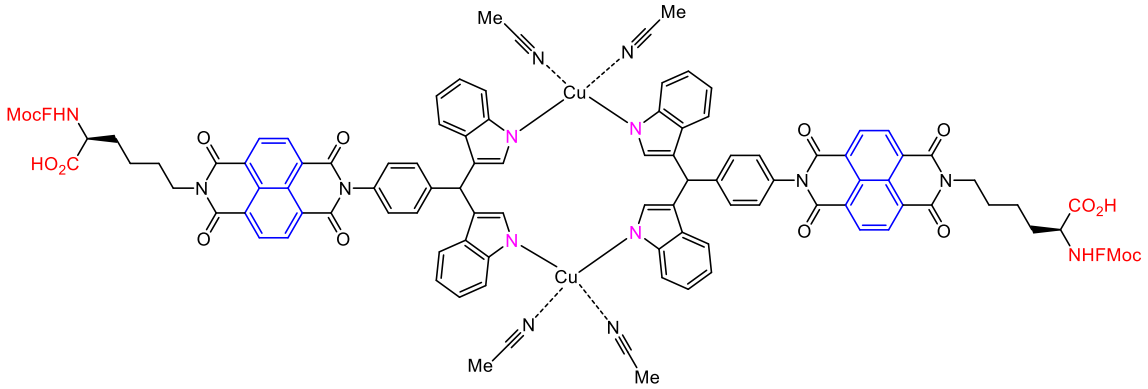

Figure 17. Proposed structure for tetrahedral dimer complex ([**3**·$Cu(MeCN)_2$]$_2$).

■ CONCLUSION

The synthesis of water-soluble molecules for the formation of nano-sized structures is of great importance. In conclusion, we have designed and synthesized novel NDI-based amphiphiles containing

bis(indolyl)methane unit, which can undergo a structural reorganization to self-assembly. For amine-functionalized amphiphile **2**, the self-assembly of at neutral pH provides irregular nanofibers, whereas the acidic medium (pH 2) afforded pretty regular nanotubes. Also, the self-assembly of Fmoc-protected amphiphile **3** at pH 2 and 7 allowed the formation of nanospheres and quite regular nanotubes, respectively. In addition to the self-assembly studies at different pHs, the interactions of amphiphile **3** with cations were investigated and high selectivity of **3** against Cu^{+2} was determined. The **3**-Cu complexe self-assembled into metallo-liposomes in MeCN-H_2O (v/v, 1:1). Molecular coordination between indole chromophores and Cu (II) cation was probed by DSL, XRD, XPS, CD and UV-Vis spectroscopy. The present study can further capitalize on the colorimetric response triggered by Cu2+ in the development of bioinspired material, which may open a new avenue towards the mimicry of chromatophore for pigment translocation in structural colour for camouflage, biosensor, and drug delivery applications.

[1] (a) Wu, M.; Ye, Z. Y.; Liu, Y. F.; Liu, B.; Zhao, X. J. *Mol. Biosyst.* **2011**, *7* (6), 2040-2047. (b) Chatzinikolaidou, M.; Simantirakis, E.; Terzaki, K.; Farsari, M.; Vamvakaki, M.; Mitraki, A. *J Tissue Eng Regen M.* **2012**, *6*, 226-226. (c) Sun, Y.; Li, Z. B.; Wang, Z. H. *J. Mater. Chem.* **2012**, 22(10), 4312-4318.

[2] (a) Bayindir, S.; Erdogan, E.; Kilic, H.; Saracoglu, N. *Synlett* **2010**, 10, 1455-1458. (b) Kilic, H.; Bayindir, S.; Erdogan, E.; Saracoglu, N. *Tetrahedron* **2012**, 68, 5619-5630. (c) Bayindir, S.; Erdogan, E.; Kilic, H.; Aydin, O.; Saracoglu, N. *J. Heterocyclic Chem*. **2015**, 52, 1589-1594. (d) Aydin, O.; Kilic, H.; Bayindir, S.; Erdogan, E.; Saracoglu, N. *J. Heterocyclic Chem*. **2015**, 52, 1540-1553. (e) Kilic, H.; Bayindir, S.; Saracoglu, N. *Curr. Org. Chem.* **2014**, 11, 167–181. (f) Aydin, O.; Kilic, H.; Bayindir, S.; Saracoglu, N. *J. Heterocyclic Chem*. **2016**, 53, 2096-2101. (g) Bayindir, S.; Saracoglu, N. *RSC Adv.* **2016**, 6, 72959–72967.

[3] Martin, A. D.; Robinson, A. B.; Mason, A. F.; Wojciechowski, J. P.; Thordarson, P. *Chem. Comm.* **2014**, 50(98), 15541-15544.

[4] (a) Deb, M. L.; Baruah, B.; Bhuyan, P. J. *Synthesis* **2008**, 2, 286-292. (b) Su, J. Y., Lo, C. Y.; Tsai, C. H.; Chen, C. H.; Chou, S. H.; Liu, S. H.; Wong, K. T. *Org. Lett.* **2014**, 16(12), 3176-3179.

[5] (a) Lowik, D. W. P. M.; Leunissen, E. H. P.; Heuvel, M.; Hansen M. B.; Hest J. C. M. *Chem. Soc. Rev*. **2010**, 39, 3394–3412. (b) Yucel, T.; Micklitsch, C. M.; Schneider, J. P.; Pochan, D. J. *Macromolecules* **2008**, 41, 5763–5772. (c) Tu, S.; Kim, S. H.; Joseph, J.; Modarelli, D. A.; Parquette, J. R. *J. Am. Chem. Soc.* **2011**, 133, 19125–19130.

[6] (a) Pu, L., *Chem Rev.* **2004**, 104 (3), 1687-1716. (b) Kim, J.; McQuade, D. T.; McHugh, S. K.; Swager, T. M. *Angew. Chem. Int. Ed.* **2000**, 39 (21), 3868-3872. (c) Sarkar, S.; Shunmugam, R. *ACS Appl. Mater. Interfaces* **2013**, 5, 7379−7383. (d) Busschaert, N.; Caltagirone, C.; Rossom, W. V.; Gale, P. A. *Chem. Rev.* **2015**, 115 (15), 8038–8155.

[7] (a) Wang, B.; Gao, Y.; Li, H. W.; Hu Z. P.; Wu, Y. *Org. Biomol. Chem.* **2011**, 9, 4032-4034. (b) Chereddy, N. R.; Janakipriya, S.; Korrapati, P. S.; Thennarasu, S.; Mandal, A. B. *Analyst.* **2013**, 138, 1130–1136. (c) Du, J.; Hu, M.; Fan, J.; Peng, P. *Chem. Soc. Rev.* **2012**, 41, 4511–4535. (d) Kaur, P.; Kaur, S.; Singh, K. *Org. Biomol. Chem.* **2012**, 10, 1497–1501. (e) Park, H.; Chang, S. K. *Sens. Actuators B Chem.* **2015**, 220, 376–380.

[8] Gunnlaugsson, T.; Leonard, J. P.; Murray, N. S. *Org. Lett.* **2004**, *6* (10), 1557-1560.

[9] (a) Ajayaghosh, A.; George, S. J. *J. Am. Chem. Soc.* **2001**, *123* (21), 5148-5149. (b) George, S. J.; Ajayaghosh, A.; Jonkheijm, P.; Schenning, A. P. H. J.; Meijer, E. W. *Angew. Chem. Int. Ed.* **2004**, *43* (26), 3422-3425.

[10] Dujols, V.; Ford, F.; Czarnik, A. W. *J. Am. Chem. Soc.* **1997**, *119* (31), 7386-7387.

[11] (a) Zhou, Y.; Wang, F.; Kim, Y.; Kim, S. J.; Yoon, J. *Org Lett.* **2009**, *11* (19), 4442-4445. (b) Li, G. K.; Xu, Z. X.; Chen, C. F.; Huang, Z. T. *Chem. Commun.* **2008**, (15), 1774-1776. (c) Xu, Z. C.; Qian, X. H.; Cui, J. N. *Org. Lett.* **2005**, *7* (14), 3029-3032. (d) Martinez, R.; Espinosa, A.; Tarraga, A.; Molina, P., *Tetrahedron* **2008**, *64* (9), 2184-2191.

[12] Siyu, T., Se H. K., Jojo J., David A. M., Jon R. P. *J. Am. Chem. Soc.* **2011**, 133, 19125–19130.

[13] Ludwig, V., Krebs, A., Stoll, M., Dietrich, U., Ferner, J., Schwalbe, H., Scheffer, U., Dürner, G., Gobel, M. W. *ChemBioChem.* **2007**, 8, 1850 – 1856.

[14] (a) Shao, H.; Seifert, J.; Romano, N. C.; Gao, M.; Helmus, J. J.; Jaroniec, C. P.; Modarelli, D. A.; Parquette, J. R. *Angew. Chem. Int. Ed.* **2010**, *49* (42), 7688-7691. (b) Shao, H.; Parquette, J. R. *Chem. Commun.* **2010**, *46* (24), 4285-4287. (c) Shao, H.; Nguyen, T.; Romano, N. C.; Modarelli, D. A.; Parquette, J. R. *J. Am. Chem. Soc.* **2009**, *131* (45), 16374-16376. (d) Shao, H.; Gao, M.; Kim, S. H.; Jaroniec, C. P.; Parquette, J. R. *Chem. Eur. J.* **2011**, *17* (46), 12882-12885.

[15] Zhang, W. H.; Carravetta, V.; Plekan, O.; Feyer, V.; Richter, R.; Coreno, M.; Prince, K. C. *J. Chem. Phys.* **2009**, *131* (3), 174319.

[16] Yu, Y.; Shapter, J. G.; Popelka-Filcoff, R.; Bennett, J. W.; Ellis, A. V. *J Hazard Mater* **2014**, *273*, 174-182.

[17] Shuvaev, S.; Bushmarinov, I. S.; Sinev, I.; Dmitrienko, A. O.; Lyssenko, K. A.; Baulin, V.; Grunert, W.; Tsivadze, A. Y.; Kuzmina, N. *Eur. J. Inorg. Chem.* **2013**, 27, 4823-4831.

Light-controlled self-assembly of dithienylethene bolaamphiphiles in water.

Haydar Kilic,[b,c] Kwang Soo Lee,[a] Nurullah Saracoglu *[b] and Jon R. Parquette*[a]

This manuscript is undergoing revision to address reviewer comments. Several new experiments are being conducted with the addition of two more authors: Dr. Mingyang Ji and Cassidy Creemer.

Abstract. The self-assembly of bolaamphiphiles comprised of a central photochromic dithienylethene (dte) chromophore was investigated in aqueous media. Irradiation at 254 nm induced a conversion from the open to closed states of the DTE chromophores. The open→closed transition was accompanied by a change from nonspecific aggregates to 1D nanofibers and from sheets to liposomal structures for 1 and 2 in aqueous media, respectively.

Many biomolecular systems achieve and modulate their functional characteristics via noncovalent self-assembly.[1] Self-assembly provides a convenient, albeit often empirical strategy, to fabricate materials in the nanoscale regime.[2] Strategies to create nanostructured materials by controlled self-assembly offer a diverse array of applications in optoelectronics,[3,4] biomaterials[5-7] and drug delivery,[8] inter alia.[9] The potential for these materials to display adaptivity, self-healing and other forms of "intelligent" behavior would be enhanced by a capability to transition between multiple states.[10] However, methods to dynamically modulate their structural features via external triggers are currently limited.[11,12] Molecules, termed "molecular switches,"[13,14] that switch between multiple configurational states upon irradiation[15] have potential to induce changes in local monomer packing as a mechanism to modulate

long-range nanostructural order. Although photoswitches have been exploited to modulate supramolecular structure and morphology in organic media, the control of self-assembly in water with light has been less studied.[10,16-19]

A potential strategy to control the nanoscale organization of a self-assembled material would incorporate a photoresponsive chromophore within the building blocks that comprise the nanostructure. Dithienylethene (DTE) photoswitches[20] have been employed to control the morphology of modified surfaces,[21-23] polymers,[24] organogels,[25] nanofibers,[26] and liquid crystals.[27] Herein, we report the light-controlled self-assembly of photoresponsive DTE-bolaamphiphiles in aqueous media. We have recently demonstrated that lysine-1,4,5,8-naphthalenetetracarboxylic acid diimide (Lys-NDI) amphiphiles and bolaamphiphiles undergo efficient self-assembly into 1D-nanostructures in water.[28-30] In these systems, self-assembly was driven by the

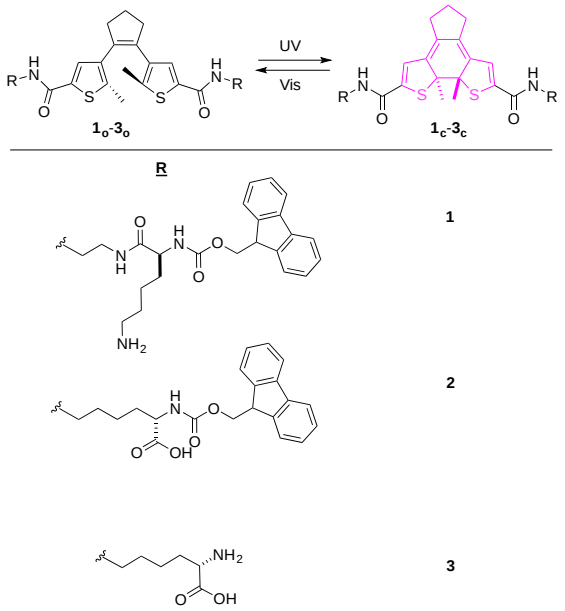

Figure. 1 Photoisomerization of DTE photochromic unit and structures of DTE bolaamphiphiles **1-3**.

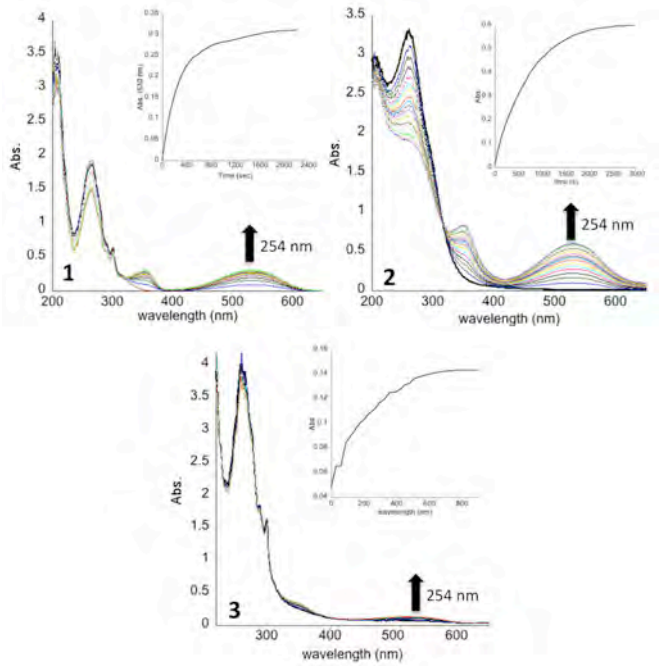

Figure 2. Photochromic behavior of **1**-**3.** UV/Vis absorption spectra in water (1 mM) during the course of irradiation at 254 nm from the open state to the photostationary state. Inset: time-dependent absorption changes at 524 nm.

intermolecular π-stacking of the NDI group in addition to amphiphilic phase separation. Therefore, based on these systems, photoresponsive monomers **1**-**3** were designed by replacing the NDI chromophores with a light-responsive, dithienylethene (DTE) chromophore,[31] which serves as the hydrophobic, aromatic component (Fig. 1). The tendency of bolaamphiphiles to form 1D rods or tubes over spherical structures has been shown to increase for monomers having rigid internal segments, which results in a more ordered packing of the hydrophobic core.[32] Thus, we reasoned that the cyclization/cycloreversion reaction between the open- and closed-ring isomers of DTE upon irradiation would alter both the conformational flexibility and/or the π-stacking capability of the monomer, thereby modulating the rigidity of the interior segments, and the resulting structure, of the assemblies.

A series of DTE-lysine bolaamphiphiles displaying positive, negative or zwitterionic headgroups (**1-3**) were prepared by amidation of 4,4'-(cyclopent-1-ene-1,2-diyl)bis(5-methylthiophene-2-carboxylic acid)[33] (**DTE-CO_2H**) as described in the supporting information (Scheme S1). Bolaamphiphile **1**, displaying ammonium head groups was prepared by bisamidation of **DTE-CO_2H** with *tert*-butyl(2-aminoethyl)carbamate followed by acidic removal of the *t*-Boc groups, amide coupling with Fmoc-Lys(Boc)-OH and final deprotection. Similarly, bolaamphiphiles **2** and **3**, containing negative or zwitterionic headgroups, respectively, were obtained by coupling two equivalents of N_α-Fmoc-L-Lys-OMe with **DTE-CO_2H** and subsequent deprotection.

The bolaamphiphilic monomers **1-3** contain a central dithienylethene (DTE) photochromic unit capable of undergoing a reversible cyclization/cycloreversion reaction between open- and closed-ring isomers upon irradiation.[34] The photochromic behavior of **1-3** was studied by UV-Vis spectroscopy in water (**1**/**3**); 10% THF/H_2O (**2**) or $CHCl_3$ (**1-3**) (Fig. 2). The lower solubility of **2** necessitated the addition of 10% THF to obtain sufficiently concentrated solutions for the self-assembly studies. The open forms of bolaamphiphiles **1-3** exhibited absorption bands in the range of 259-264 nm in the UV-Vis spectra. Irradiation of the colorless open form of **1** in water (10 mM) at 254 nm produced a photo-stationary state (PSS) after ~ 35 minutes, resulting in the formation of a violet colored solution with absorption bands at 354 and 524 nm, and a concomitant decrease in the 264 nm band. The open/closed ratios were determined using ^{1}H-NMR by lyophilizing the aqueous solution then redissolving in $CDCl_3$ to reduce the aggregation that occurs in water. The amount of the closed form of the DTE chromophore produced at the PSS correlated with the extent of aggregation of the open form of the bolaamphiphile, which qualitatively decreased in the order **3**>**1**>**2**. Accordingly, the ratio of the open to closed forms of **1** at the PSS was determined to be 66:34 ($\mathbf{1}_{open}$:$\mathbf{1}_{closed}$) in water. However, photoisomerization in $CHCl_3$, in which $\mathbf{1}_{open}$ was monomolecular,

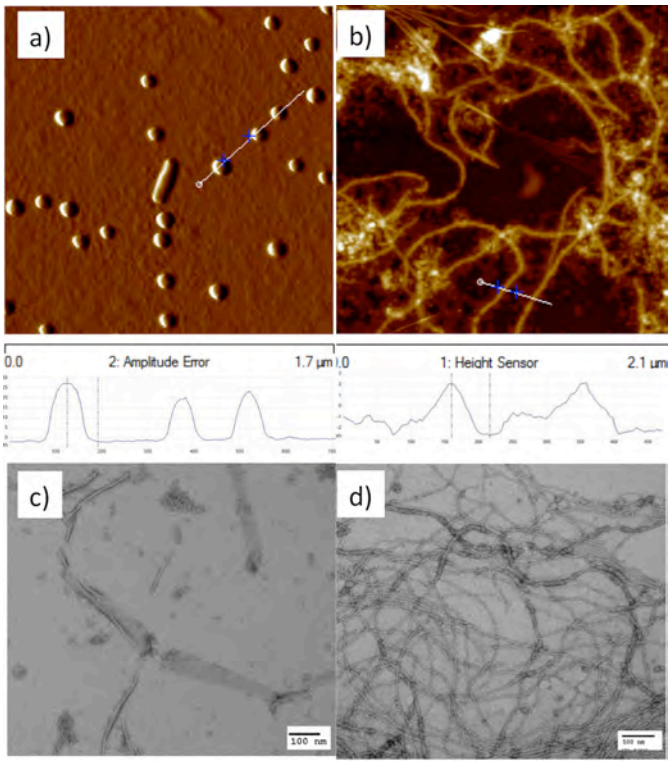

Figure 3: Tapping-mode AFM images of **1** (a) in the open state and, (b) 24 h after irradiation with 254 nm light. (c) TEM images of **1** after exposure to 254 nm light and subsequent aging for (c) 0 h and (d) 24 h. Samples were prepared by dissolving **1** in water (10 mM), prior to diluting to 500 μM (TEM) and evaporating onto a carbon-coated copper grid with uranyl acetate as a negative stain (TEM) or diluting to 100 μM and evaporating onto freshly cleaved mica (AFM).

produced a PSS with a 44/56 open/closed ratio. Similarly, only 23% of the closed form was present at the PSS for **2** in 10% THF/water; whereas, 70% of the closed form was produced in $CHCl_3$. In contrast to **1** and **2**, zwitterion **3** did not undergo significant self-assembly in water or $CHCl_3$. Thus, the amount of $\mathbf{3}_{closed}$ present at the PSS was similar in water and $CHCl_3$ (48% and 58%, respectively).

The self-assembly characteristics of **1-3** were explored by transmission electron microscopy (TEM) and atomic force microscopy (AFM) in both the open state and at the PSS following irradiation with 254 nm light. Accordingly, imaging a sample of $\mathbf{1}_{open}$, prepared by diluting a colorless 10 mM solution to 0.5 mM, revealed minimal, nonspecific aggregation with a few liposomal aggregates (Figs. 3a, S2). Irradiation with 254 nm light for ~45 mins produced a violet solution due to the formation of the closed form of the DTE chromophore (Fig. 2). TEM and AFM images of the solution at the PSS revealed a transition in morphology from the nonspecific aggregates to uniform 1D nanofibers with diameters of 14 nm and heights of 2.8-4.8 nm (Fig. 3b). Immediately following irradiation, a transition to ribbons was observed by TEM that fully converted to nanofibers after 24 h (Figs. 3c-d). Helical twisting and thickening of a portion of the nanofibers were also apparent in the images. Similar to **1**, the open state of **2** produced a clear solution in 10% THF/H_2O (10 mM) that became violet at the PSS produced by irradiation at 254 nm. TEM images of the diluted solution (0.5 mM) of $\mathbf{2}_{open}$ revealed sheet-like aggregates (Fig. 4a). At the PSS, the sheets transformed into a series of liposomal assemblies, with diameters ranging from 68-87 nm, which were fused into bead-like strands immediately following irradiation (Fig. 4b). After 12 h, the bead-like arrays partially separated into distinct, well-defined liposomal structures with less agglomeration, as observed by both TEM and SEM imaging (Figs. 4c-d). Dynamic light scattering measurements reported liposomal diameters of 396 nm, which were significantly larger than the isolated liposomal dimensions, measured by electron microscopy, due to the tendency of some of the liposomes to adhere together (Fig. S3). The zwitterionic bolaamphiphile **3** did not exhibit any specific self-assembly in water in either the open or closed state by TEM imaging.

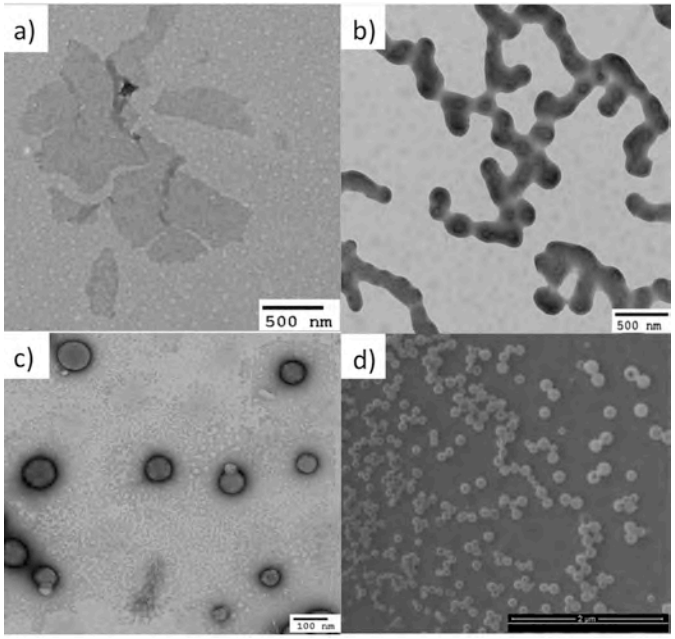

Figure 4: TEM image of **2** (a) in open form; and (b) 12 h and (c) 24 h after irradiation with 254 nm light. (d) SEM image of **2** following 254 nm irradiation after 24 h. Samples were prepared by irradiating **2** in water (10 mM), prior to diluting to 500 μM for imaging.

The photoisomerization of the DTE ring system leads to conversion from a non-planar, conformationally flexible structure to rigid, planar ring. However, a comparison of the CD spectra of the open and closed forms of **1** and **2** exhibited transitions only in the region 200-350 nm (Fig S1). In the spectral region of 520-530 nm, corresponding to the π–π absorption of the closed DTE chromophore, no Cotton effects were observed, suggesting that π–π aggregation of the DTE chromophore was not driving self-assembly. Rather, changes in the flexibility of the bolaamphiphile induced by photoisomerization of the DTE unit, likely mediated the observed changes in self-assembly process.

Conclusions: The self-assembly of bolaamphiphiles containing a central DTE chromophore was controlled by photochemical interconversion between open and closed states. The open→closed transition induced a change from nonspecific aggregates to 1D nanofibers and from sheets to liposomal structures for **1** and **2** in aqueous media, respectively. It is noteworthy that although a mixture of the open and closed forms was produced at the PSS for both **1** and **2**, a significant perturbation of the morphology of the aggregates was observed by electron microscopy.

Notes and references

1. R. N. Perham, *Philos. T. Roy. Soc. B*, 1975, **272**, 123-136.
2. G. M. Whitesides, J. P. Mathias and C. T. Seto, *Science*, 1991, **254**, 1312-1319.
3. T. E. Kaiser, H. Wang, V. Stepanenko and F. Wurthner, *Angew. Chem. Int. Ed.*, 2007, **46**, 5541-5544.
4. M. Gao, S. Paul, C. D. Schwieters, Z.-Q. You, H. Shao, J. M. Herbert, J. R. Parquette and C. P. Jaroniec, *J. Phys. Chem. C*, 2015, **119**, 13948-13956.
5. H. G. Cui, M. J. Webber and S. I. Stupp, *Biopolymers*, 2010, **94**, 1-18.
6. T. Dvir, B. P. Timko, D. S. Kohane and R. Langer, *Nat. Nanotech.*, 2011, **6**, 13-22.
7. S. G. Zhang, *Nat. Biotechnol.*, 2003, **21**, 1171-1178.

8. S. H. Kim, J. A. Kaplan, Y. Sun, A. Shieh, H. L. Sun, C. M. Croce, M. W. Grinstaff and J. R. Parquette, *Chem.-Eur. J.*, 2015, **21**, 101-105.
9. K. Thorkelsson, P. Bai and T. Xu, *Nano Today*, 2015, **10**, 48-66.
10. I. Tomatsu, K. Peng and A. Kros, *Adv. Drug Deliver. Rev.*, 2011, **63**, 1257-1266.
11. B. A. Grzybowski, C. E. Wilmer, J. Kim, K. P. Browne and K. J. M. Bishop, *Soft Matter*, 2009, **5**, 1110-1128.
12. T. Fenske, H. G. Korth, A. Mohr and C. Schmuck, *Chem.-Eur. J.*, 2012, **18**, 738-755.
13. B. L. Feringa, *J. Org. Chem.*, 2007, **72**, 6635-6652.
14. G. Vives and J. M. Tour, *Acc. Chem. Res.*, 2009, **42**, 473-487.
15. M. Natali and S. Giordani, *Chem. Soc. Rev.*, 2012, **41**, 4010-4029.
16. J. T. van Herpt, J. Areephong, M. C. Stuart, W. R. Browne and B. L. Feringa, *Chem.-Eur. J.*, 2014, **20**, 1737-1742.
17. T. Hirose, K. Matsuda and M. Irie, *J. Org. Chem.*, 2006, **71**, 7499-7508.
18. K. Higashiguchi, G. Taira, J. Kitai, T. Hirose and K. Matsuda, *J. Am. Chem. Soc.*, 2015, **137**, 2722-2729.
19. A. C. Coleman, J. M. Beierle, M. C. Stuart, B. Macia, G. Caroli, J. T. Mika, D. J. van Dijken, J. Chen, W. R. Browne and B. L. Feringa, *Nat. Nanotechnol.*, 2011, **6**, 547-552.
20. M. Irie, *Chem. Rev.*, 2000, **100**, 1683-1683.
21. K. Uchida, Y. Yamanoi, T. Yonezawa and H. Nishihara, *J. Am. Chem. Soc.*, 2011, **133**, 9239-9241.
22. D. Frath, T. Sakano, Y. Imaizumi, S. Yokoyama, T. Hirose and K. Matsuda, *Chem.-Eur. J.*, 2015, **21**, 11350-11358.
23. S. Bonacchi, M. El Garah, A. Ciesielski, M. Herder, S. Conti, M. Cecchini, S. Hecht and P. Samori, *Angew. Chem. Int. Ed.*, 2015, **54**, 4865-4869.
24. Z. Chen, Y. He, Y. Wang and X. Wang, *Macromol. Rapid Commun.*, 2011, **32**, 977-982.
25. J. J. D. de Jong, L. N. Lucas, R. M. Kellogg, J. H. van Esch and B. L. Feringa, *Science*, 2004, **304**, 278-281.
26. Y. Hotta, S. Fukushima, J. Motoyanagi and A. Tsuda, *Chem. Commun.*, 2015, **51**, 2790-2793.
27. C. Denekamp and B. L. Feringa, *Adv. Mater.*, 1998, **10**, 1080-+.
28. H. Shao, M. Gao, S. H. Kim, C. P. Jaroniec and J. R. Parquette, *Chem.-Eur. J.*, 2011, **17**, 12882-12885.
29. S. Y. Tu, S. H. Kim, J. Joseph, D. A. Modarelli and J. R. Parquette, *J. Am. Chem. Soc.*, 2011, **133**, 19125-19130.
30. M. Gao, S. Paul, C. D. Schwieters, Z. Q. You, H. Shao, J. M. Herbert, J. R. Parquette and C. P. Jaroniec, *J. Phys. Chem. C*, 2015, **119**, 13948-13956.
31. M. Irie, *Chem. Rev.*, 2000, **100**, 1685-1716.
32. X. F. Wang, Y. Z. Shen, Y. Pan and Y. Q. Liang, *Langmuir*, 2001, **17**, 3162-3167.
33. L. N. Lucas, J. J. D. de Jong, J. H. van Esch, R. M. Kellogg and B. L. Feringa, *Eur. J. Org. Chem.*, 2003, 155-166.
34. T. Yamaguchi, K. Uchida and M. Irie, *J. Am. Chem. Soc.*, 1997, **119**, 6066-6071.

Photo-crosslinking the Kinetic States of Self-Assembled Nanotubes.

Nicholas Bewick and Jon Parquette

Introduction. Molecular self-assembly is governed by the collective action of numerous weak, noncovalent forces that drive the intermolecular association of the primary building blocks toward a structure that typically represents a free-energy minimum. Creating adaptive nanoscale systems exhibiting both adaptability and robustness is a challenging endeavor because stability and responsiveness would seem to be opposing characteristics. One strategy to increase the physical stability of these nanostructured systems is to covalently cross-link the individual components of the assembly. Cross-linking the formed nanostructures could be achieved by incorporating multiple cysteine residues to permit intermolecular disulfide bond formation or installing strained alkenes for ring-opening metathesis polymermization. However, a particularly attractive strategy that avoids the need to add exogenous reagents is the light-initiated polymerization of diacetylene.[1] This polymerization produces conjugated polymers with an intense color that are extremely sensitive to environmental and conformational variation. Variations in pH, temperature, and mechanical stress result in variable colors ranging from blue to red. Consequently, the crosslinking process would serve both to stabilize the assemblies and to respond colorimetrically to extrinsic input or structural changes. The polymerization of diacetylene requires that the monomers be positioned within 4.9 Å of each other and at a relative angle of ~45°. Thus, self-assembly must precede polymerization to proximally position the diacetylene groups for polymerization. We will then explore light responsiveness (color and structure) of the cross-linked assemblies to ascertain how the increased stability impacts structural adaptability. This two-component colored system (merocyanine-spiropyran/polydiacetylene) would be expected to produce a wider range of tunable colors compared with a single chromophore assembly.

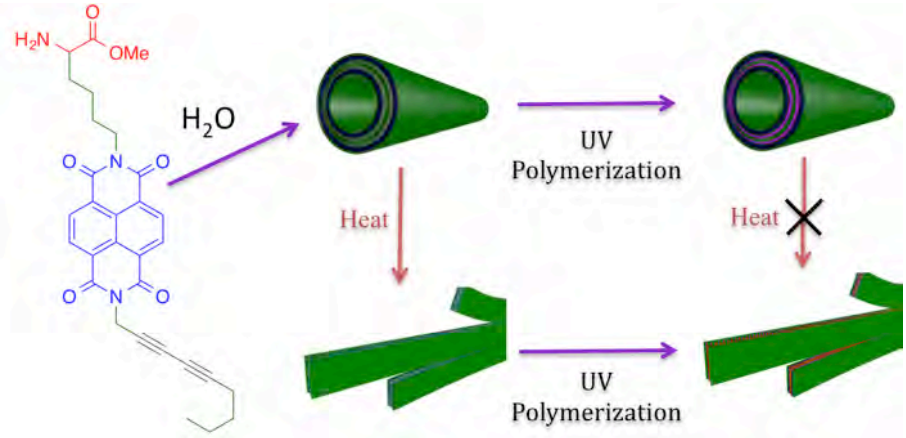

Summary. In this study, we incorporated a diacetylene group into the hydrocarbon tail of the nanotube monomers with positive (**A**) or zwitterionic (**B**) head groups, to allow photo-crosslinking of the nanostructures subsequent to self-assembly. We found that the amphiphile assembled into nanotubes upon dissolving in water at 300 M. However, upon heating to 65°C, the assemblies converted into nanosheets/nanotapes. Irradiation at either of these stages, produced colored polydiacetylene structures that retained the prior morphology. Furthermore, if the photocrosslinked nanotubes, which were likely the kinetically formed state, were heated to 65°C, they remained stable rather than transitioning to the nanosheets.

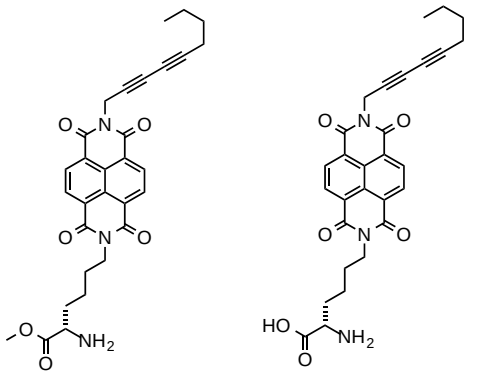

A **B**

Examining the TEM images of the of the assembled monomer **B** in water indicated the presence of nanotube structures, measured 170 nm in diameter and *ca.* 1200 nm in length. When polymerized, the tubes were maintained the same dimensions. To ascertain the stability of the pre- and post-crosslinked nanotubes, dilution experiments were conducted. Pre-crosslinked nanotubes were present in water at concentrations 100 μM. When the pre-crosslinked nanotubes in water were added to THF to make a mixture of 30% THF in water, the tubes dissociate into monomers. However, crosslinked nanotubes retain their nanostructures in 30% THF/water due to the stability afforded by polymerization. This photocrosslinking procedure will expand the utility of these structures by allowing use under conditions that normally induce disassembly.

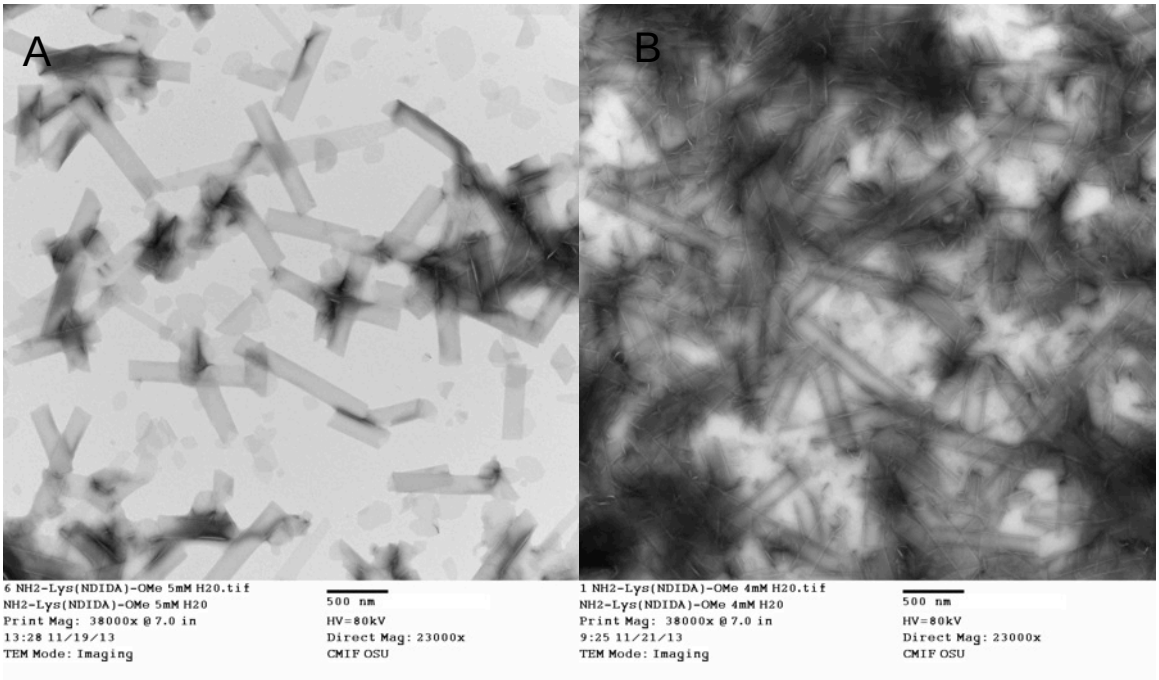

Figure 1. TEM images of nanotubes in water. (left) prior to polymerization in water. (right) after uv irradiation.

Details of Study: Compound **A** was soluble in neutral water due to the positive charge produced from the protonated amine. Zwitterion **B** has a formal charge of zero and a large crystalline lattice energy resulting in very low solubility in water at neutral conditions.[2] At pH 11, compound **B** was sufficiently soluble to obtain solutions at low concentrations (50 μM).

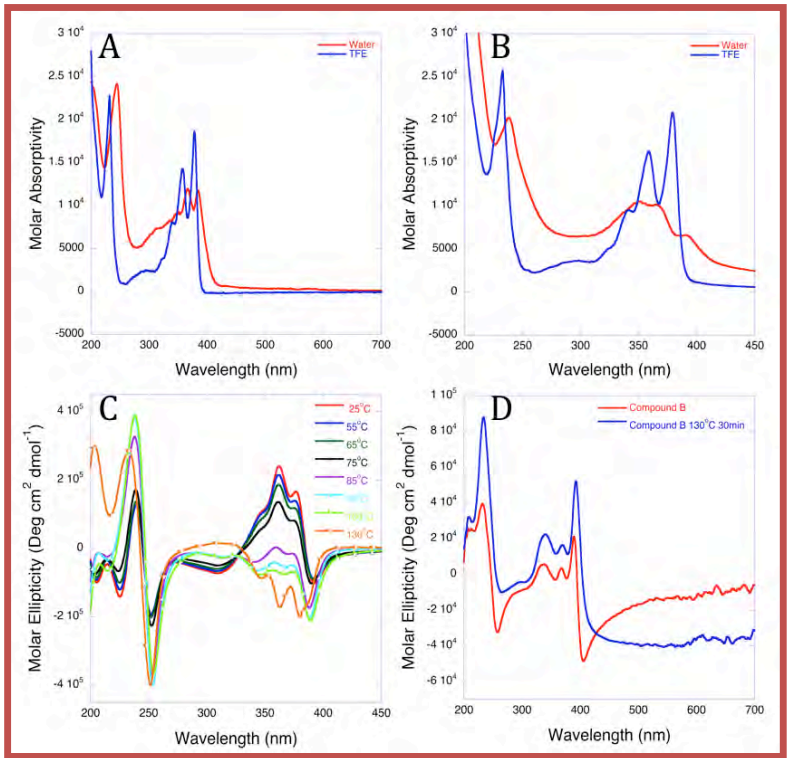

Figure 2. CD and UV Spectra of A and B. 1: UV-Vis of **A** (aged for 12h at 5 mM) in TFE and water (0.30 mM) (A). UV-Vis of **B** in TFE and water (0.05 mM) (B). Temperature dependent CD of **A** (1 mM) (C). Temperature dependent CD of **B** (0.05 mM) (D).

Initially, the amphiphiles were analyzed by ultra-violet spectroscopy (UV) in TFE and water (Figure 2). The NDI chromophore π-π* band I (300 nm to 400 nm) and band II (220 nm to 280 nm) were observed as intense sharp absorbance.[3] When **A** and **B** were dissolved in water, the intensities of band I decreased in intensity and a red shift of bands I and II occurred indicating *J*-type aggregation of the NDI.[4] The red shift of compound **A** was 6 nm while compound **B** had a larger shift of 10 nm. The long-range NDI organization was examined with CD in water. Both compound **A** and **B** displayed cotton effects in the corresponding π-π* NDI I and II absorbance regions. Compound **A** shows a negative excitonic couplet cotton effect, which indicates that NDI adopts on *M*-helix. When the solution was heated (2 mM at 130ºC in a pressure tube for 30 min), the negative signature became more pronounced at 242 nm and the band I signals between 330 nm and 390 nm flip from a positive signal to a negative signal (Figure 2c). Also, the solubility decreases as the solution undergoes prolonged heating treatment. Examining the TEM images of Compound **A**, nanotubes with a width of 140 nm and lengths up to 2 microns were observed with the wall width of 4 nm (Figure 3). After heat treatment of compound **A** at 130ºC for 30 min in a pressure tube, the nanotubes transformed to sheets and helical coil assemblies (Figure 3b). The TEM image of compound **B** exhibited nanostructures that resembled 2D sheets (Figure 3 c). Interestingly, when compound **B** was heated to 130 ºC for 30 minutes in a pressure tube, the NDI CD signals exhibited only a slight increase in intensity and the sheet nanostructures remained (Figure 2 and 3d).

The cause of the change in chirality of the band I region was an interesting feature that needed further exploration. At an elevated temperature, hydrolysis can take place in a reactive media such as water.[5] Even though hydrolysis of amino acid methyl esters at neutral pH is slow, this reaction may be promoted in an assembly with protonated amines and catalyze hydrolysis of an neighboring ester. Functionalities that are regional to the labile group have been shown to effect the rate of hydrolysis.[6] To examine hydrolysis of compound **A**, analytical HPLC was used since both the methyl ester and zwitterion retention times are known. Compound **A** was dissolved in neutral water and left in the dark at room temperature. Measurements were taken at different intervals of time and the zwitterion was detected after 8 hours (Figure 4). After 144 h the hydrolysis leveled off to yield 20% compound **A** and 80% compound **B**. TEM of the sample aged for seven days showed that the tubes were deteriorating and slowly converting to sheets (Figure 4a). As the hydrolysis occurs, sheet formations are promoted due to the nature of compound **B**.

The transformation to sheets was much slower when the hydrolysis occurs at room temperature, even after 80% of **A** was hydrolyzed. To compare, a fresh sample of compound **A** was heated for 30 min at 130ºC in a sand bath, and only 37% hydrolysis conversion was observed (Figure 4b). The TEM revealed that the nanotubes converted to sheets and helical coils (Figure 5b). The complete conversion (>96%) to zwitterion **B** was accomplished in two ways: heating at 130ºC for 4 h in an oil bath, and aging the sample at pH=11 for 2 days at a concentration of 2 mM. Both methods resulted in large decrease of solubility and most of the material precipitated of out solution, which was expected due to the low solubility of compound **B**. The TEM images displayed nanosheets when **A** was aged at pH=11 for two days (Figure 5c). The CD spectrum decreased in intensity due to solubility, but the band I cotton effect was similar to compound **A** (Figure 5d).

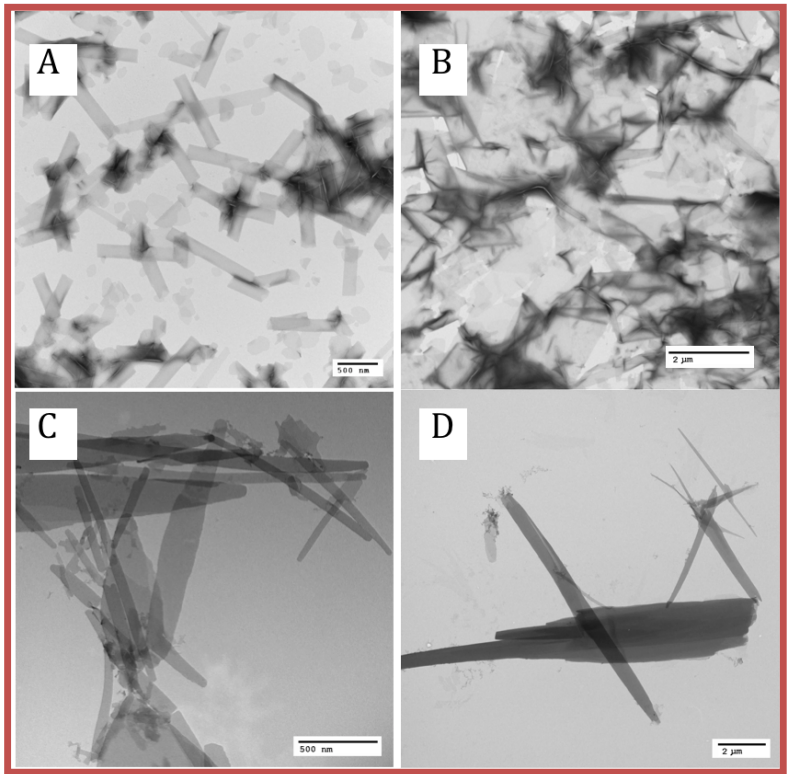

Figure 3. TEM images of A and B: TEM of A (aged (12h) and examined at 4 mM; carbon-coated grid and stained with 2% (w/w) uranyl acetate negative stain) (A) and **A** heated to 130ºC for 30 min (B). TEM of **B** (0.05 mM) (C) and compound **B** heated to 130ºC for 30 min (D).

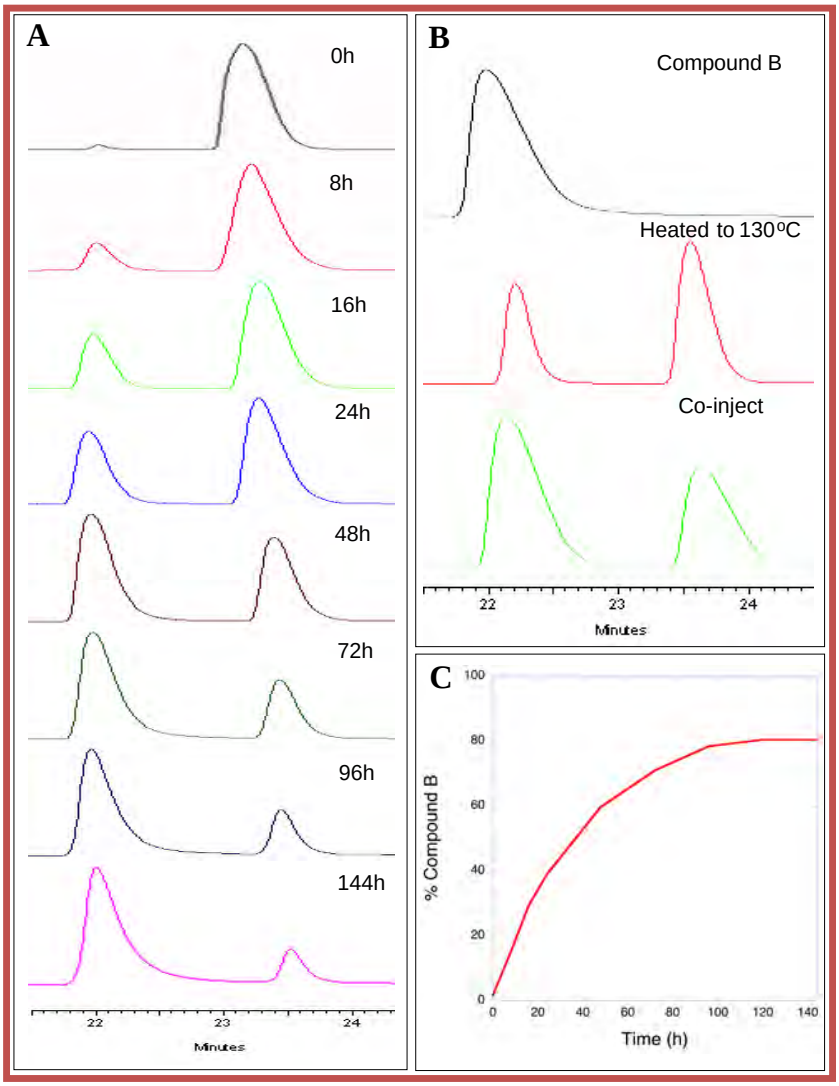

Figure 4: (a) Time dependent hydrolysis of compound **A** at neutral pH and room temperature (2 mM) (b). HPLC analysis of **A** and **B** heated in a sand bath (130 ºC for 30 min in a pressure tube at 2 mM), and a co-injection of **A** and **B** (c). Time dependent hydrolysis of compound **A** at neutral pH and room temperature.

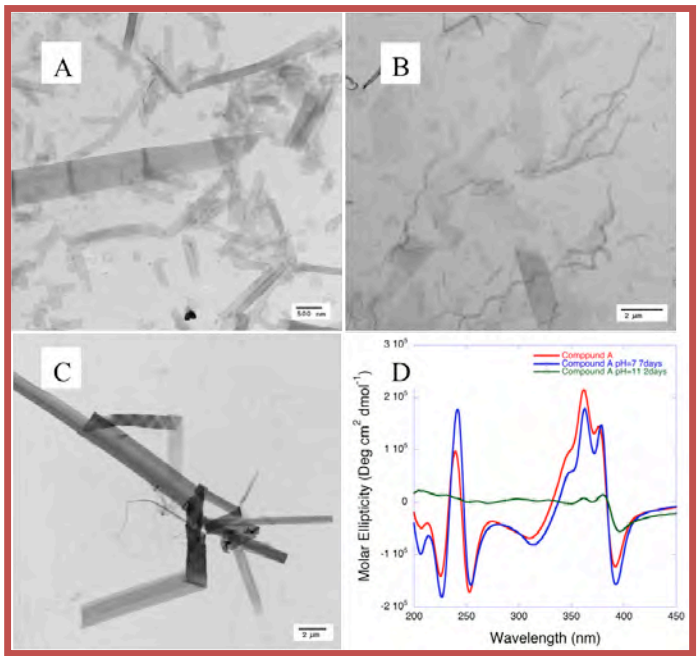

Figure 5: (a) TEM of **A** aged for 7 days at pH=7 (2 mM). (b) TEM of **A** heated to 130ºC for 30 min (1 mM). (c) TEM of **A** aged for 2 days at pH=11. (d) CD of the hydrolysis of **A** after 7 days at pH=7 (Blue) and 2 days at pH=11 (Green).

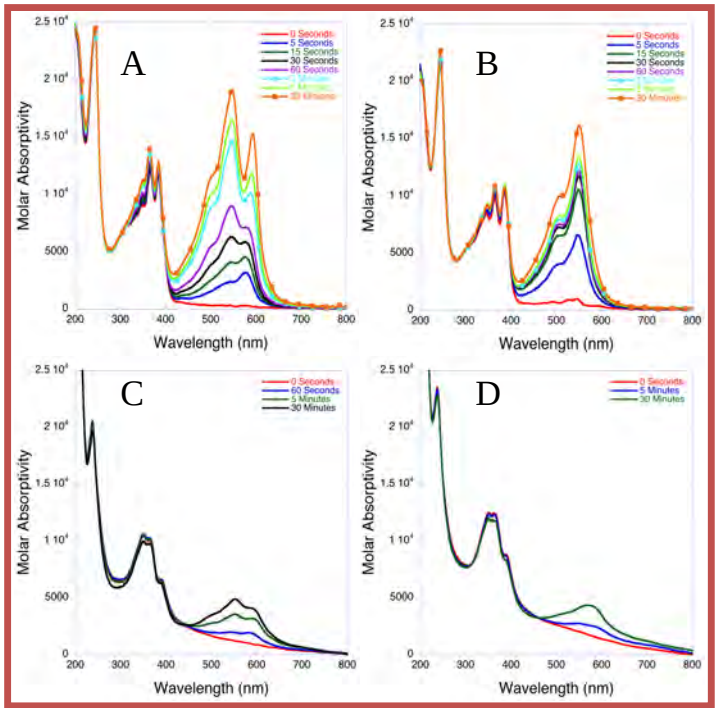

Figure 6. (a) Time dependent polymerization of **A** in water (254 nm (19 W); aged at 5 mM then diluted to 0.30 mM) irradiated over a 30 min period, (b) **A** heated to 130ºC for 30 min in water in a pressure tube (0.30 mM), irradiated over a 30 min period, (c) **B** in water (0.30 mM) irradiated over a 30 min period, (d) and **B** heated to 130ºC for 30 min in water in a pressure tube (0.30 mM), irradiated over a 30 min period.

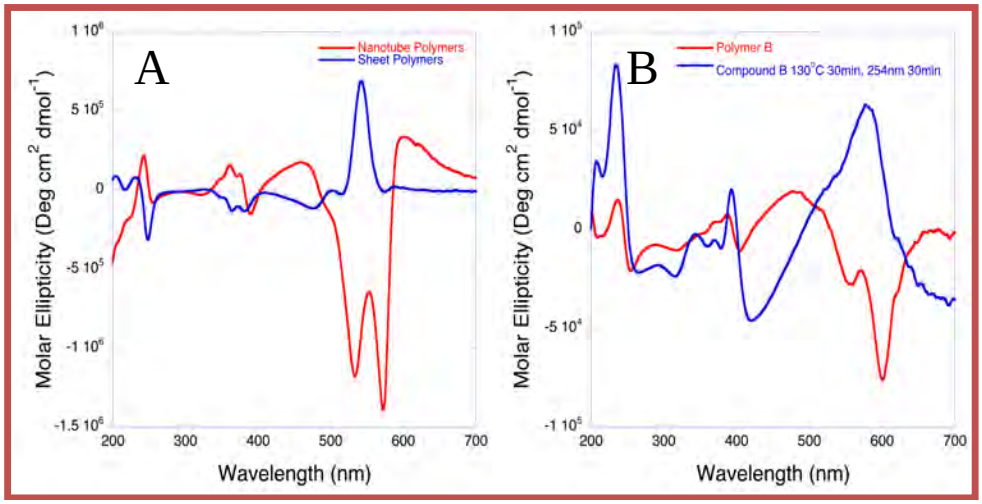

Figure 7. (a) CD of polymer **A** nanotubes (aged for 12h 5 mM, diluted to 0.3 mM, and then polymerized via UV irradiation at 254 nm (19 W) for 30 minutes) and **A** heated to 130ºC (Pressure tube, 30 minutes, 2 mM) to yield sheets, then polymerized (UV irradiation at 254 nm (19 W) for 30 minutes) (0.3 mM). (b) CD of polymer **B** and compound **B** heated to 130ºC then polymerized (0.05 mM).

Diacetylene compounds are known to have a strong UV signal at ca. 500 nm and/or ca. 650 nm after UV induced polymerization.[7] When solutions of nanotubes, created from **A** (300 μM water), were exposed to UV light (254 nm, 19 W), a strong absorbance was observed at 593 nm, 540 nm, and 504 nm within 30 minutes and the solution turned a purple color (Figure 6a). Previous reports have described the purple PDA color emerge from to the 593 nm absorbance.[8-11] The nanosheets (From **A** heated to 130ºC for 30 minutes in a pressure tube) were also exposed to UV light for 30 minutes, causing the 593 nm absorbance to disappear and the solution turned red (Figure 6b). Compound **B**, when irradiated with UV light polymerizes to give the same PDA absorbance as compound **A**: 593 nm, 547 nm, and 504 nm (Figure 6c). The intensity of the PDA absorbances were not as strong. Compound **B** (50 μM) was heated to 130ºC for 30 minutes and then cooled to room temperature, followed by 30 minutes of UV irradiation to see if the behavior of **B** was similar to **A**. Once again the 593 nm absorbance disappeared and the color of the solution was red (Figure 6d). Hydrolysis does not cause the change of the two PDA organizations, but appeared to be promoted with heat. The NDI chromophores of **A** (300 μM) before heat treatment, displays a positive band I excitonic cotton effect and when irradiated with UV for 30 minutes, the polymer helicitywas *M* due to the negative signals centered at 550 nm (Figure 7a). When **A** was heated (130 ºC, 30 minutes), a negative NDI band I excitonic cotton effect, the polymer helicity was *P* due to the positive signal centered at 550 nm. CD of polymer **B** displayed the similar effect for both preheated and heated samples (Figure 7b). The NDI organization regulates the helicity of the polymer backbone. When a positive signal was observed for the NDI chromophores, a negative signal emerged from the PDA chromophores.

In order for diacetylene materials to polymerize, the diacetylene groups must be 4.8 nm from one another. Compound **A** polymerizes quite readily, which hints that the internal organization of the monomeric units are highly ordered (Figure 8). XRD of the centrifuged nanoparticles from compound **A** yielded a 2Θ of 25.7, which indicates a *d*-spacing between the NDI chromophores of 3.5 Å. Since the diacetylene group and the NDI have only a ridged one-carbon spacer between them and that the polymerization occurs readily, the *d*-spacing of the diacetylene should be less then 4.8 Å. If the spacer was larger the diacetylene groups could be further apart due to increased tail flexibility, which would slow PDA formation. The XRD also has a 2Θ of 4.3, which relates to the molecular length with a *d*-spacing of 2.1 nm. This correlates with the measured bilayer tube wall thickness (~4 nm), but is slightly less then the calculated molecular length (2.3 nm). Since the calculated length was less then the *d*-spacing, we hypothesized that the molecular stacking was not straight, but has a slight tilt. The tilt would result in a smaller *d*-spacing value. Tilted molecules within the matrix were common in chiral amphiphilic assemblies.[12]

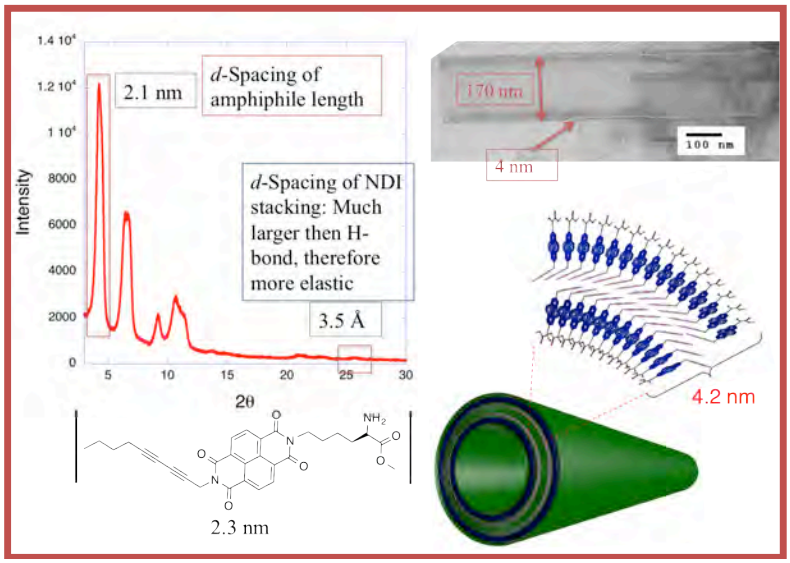

Figure 8: XRD of compound **A** (left) and a model of the nanotube assembly.

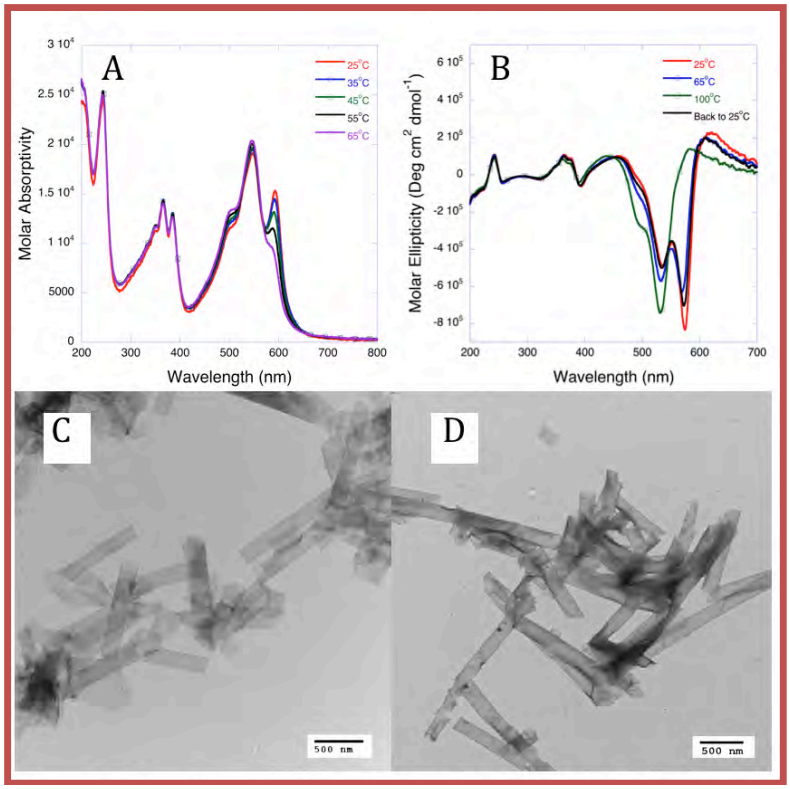

Figure 9: CD and UV-Vis of polymer **A** nanotubes aged for 12h 5 mM, diluted to 1 mM, and then polymerized via UV irradiation at 254 nm (19 W) for 30 minutes. (a) Temperature dependent UV-Vis of polymer **A** (0.3 mM). (b) Temperature dependent CD of Polymer **A** (0.3 mM). (c) TEM of polymer **A** before heating to 100ºC (1 mM). (d) TEM of polymer **A** after heating to 100ºC (1 mM) (D).

Polymerized assemblies have shown improved robust characteristics toward thermal and chemical treatments.[13,14] The UV absorbance at 593 nm decreased and the absorbances at 547 nm and 504 nm intensified as the result of the elevated temperature (Figure 9a). Also when visually inspecting the solution color, the initial purple solution changed to red.

When the solution was allowed to cool, the color changed back to purple and the absorbance of 593 nm reappeared. The decrease of the 593 nm absorbance indicated the loss of conjugation within the polymer backbone.[15] A similar effect can also be seen in the CD spectrum where the negative excitonic cotton signal corresponding to the absorbance at 593 nm also loses intensity and while the signals at 547 nm and 504 nm intensifies. The NDI CD regions remain unchanged and suggesting the organization of the structure was stable even after 30 minutes at 100ºC (Figure 9b). When polymer **A** was cooled back to room temperature, the 597 nm absorbance intensified again reestablishing the lost conjugation. TEM of a sample heated to 100ºC for 30 minutes at a concentration of 1 mM confirms that the nanotubes are retained (Figure 9d).

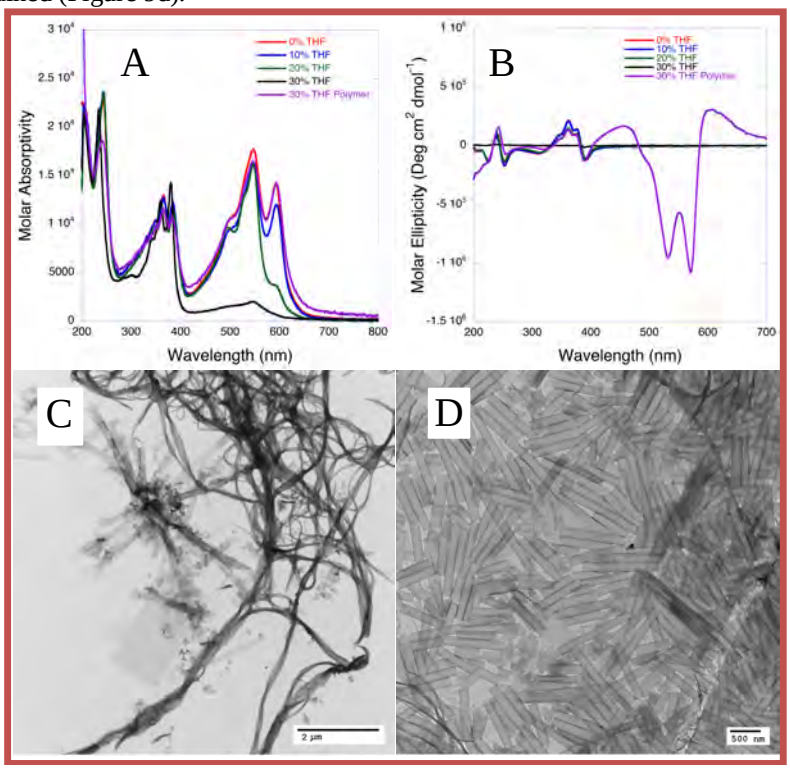

Figure 10: UV-Vis of time dependent polymerization of **A** in THF/water solutions (0% to 30%, v/v). (a) Purple line is polymer **A** in 30% THF/water (v/v). (b) CD of **A** in increasing THF solutions. Purple line is polymer **A** in 30% (v/v) THF/water solution. (c) TEM of **A** in 30% (v/v) THF/water solution. (d) TEM of polymer **A** in 30% (v/v) THF/water solution.

The tube morphology and internal organization of compound **A** were destabilized in 30% THF/Water solution. As the percentage of THF increased in solution from 0% to 30%, the polymerization was hindered as evident by the decreased PDA absorbances centered at 550 nm (Figure 10a). In 30% TFE/water solution, the PDA absorbanceswere significantly less intense. This indicates that the diacetylene groups were no longer adjacent to one another within the structural matrix and cannot polymerize.[16] Compound **A** lacked a PDA CD signal (centered at 550 nm) when THF was added to 30% (v/v) while polymer A showed stability in THF solutions where similar CD positive couplet was observed in the band I range in 30% THF/water (v/v) solutions (Figure 10b). TEM demonstrated the induced robustness of polymer **A**. The non-polymerized nanotubes were destroyed in 30% THF/water (v/v) solutions and transforms into large fibers, while the polymer retains the tube morphology (Figure 10c-d).

The hydrolysis of the methyl ester for compound **A**, as stated above, was fast at elevated temperatures. In an attempt to hydrolyze the polymer, polymer **A** (1 mM) was heated to 130ºC for four hours in a pressure tube. The CD spectrum showed that the NDI organization has a signature similar to the zwitterion, but the nanotubes were not stable under these conditions; sheets, helical coils, and fibers were observed (Figure 11f). In order to determine that polymer has undergone hydrolysis, FT-IR spectroscopy was used to detect changes in the carbonyl region (1800 cm^{-1} to 1600 cm^{-1}). The IR for compound **A** and **B** differ at two wavelengths: the intensity at ca. 3550 cm^{-1} increased for zwitterion **B** due to the carboxylic acid and two carbonyl absorptions (NDI imines and carboxylic acid) at 1659

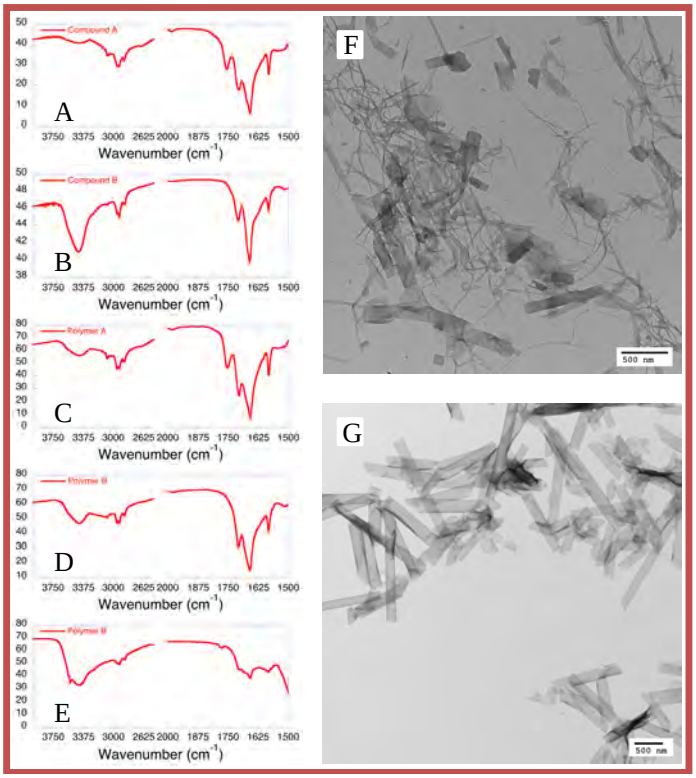

Figure 11. FT-IR of compound **A** (A), compound **B** (B), polymer **A** (C), polymer **A** after thermal hydrolysis at 130ºC for 4h in water in a pressure tube (1 mM) (D), polymer **A** after chemical hydrolysis at pH=11 for 2 days (2 mM) (E). TEM of polymer **A** after thermal hydrolysis (F) and chemical hydrolysis (G).

cm^{-1} and 1706 cm^{-1}. Compound **A** has a distinct methyl ester carbonyl absorption at 1754 cm^{-1}, which compound **B** lacks (Figure 11a-b). The IR spectrum of polymer **A** was similar to that of compound **A**, where the absorption of 1754 cm^{-1} were observed for both (Figure 11c). When polymer **A** undergoes hydrolysis, similar IR absorption changes should be observed. The heat treated polymer **A** did show an increase at ca. 3550 cm^{-1} and lacked the 1754 cm^{-1} absorption indicating hydrolysis occurred similar to compound **A** (Figure 11d). The pH was increased to 11 to retain the polymer's tube morphology due to less destructive conditions. Polymer A was subjected to a two day aging period at pH=11 (2 mM, pH adjusted with 1 mM NaOH), the solution was lyophilized and IR once again showed and increase of the ca. 3550 cm^{-1} absorption and the absence of the absorption at 1754 cm^{-1} the same as the heat treated sample (Figure 11e). TEM revealed the tubular structure was maintained (Figure 11b. The CD of the chemically hydrolyzed polymer **A** displayed a similar spectrum as compound **A** (Figure 12b). Also, the solubility of hydrolyzed polymer **A** was improved when compared to the zwitterion. The morphology of the nanostructure can affect solubility.

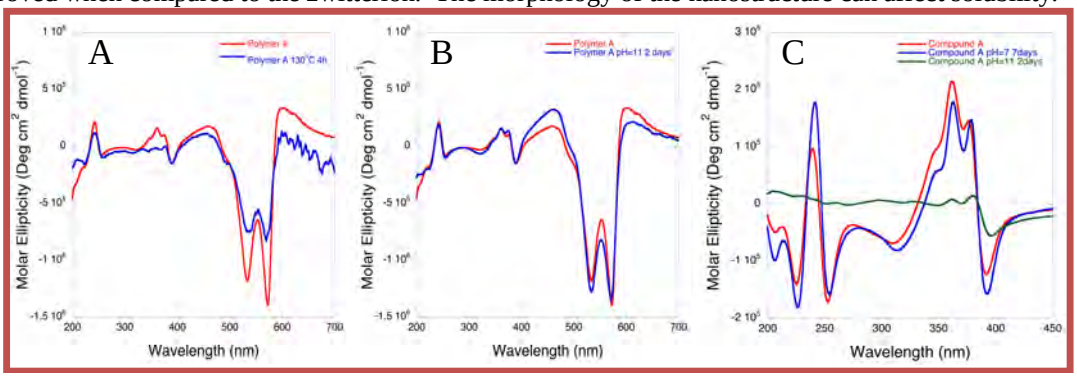

Figure 12: CD of polymer **A** heated at 130ºC for 4 hours in water in a pressure tube at 1 mM (0.3 mM) (A). CD of polymer **A** at pH=11 for 2 days at 2 mM (0.3 mM) (B). CD of **A** (0.3 mM)**, A** at pH=7 for 7 days at 2 mM (0.3 mM) (Blue) and pH=11 for 2 days at 2 mM (0.3 mM) (Green) (C).

Self-Assembled Nanotube Templates for Gold Nanoparticles

Introduction. Gold nanoparticles have gained interest during the past decades due to their optical, electronic, and chemical properties.[17-19] These properties show application potential in optics,[20] sensing,[21] nanoelectronics,[22] catalysis,[23,24] biotechnology,[25,26] and medicine.[27,28] The properties of gold nanoparticles are heavily dependent on the size and shape of the particle.[29,30] For example, gold nanoparticle catalysts are more reactive when the surface area is increased, therefore a smaller diameter particle will yield higher reactivity.[31] Also, the absorbance of the gold nanoparticle increases in wavelength was the size increases, resulting in near IR absorbance useful for biomedical imaging.[32] During the reduction of gold salt, the gold nanoparticle growth can be hard to control because of the lack of a stabilizing agent that will prevent agglomeration and reduce surface area. Synthesis occurs through a reduction gold(III) to gold(0) using chemical reducing agents such as citrate, sonochemical, and photochemical.[33] Usually a stabilizing agent (thio-ligand) is added that will surround the nanoparticle and prevent agglomeration or growth of the nanoparticle.[34]

Besides using small molecular stabilizing agents to control shape and size, templates made from polymers,[35-37] inorganic particles,[38,39] or assembled 1-D nanostructures can be used.[40,41] Templates with amine and thio- attractive functionalities have had success for gold nanoparticle formation on the template surfaces.[42] Amphiphilic lysine-NDI molecules have an amine in the polar head that has a positive charge that can attract anionic gold tetrachloride salts and gold nanoparticles stabilize by negatively charged citrate. This chapter will go into detail on the exploration of robust nanotube assemblies comprised of lysine-NDI-diacetylene amphiphiles used as a template for gold nanoparticles.

Research Design. The most common way to synthesize gold nanoparticles would be to reduce the strong acid tetrachloroauric acid ($HAuCl_4$) with sodium citrate in water at 75ºC (Figure 13).[43] The auric acid will dissociate into water as a gold(III)tetrachloride anion, which can electrostatically be attracted to a cationic species.[44] During the reduction reaction, agglomeration can be hindered by the citrate coating the gold particle, acting as a stabilizing agent. The citrate coating is also anionic and is attracted to cations.[45] Therefore the gold was attracted to a cationic surface in both ionic and colloidal forms.

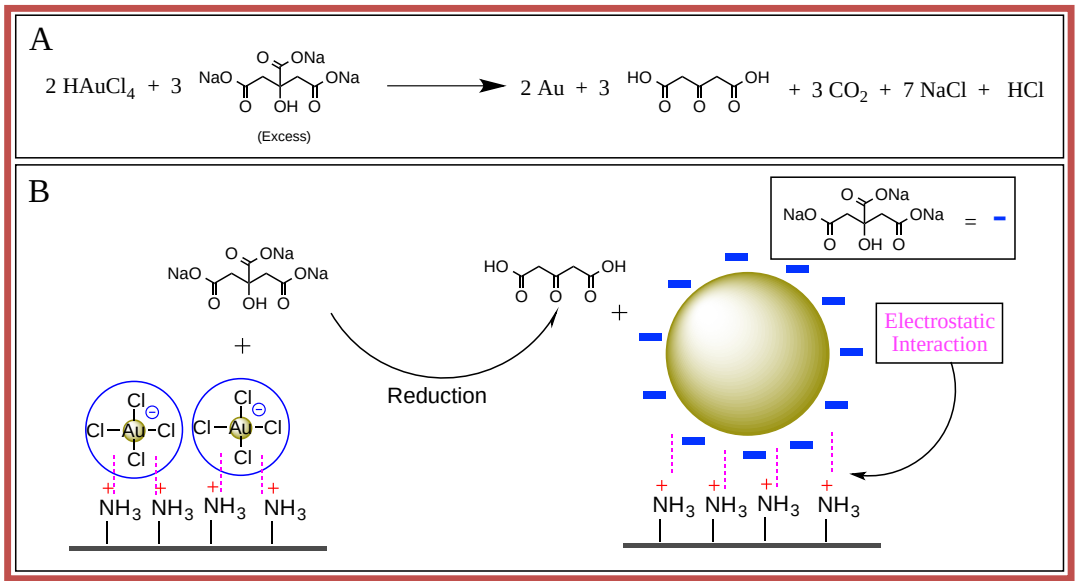

Figure 13. (a) Turkevich method to reduce gold(III) to gold(0). (b) Two different ways gold can electrostatically interact with cations; gold(III)tetrachloride anion or citrate coated colloidal gold can interact with the positively charged surface.

Research. Lysine-NDI amphiphilic molecules exhibit an ammonium cation in the polar head group.[3] The NDI amphiphiles with diacetylene functionality displayed some robust characteristics toward conditional changes especially after polymerization, where the nanotube morphology was stable to elevated temperature and pH change. The directional
assembling interaction was π-π stacking of the NDI core and the diacetylene tail, which enforces the robustness of the nanotube assembly. Small simple amphiphilic molecules that undergo self-assembly and lack intermolecular interactions, such and hydrogen-bonding and π-π stacking, are sensitive to conditional changes.[46] Many surfactants are known to cover the surface of the colloidal nanoparticle, so the assembly will most likely fall apart and coat the

gold nanoparticle due to stronger gold-ligand interaction.[47] Amphiphilic assemblies used as gold nanoparticle templates are more rare and most templates designed for gold nanoparticle decoration involved a fixed surface such as carbon nanotubes, silica oxide, titanium oxide, and other inorganic surfaces.[39,48,49] Larger molecules that undergo self-assembly with very strong intermolecular interactions such as peptides and larger proteins have shown to be stable enough to provide a compatible surface for in situ gold nanoparticle synthesis.[50] The lysine-NDI-diacetylene (compound **A**) nanotube assembly would be stable to citrate addition and the gold(III) tetrachloride reduction because of the intermolecular π-π stacking between the NDIs and diacetylene. The ammonium on the lysine will attract citric acid/citrate coating the tube in reducing agent, followed by the addition of tetrachloroauric anion and reduce the gold(III) on the tube surface decorating the tube with gold nanoparticles coat (Figure 4.10).

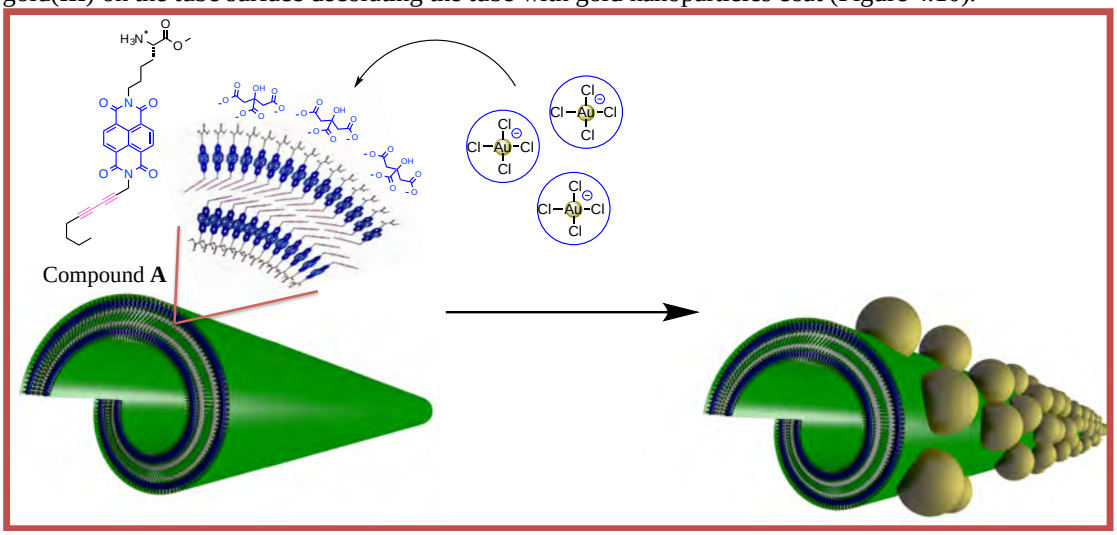

Figure 14: Depiction of the **A** amphiphilic assemblies being decorated with gold nanoparticles.

Results and Discussion. Compound **A** was soluble in neutral water and formed nanotube assemblies at a concentration of 2 mM. When citric acid (2 mM, 1 eq, pH = 3.4) was added to the solution, the pH decreased, and the nanotube morphology was similar to that found at pH = 7.0. When tetrachloroauric acid (0.67 mM, 0.67 eq) was added, the pH dropped slightly to 3.0. Examining the sample by TEM, spherical gold nanoparticles were observed on the surface of the nanotube (Figure 15). When these gold nanoparticles were compared to the same conditions in the absence of compound **A**, non-spherical particles were also observed. The nanotube template controls the growth of the nanoparticles similar to a stabilizing agent.[34] The gold nanoparticles were measured to have a diameter of an average 7.6 nm for these conditions.

The order of addition, citric acid to the nanotube solution followed by the addition of tetrachloroauric acid, was critical in order to obtain spherical gold nanoparticles. The hypothesis was that the tetrachloroauric anion would interact with the ammonium cation and coat the tube surface where the citric acid would reduce the gold(III) giving an evenly decorated nanotube. When the citric acid (1 equiv., 1 mM) was added to the gold(III) (667 μM) and compound **A** solution (1 mM), irregular gold nanoparticles formed (Figure 16). As seen in previous reports, citric acid coordinates to the ammonium cations and allows controlled growth of the gold nanoparticle because the tube surface provides stability.[44] Citric acid also acts as a stabilizing agent, so if the citric acid was added to the gold(III) coated nanotube the citric acid would be diluted and not concentrated on the tube. Therefore, as the nanoclusters of colloidal gold form, the lack of citric acid allows for agglomeration to occur. Another possibility for the behavior could be due to hydrolysis of the tetrachloroauric anion to trichloroauric hydroxide. The tetrachloroauric anion exists in water/NaCl solutions because of an increase in chloride ion and ligand exchange was slowed.[51] Perhaps the trichloroauric hydroxide was protonated in the acid pH forming a neutral species and had less affinity to the ammonium surface.

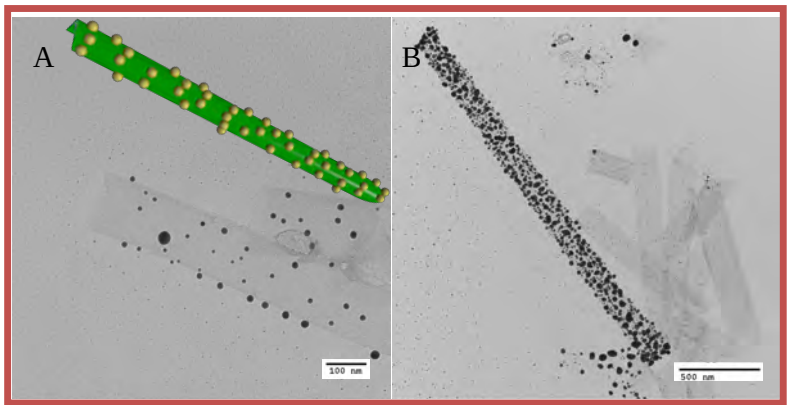

Figure 15: (a) Control: TEM (carbon-coated grid and not stained) of citric acid and tetrachloroauric acid (3:2, 500 μM citric acid) in water, aged for 1 d at pH = 3.3 (b) TEM of 1 eqiv. of citric acid in a solution of compound **A** (500 μM), followed by an addition tetrachloroauric acid (0.67 eqiv.) and aged for 1 day at pH = 3.0.

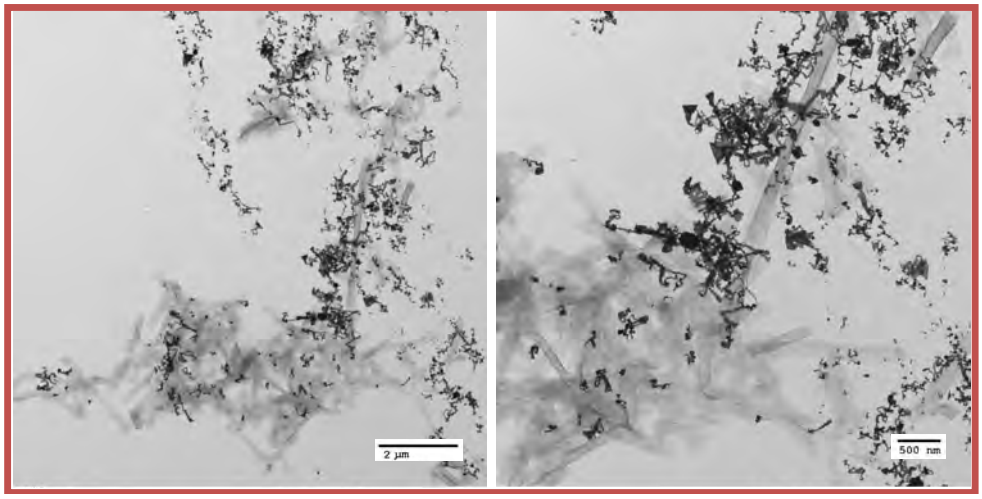

Figure 16. TEM of **A** (500 μM) and tetrachloroauric acid (333 μM) after the addition of citric acid (500 μM).

A titration of a solution of compound **A** and citric acid (500 μM) with tetrachloroauric acid (1.0 mM) was performed to show the growth of the gold nanoparticles. Initially, the gold nanoparticles quickly grew as the ratio of gold(III): compound **A** reached a ratio of 0.8, where the diameter of the gold nanoparticles went from 8.4 nm at a ratio of 0.2 to 21.2 nm at a ratio of 0.8. Upon further increase of the gold(III): compound **A** ratio, the size growth stagnated due to the lack of available reducing agent and reached a diameter of 23.9 nm when a ratio of 1.6 was reached. At a ratio of 3.2, gold(III): compound **A**, the concentration of compound **A** had been diluted (60 μM) enough, that the critical micellar concentration has been reached and the tubes started to break apart. The gold nanoparticle diameter in this sample increased significantly to 29.5 nm. The zoomed in image of the gold nanoparticles showed the amphiphile coating the particles. The gold nanoparticle diameter increase that occurred between a ratio of 1.0 and 1.6 was small (1.4 nm). To determine if the gold nanoparticle did have a surfactant coating, tetrachloroauric acid (5 mM, 10 equiv.) was added to compound **A**: citric acid (1:1, 500 μM) (1:1 v:v) resulting in a 250 μM concentration of compound **A**. This will yield a concentration where the nanotubes do not deteriorate. Most nanotubes did show an even coating of gold nanoparticles between 6 nm to 25 nm in diameter. Close examination of the gold nanoparticles revealed that the particles had clean curved edges without a noticeable surfactant coating.

Gold nanoparticles have been shown to have an affinity to acetylene functionalities and acetylene groups are known to coordinate to metal.[52] With cationic surfactants, gold nanoparticles with a citrate coating interact through electrostatic charge. To rule out acetylene coordination and demonstrate that the decoration process was electrostatic, auric acid was reduced in the presence of nanotubes assembled from NH_2-Lys(NDI-*n*Bu)-OMe (**C**), a monomer not

containing disacetylene functionality, and citric acid. Unfortunately, the nanotube morphology was not stable under these conditions (500 μM **C**, 500 μM citric acid, and 333 μM) and irregular

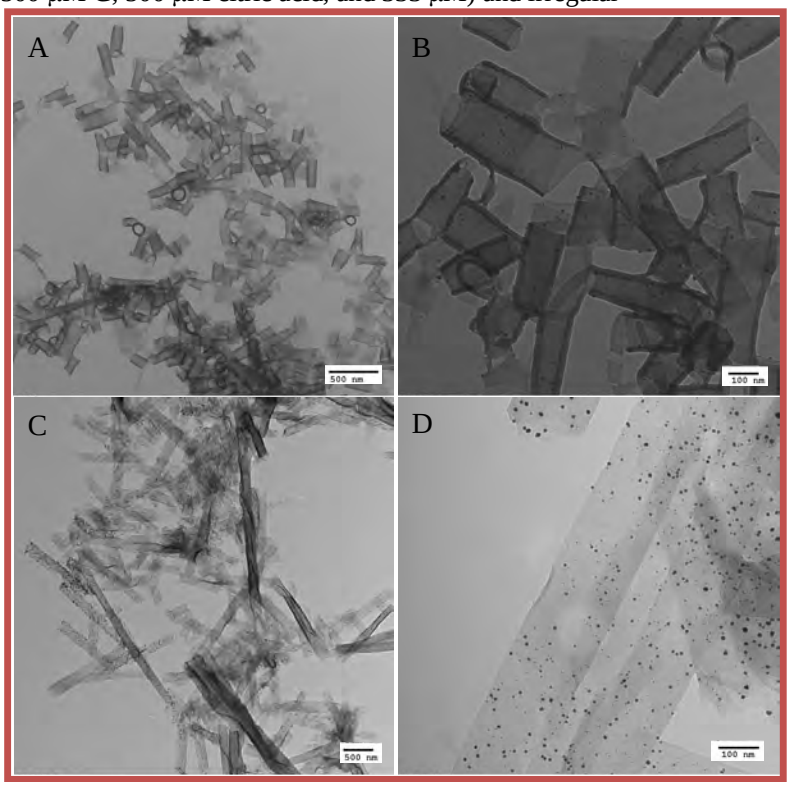

Figure 17. TEM of NH_2-Lys(NDI-*n*Bu)-OMe (**C**) in water (500 μM, 1 eq sodium citrate, 0.67 eq $HAuCl_4$) at pH = 5.2 (A and B). TEM of compound **A** in water (500 μM, 1 eq sodium citrate, 0.67 eq $HAuCl_4$) at pH = 5.2 (C and D). aggregates were observed.

The citric acid was replaced with sodium citrate to increase the pH to 5.2. Although the original long narrow nanotube morphology was not observed when the assembly was at neutral pH, shorter and wider nanotubes formed (Figure 17a/b).[3] In a solution of **C**(1 mM) and sodium citrate (1 mM) was added gold(III) (0.67 mM) and gold nanoparticles once again formed on the surface of the nanotubes, which suggested strong electrostatic interactions do occur between the gold nanoparticles and the nanotube surface. The gold nanoparticles were very uniform in size ranging 9.0 to 13 nm in diameter and evenly dispersed.

Under the same condition but with compound **A** (1:1 sodium citrate, 0.67 equiv. tetrachloroauric acid), the nanotube morphology was retained and the gold nanoparticles were dispersed evenly, more so than the samples using citric acid. The sizes of the gold nanoparticles were once again in the range of 9.0 to 13 nm in diameter. As seen with other research involving the gold decorating of templates, the pH was an important factor.[42] The sodium citrate will be attracted to the positive nanotube surface more so than more neutral citric acid. The pKa of the mono- and disodium citrate was 4.77 and 5.19 respectively and the pKa of citric acid was 3.15. The more basic the solution, sodium citrate formation would be more favorable, therefore having an increased negative formal charge. The increase in formal negative charge increases the electrostatic interaction with ammonium tube surface. Having more reducing agent on the surface of the nanotube will result in more colloidal gold nanocluster nodes, which will further grow into evenly dispersed nanoparticles.

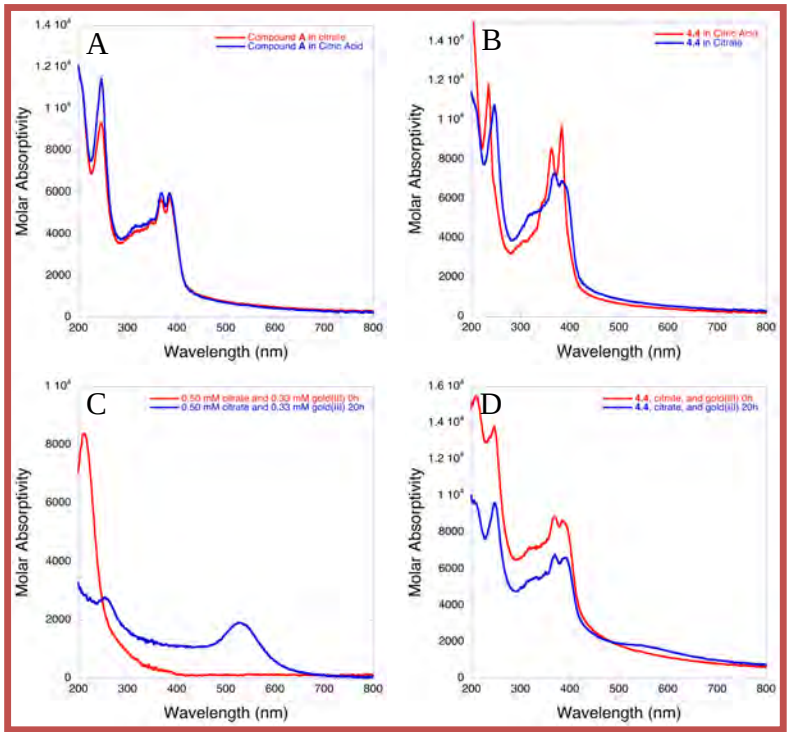

Figure 18: (a) UV-Vis of **A** in sodium citrate (red) or citric acid (blue), and **C** in sodium citrate (red) or citric acid (blue). (b) Time dependent UV-Vis of the reduction of tetrachloroauric acid (333 μM) with sodium citrate (500 μM): 0h (red) and 20h (blue). (c) Time dependent UV-Vis of the reduction of tetrachloroauric acid (333 μM) with sodium citrate (500 μM) in the presence of **C:** 0h (red) and 20h (blue).

The main purpose of a template for gold nanoparticles was to increase the stability of a gold nanoparticle and prevent agglomeration. A solution of tetrachloroauric acid (0.67 mM, 0.67 equiv.) was added to a solution of **A** (1 mM) and sodium citrate (1 mM) and aged for up to 4 days (Figure 4.15). After 4 days of aging, the gold nanoparticles did not agglomerate according to the measured average gold nanoparticle diameter. The average diameter of the gold nanoparticles in each sample ranged from 12.0 nm to 14.4 nm. The nanotubes showed to stabilize the gold nanoparticles and prevented agglomeration for up to 4 days. Nano-sized gold nanoparticles can absorb UV light due to surface plasma ocillations.[50] The size of the particle was determined to be directly related to the absorption wavelength.[53] The absorption of **C** showed the NDI band I (330 nm to 390 nm) and II (240 nm to 270 nm) absorptions, but lacks any absorption higher than 400 nm (Figure 4.16 B). When gold(III) (333 μM) was reduced without amphiphile **A** or **C** in sodium citrate (500 μM) in 20h at room temperature, an absorption of 525 nm appeared, indicating gold nanoparticle formation. In the presence of amphiphile **C**, a similar absorption appeared in the same region, but slightly red shifted (550 nm). Therefore, the gold nanoparticles on the surface of the tube clearly exhibited different absorption properties-the red shift (an increase in absorbance wavelength) indicates a larger spherical particle.[53]

Photoresponsive Amphiphilic Nanotubes from lysine-SP/MC Hybrid. These preliminary studies focus on installation of a spiropyran photoresponsive unit on the lysine side-chain to explore how the self-assembly and photoresponsive responds to changes in the SP/MC chromophore. Two compounds were prepared: Ac-K(SP)-OH (**SP1**) and H_2N-K(SP)-NH_2 (**SP2**).

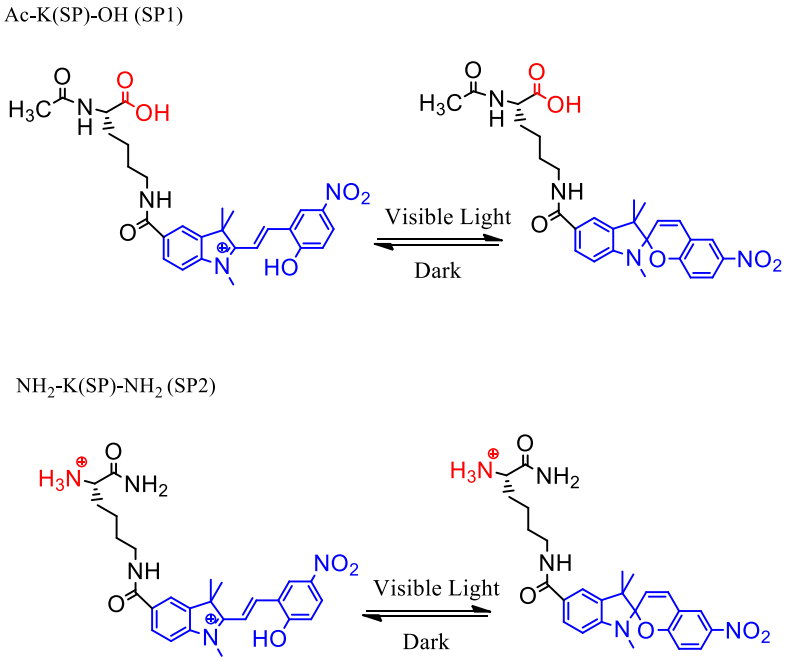

Figure 1. The structural design and of Ac-K(SP)-OH (**SP1**) and NH_2-K(SP)-NH_2 (**SP2**) which undergo structural change into the open form of protonated merocyanine form with UV=254 nm irradiation in acidic condition.

1. SP1 and SP2 Solution Preparation

The freeze-dried Ac-K(SP)-OH (**SP1**) was added to water and 1% TFA in water solution to prepare a 10 mM stock solution. Each solution was divided by half; half of the solution was aged at room temperature in dark condition for 3 days solution and named as a1 (in H_2O), b1 (in 1% TFA) and the other half was moved under visible light of table lamp and aged for 3 days and named as b1 (in H_2O), d1 (in 1% TFA) at room temperature. For NH_2-K(SP)-NH_2 (SP2), four corresponding solutions a2, b2, c2 and d2 were prepared.

2. TEM morphologies of self-assembled nanostructures.

The self-assembly behavior of the solutions (a1~d1) was investigated by transmission electron microscopy (TEM) (Fig. 2). In H_2O in the dark, SP1 predominantly remains in the open merocyanine form and self-assembles into nano-belt structure. The self-assembly of this form of the monomer is driven by the planar merocyanine form, which can provide π-π interactions. Upon visible light irradiation, SP1 changes into the closed spiropyran form and formed some amorphous aggregates with some large sheets structure, presumably due to the nonplanar structure of the closed spiropyran form. The SP form is hydrophobic and tends to aggregate in water, but in contrast the the MC form does not form ordered aggregates.

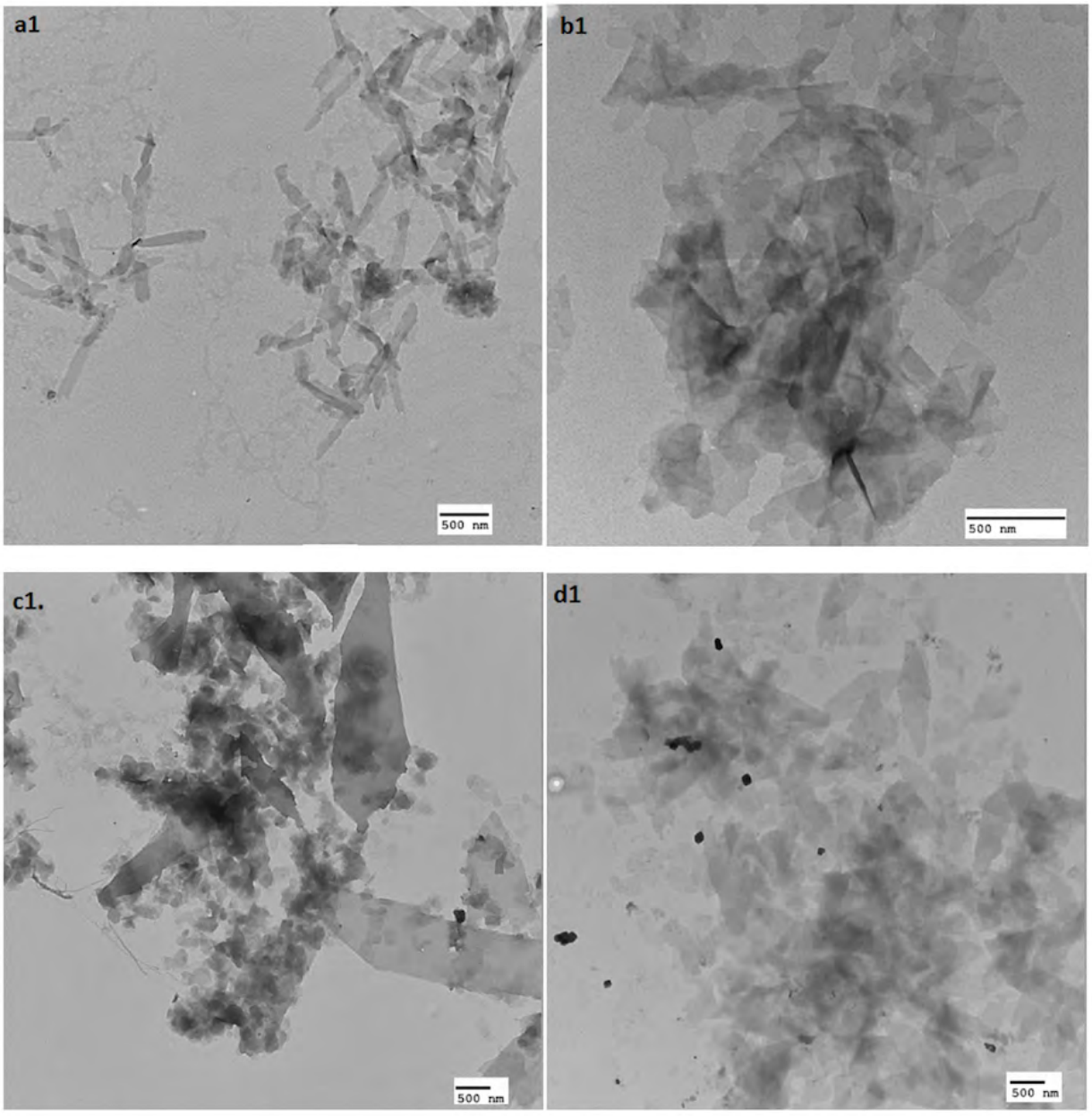

Figure 2. TEM images of solution a1(H_2O, MC form, Dark), b1(1% TFA, MC form, Dark), c1(H_2O, SP form, Visible light) and d1(1% TFA, SP form, Visible light). All solutions were prepared at 10 mM concentration and aged under corresponding condition for 3 days and freshly diluted to 1 mM for microscopy.

Self-assembly behavior of the solutions of NH_2-K(SP)-NH_2(SP2) (a2~d2) In H_2O, SP2 remains in the closed SP in the dark and predominantly self-assembles into a sheet-like structure, some of which partially roll into tubes that are not well defined or homogeneous in structure. The range of structures that are observable here may be a consequence of the presence of both SP and MC forms, due to the ready capability of the SP to interchange with the MC form with stray light (Fig. 3). However, upon visible light irradiation, which produces the closed SP form, nanostructures transitioned to well-defined short tubes as SP1 changed into the closed spiropyran form. In 1% TFA in dark after 254 nm irradiation, SP2 predominantly remains in the protonated MC open form, which does not have very distinct self-assembly conformation since the protonated open form for SP2 is too polar. The well-defined self-assembly of the closed SP form into well defined nanotubes may be a consequece of the hydrophobic nature of the SP form, which

maintains the monomer amphiphilicity. Whereas, in the MC form, although the planar structure is more capable of p-stacking the charge reduces the amphiphilic driving force for self-assembly. Work is in progress to fully understand the source of these structural changes.

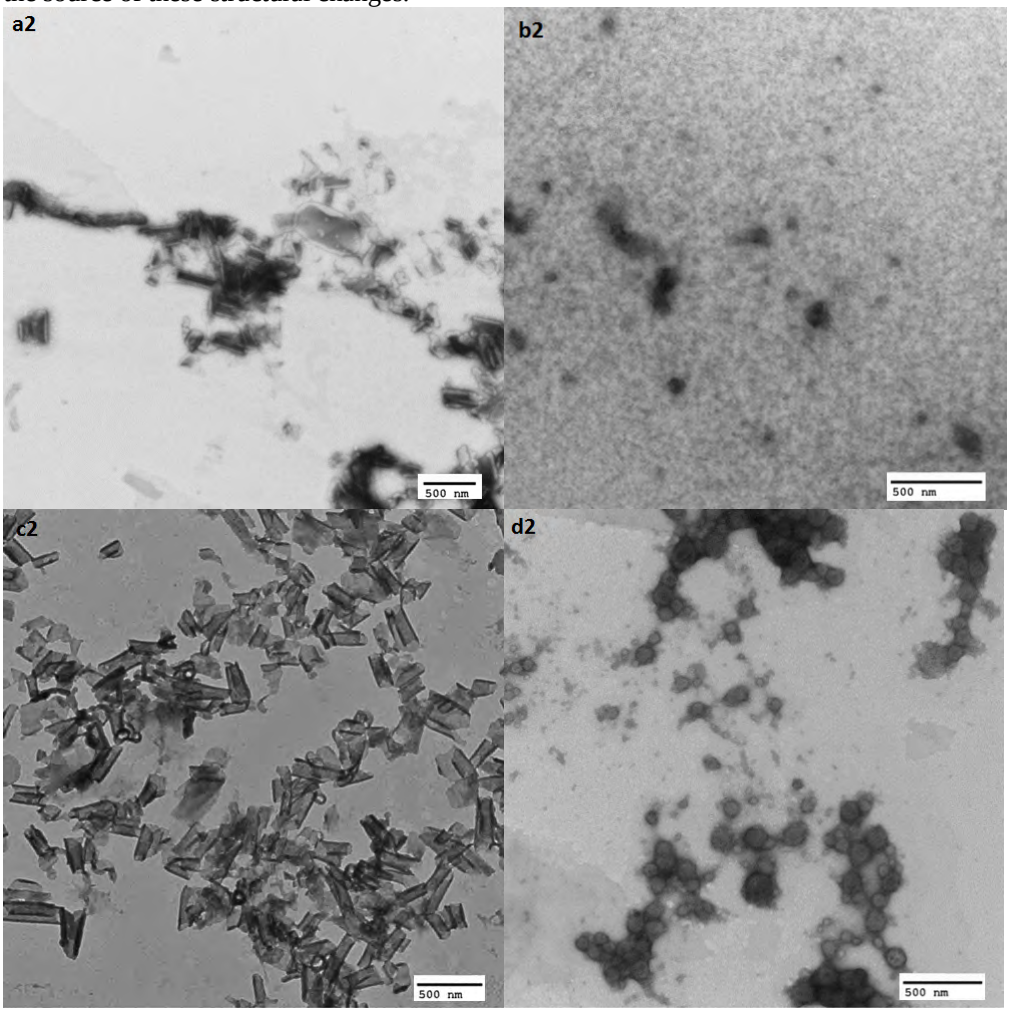

Figure 3. Self-assembly behavior of the solutions of NH_2-K(SP)-NH_2 (SP2), a2(H_2O, Dark), b2(1% TFA, Dark), c2(H_2O, Visible light) and d2(1% TFA, Visible light). All solutions were prepared at 10 mM concentration and aged under corresponding condition for 3 days and freshly diluted to 1 mM for microscopy

UV-vis/CD Spectroscopy. The conversion between closed spiropyran form and the open merocyanine form can be observed by fluorescence microscopy. In H_2O in dark, SP1 is in the protonated open merocyanine form with a distinct absorbance at 420 nm. There is a small portion of the deprotonated merocyanine form with a peak *ca*. 500 nm (Fig. 4, black line). In this condition, SP1 self-assembles into nano-belt structure. With visible light irradiation, both peaks at 420 nm and 510 nm disappeared, indicating that the SP1 change into the closed spiropyran structure (Fig. 4, blue line). The self-assembly conformation also changed into large sheets and amorphous aggregates. This may result from that the closed spiropyran is not planar and is less rigid than the open merocyanine form, so that the molecules cannot pack as closely. In 1% TFA, in dark Ac-K(SP)-OH mainly stays in the protonated open form with the peak at 420 nm (Fig. 4, red line). After visible light irradiation, it also changed into the closed spiropyran form (Fig. 4, green line).

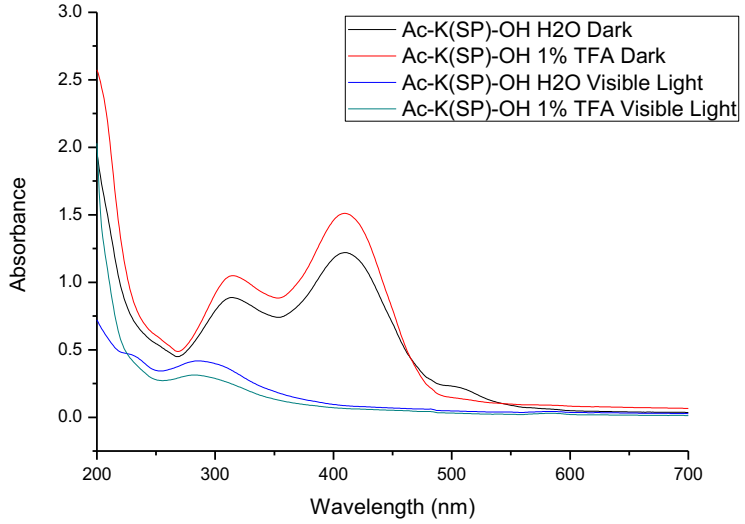

Figure 4. The UV-vis absorption of Ac-K(SP)-OH solution in H_2O Dark (a1), in 1% TFA Dark (b1), in H_2O visible light (c1), in 1% TFA visible light (d1). All solutions were prepared at 10 mM concentration and aged under corresponding condition for 3 days and freshly diluted to 1 mM for microscopy

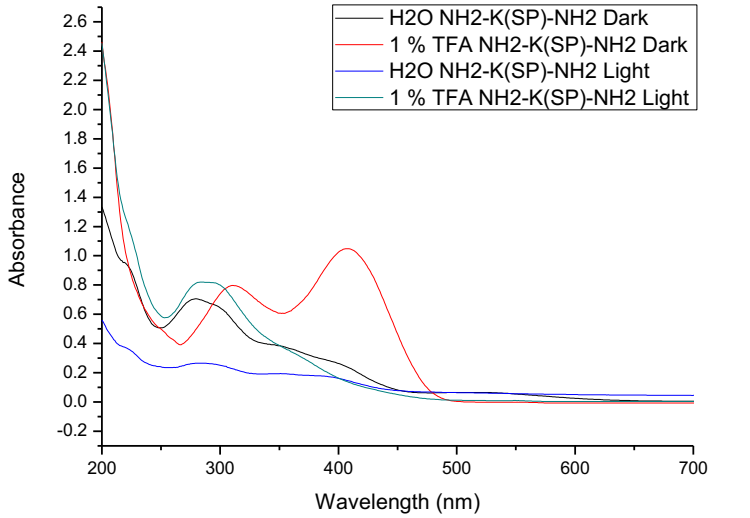

Figure 5 The UV-vis absorption of NH_2-K(SP)-NH_2 solution in H_2O Dark (a2), in 1% TFA Dark (b2), in H_2O visible light (c2), in 1% TFA visible light (d2). All solutions were prepared at 10 mM concentration and aged under corresponding condition for 3 days and freshly diluted to 1 mM for microscopy

For SP2 (Fig. 5) in aqueous solution in dark, only a small portion of SP2 maintains protonated open form as the peak at 420 nm is weak. The major form is closed form so that we can see some tube-like structure in TEM. As irradiated by visible light, more open forms change into the closed form with the decrease of 420 nm peak. In 1% TFA, the strong peak at 420 nm indicates SP2 majorly stays in the protonated open form. After visible light irradiation, it changes into the spiropyran closed form.

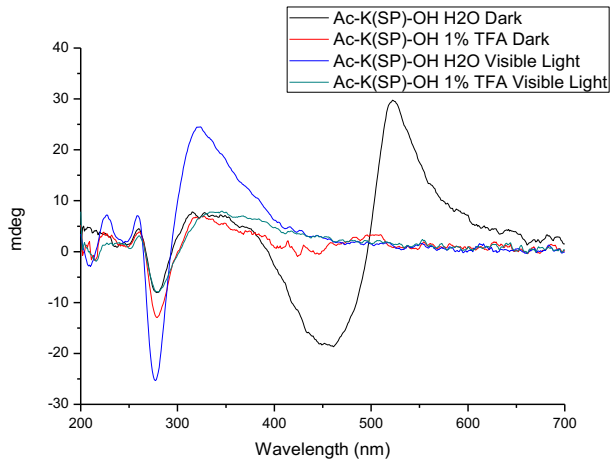

Figure 6 CD spectra of Ac-K(SP)-OHsolution a1~d1. All solutions were prepared at 10 mM concentration and aged under corresponding condition for 3 days and freshly diluted to 1 mM for microscopy

CD Spectra. The self-assembly behavior of Ac-K(SP)-OH is also investigated by CD spectra.
In aqueous solution in dark (black line), there is a strong positive peak at 510 nm, which indicates the packing involve the deprotonated merocyanine form, the strong peak over 400 nm also indicates that the protonated merocyanine form also contributes to the self-assembly (Fig. 6. black line). Under visible light irradiation, the decrease of both peaks and the increase of absorbance at 280 nm and 320 nm indicate the change into the closed spiropyran form and also the change in self-assembly (Fig. 6. blue line). The spiropyran formed self-assembly are P-type aggregates. In 1% TFA, both CD signals are not very strong, correspond to the amorphous aggregates in TEM study, which also shows that 1 % TFA interrupt the self-assembly of Ac-K(SP)-OH.

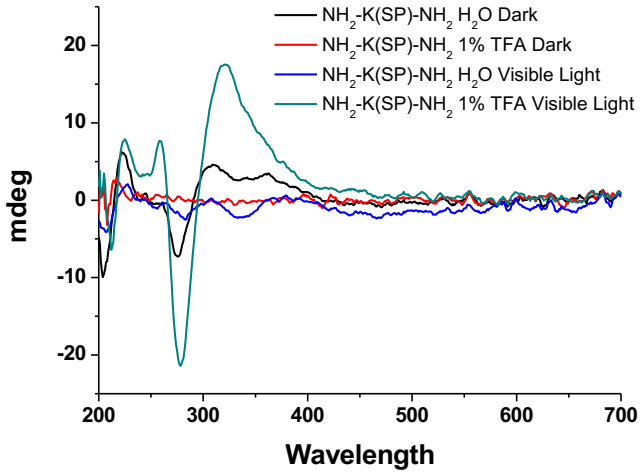

Figure 7. CD spectra of NH_2-K(SP)-NH_2solution a2~d2. All solutions were prepared at 10 mM concentration and aged under corresponding condition for 3 days and freshly diluted to 1 mM for microscopy
However, for NH_2-K(SP)-NH_2aqueous solutions, both in dark and under visible light, there are only weak CD signals, indicating that the aggregates do not have very distinct types. In 1% TFA in dark, the flat CD signal also confirm no assembly formed by the protonated open form of SP2. After visible light irradiation, a strong CD signal appear with distinct peaks at 280 nm and 320 nm, showing the self-assembly of closed spiropyran form. The positive huge peaks also identifies a p-type chirality for the aggregates.